Development of a LIM Simple Cycle Diesel Engine

By

Douglas M. Baker, Ph.D.
TECAT Engineering Inc.
Livonia, MI

February 6, 2006

Table of Contents

Executive Summary

LIM Technology, LLC has developed a camless uniflow diesel that uses unique passive pneumatic-controlled intake poppet valves to facilitate engine scavenging and to maximize trapped charge boost. Early proof of concept prototypes were equipped with lower pressure mechanical fuel injection systems and have not been thermodynamically optimized.

In the past 12 months, LIM has pursued a formal engineering approach aimed at elevating LIM technology to a competitive level within the diesel engine community. This strategy included 1) conversion of LIM engines to common-rail electronic fuel injection, 2) a testing program on an existing prototype to characterize valve behavior, and 3) numerical modeling to evaluate system potential of an optimized design. This report summarizes results from these strategic activities. Key findings include:

- A multi-pulse common rail fuel injection system successfully demonstrated improved combustion characteristics within an existing LIM engine platform
- Valve motion was observed to behave as anticipated offering potential improvements in system fuel economy and performance.
- A numerical simulation was developed and validated; simulation results indicate the potential for a supercharged, aftercooled LIM engine to reach a BSFC of 0.35lb/hp/hr and a power density of ~1.0 Hp/cuin. Better fuel economy is potentially achievable using an active valve management system.
- Clean sheet designs have potential power densities over 1.5 Hp/cuin.

The LIM engine cycle appears to offer excellent breathing characteristics and good fuel economy over a wide range of speed. Further analysis is required to fully appreciate the potential of the technology.

Project Overview

LIM currently has three running engine prototypes with LIM valves installed. The supercharged LIM 353 (i.e. – 3 cylinder, 53cuin/cyl) engine with mechanical fuel injection and four valves per cylinder with lightly sprung managed induction system was selected as the baseline prototype for the current investigation. The piston topology in this engine mimics that of the Duramax combustion system. The engine was retrofitted using a Bosch 23kpsi injection system with magneto-strictive injectors.

A TECAT fuel controller managed multi-pulse fuel delivery during all dynamometer test sessions which were conducted at McLaren Performance Engines in Livonia, Michigan. The LIM valves were instrumented with high speed sensors to better understand valve behavior during engine operation. In-cylinder high speed pressure measurements were obtained to observe combustion characteristics as well. Low speed data were recorded to evaluate system performance and fuel economy.

After testing was complete, a first principles numerical model was developed to simulate the LIM engine cycle and valve behavior. The model provides for changes to key valve dimensions, valve mass, spring tension and pre-load, and can be modified to simulate active valve control as well. Using this simulation, an extensive analysis and optimization of the existing LIM353 system was conducted to assess potential performance of this system in contrast to what was observed during actual baseline engine testing. Simulated changes in valve and/or spring design, manifold design,

porting, and supercharger design were evaluated in an attempt to improve overall system performance and fuel economy. The remainder of this report describes these activities in more detail.

Conversion to multi-pulse common rail fuel injection

TECAT has previously developed a fuel Injection Management System (TIMS) for use with high pressure common rail diesel injection systems. A key feature of this system is its ability to deliver multi-pulse injection events during an engine cycle to rate shape in-cylinder heat release and to reduce cylinder-out emissions. The system provides independent control of multiple injection events to each cylinder. This is useful for balancing cylinder performance as slight variations in injector/cylinder construction and air delivery may result in cylinder to cylinder variations. The system is also capable of supplying an initial amplified voltage to each injector ('overdrive') to improve needle opening response. This significantly enhances the fuel spray pattern at the onset of injection and provides for better control of injected fuel quantity. A LabView interface communicates command signals to the TIMS controller to provide schedule information such as number of injection pulses, pulse timing, pulse duration, and rail pressure setpoint.

TECAT has developed an enhanced version of TIMS for use with the LIM engine.

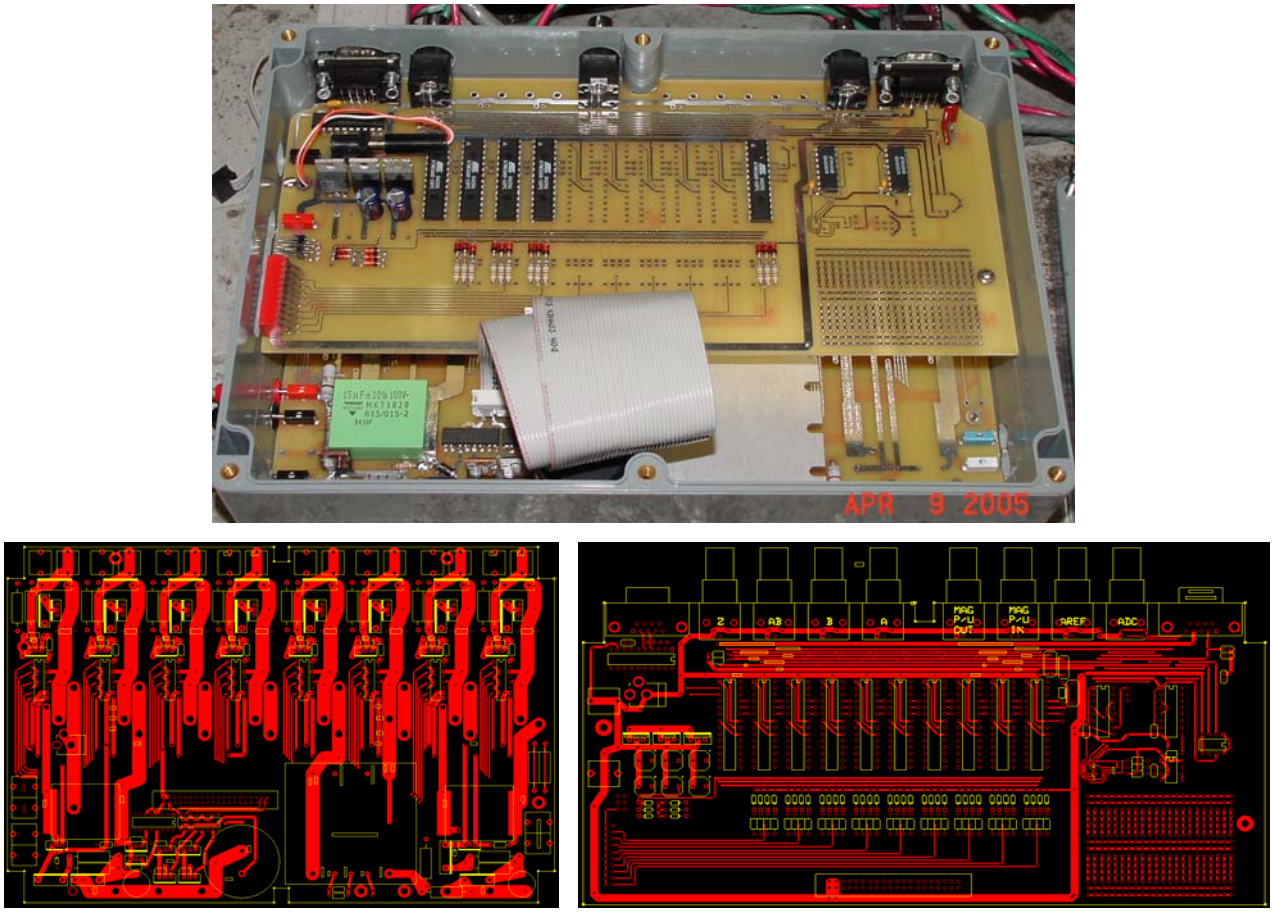

Figure 1 – Improved multi-pulse fuel injection management system. **Bottom:** New printed circuit board design. **Top:** Actual injection management hardware used for engine testing.

The new printed circuit board design, shown in Fig. 1, is currently populated with three injection controllers, one for each cylinder, a communications controller, and a rail pressure controller. The key enhancements of the new design included optical isolation between the microprocessors and the high voltage/current injector driver. This step has eliminated the potential for electrical noise to propagate from the injector driver back to the injection controller. Additionally, the hardware used to communicate with the host PC was upgraded for improved noise rejection and faster communication speeds. Finally, the ability of the system to receive different types of signals from the rail pressure sensor was improved. The system can now utilize ground referenced voltage signals, floating differential voltage signals, as well as current source transducers.

The injector driver design was also improved in several key areas. The new design can now actuate up to eight injectors where it could previously only control two injectors while utilizing the same size printed circuit board. The new design also reduces component count and, thus, cost. This significantly improved response time of the driver as well. Finally, the new system was given the ability to control a valve spring tensioning motor to dynamically adjust valve opening and closing events.

Figure 2 illustrates the Labview interface used to communicate with the TIMS controller during dynamometer testing. With the current interface, up to 8 injection pulses can be specified for each of 3 injectors. Pulse duration and timing can be independently specified for each injector; alternatively, all can be adjusted simultaneously by the same quantity. An overdrive voltage can be commanded for any pulse supplied to any injector. Valve spring tension and rail pressure setpoint can be electronically adjusted from the interface as well.

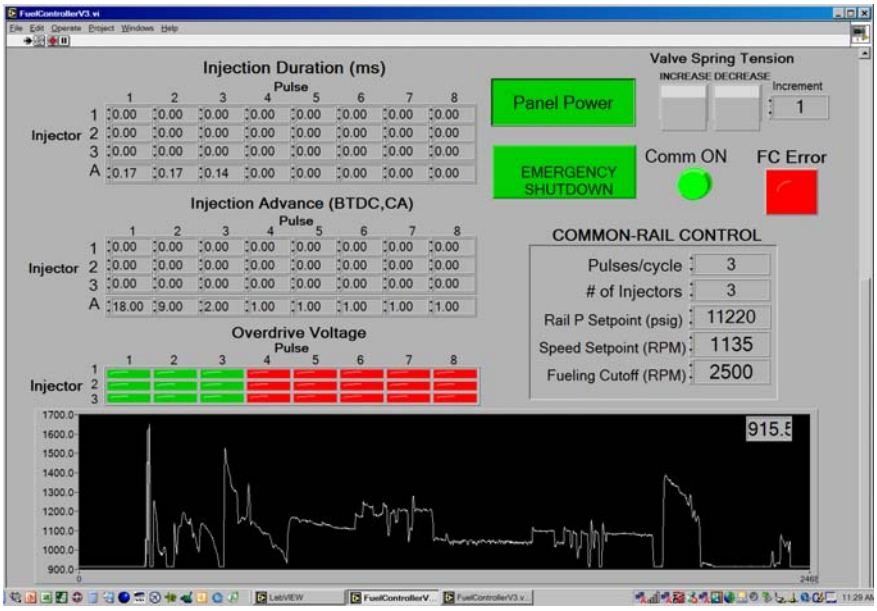

Figure 2 – Labview interface used to command the TIMS fuel controller during dynamometer testing

Preliminary testing of LIM 353

With the TIMS fuel controller installed, the LIM 353 engine was prepared for initial testing (see Fig. 3) at the McLaren Engines facility which is located adjacent to TECAT. The use of a dynamometer was not required for the initial testing period as the goal was simply to achieve smooth engine idling using the new controller. Before running the engine, an impedance test on the injectors revealed that one of the injector transducers was shorted, and thus, needed replaced.

Figure 3 – LIM 353 engine set up in test cell. Dynamometer not used for initial idle testing.

Prior to running, the injection management system was calibrated as shown in Fig. 4. Injector processor clocks were synchronized to assure that the commanded pulse duration for each injector matched the actual delivered injector signal, as illustrated in the figure. The injector phasing was also verified to assure correct injection timings for each cylinder. The engine was then run to assure proper operation of all mechanical and electronic systems. A video of this operation was recorded.

Several minor problems were noted during the initial run. Intake runner volume was insufficient to minimize intake manifold pressure fluctuations. Thus, cylinder charge delivery was limited. Additionally, the intake runner for cylinder #1 had a significant leak. These problems were alleviated through a design modification in which an intake plenum replaced the intake runners. It was also discovered during initial testing that the exhaust manifold did not seat properly on the block (see Fig. 5). This problem was alleviated by machining the exhaust manifold for a proper fit. Additionally, a gasket was fabricated by McLaren to improve sealing of the manifold. An additional point of concern was due to a moderate oil leak into the exhaust ports. As the piston rings began to seat with extended run time, the leak improved, however, it was noted that a known insufficiency in how the exhaust ports clamped onto the cylinder sleeve was the primary cause of the leak. This was an accepted consequence of the low budget prototype that can be easily corrected with a new block casting. Other minor concerns included a high pressure rail port which had been previously capped using a non-functional injector. This port was properly sealed off. Engagement of the starter gear to the flywheel was also improved by machining the starter gear.

Once idle operation of the LIM353 with the TIMS system was achieved, the engine was equipped with low speed instrumentation and set up in a dynamometer test cell as shown in Fig. 6. Low speed instrumentation for this test session included exhaust gas temperatures for each cylinder on each side of the engine, torque, speed, coolant temperature, oil temperature, fueling rate, and manifold absolute pressure. A Tektronix digital oscilloscope was utilized to monitor and record high speed injection signals. Note

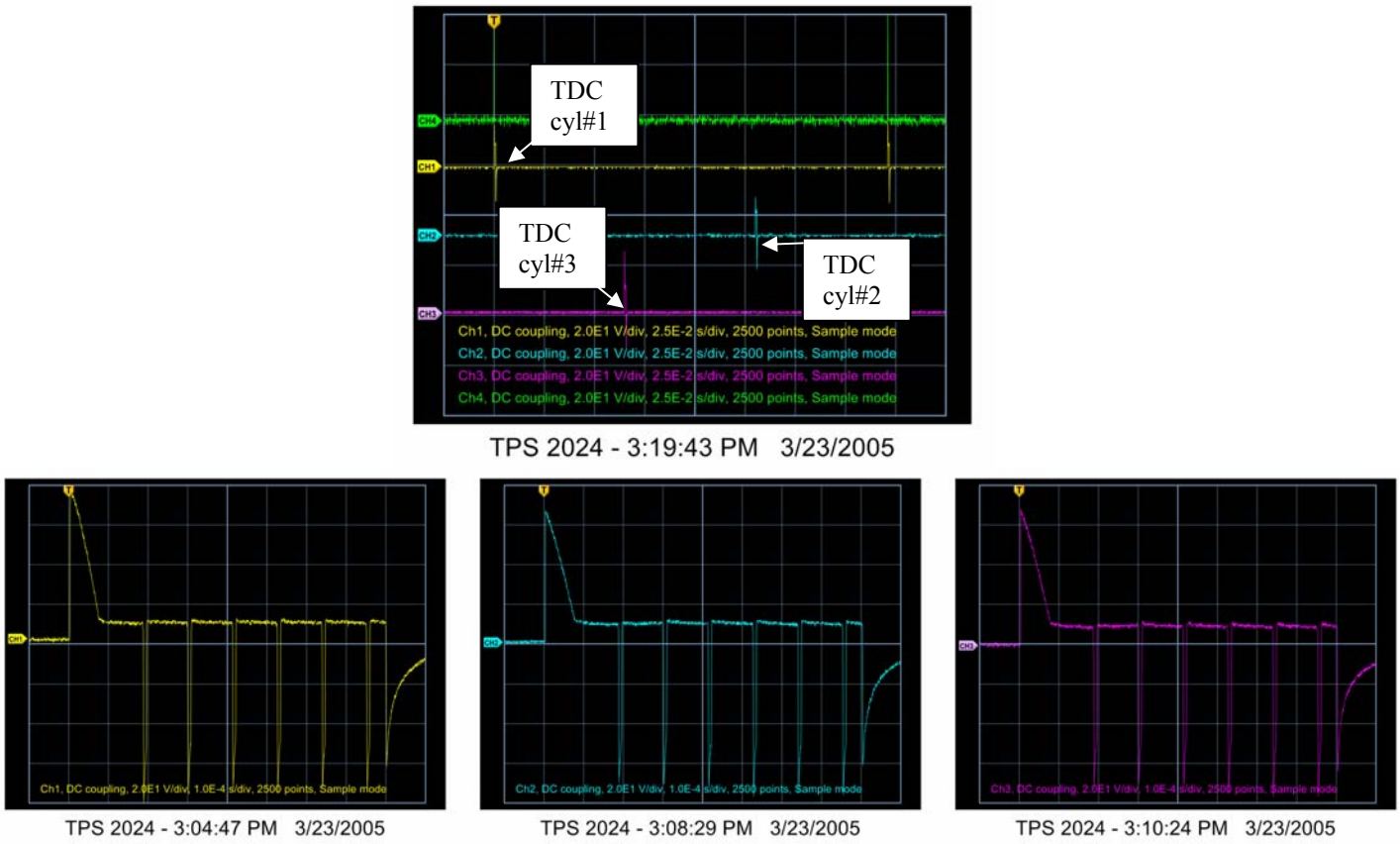

Figure 4 – Top: Verification of injector phasing with respect to reference TDC pulse. **Bottom:** Calibration of injection durations to 0.8ms for each of three injectors.

that the intake plenum design change was not yet implemented for this test session. The small intake runner volume continued to limit engine performance.

Prior to the next testing session, the intake runners were replaced with a plenum box on top of the head as shown in Figure 7. The plenum box has a Plexiglas top to observe valve motion. The box volume was sized to reduce cycle pressure swings within the intake manifold as a result of cylinder scavenging. Large manifold pressure swings cause significant losses in the blower which in turn results in undesirable heating of the compressed manifold air. Instrumentation for the next test session was also improved to include the signal from the rail pressure transducer. This allowed for observation and calibration of the pressure transducer so that closed loop pressure control could be achieved. Additional high speed and low speed data were recorded similar to the previous test session. However, a failure in the dyno speed sensor prevented loading of the engine during this testing session.

High-speed instrumentation

The third phase of testing focused on obtaining data appropriate for characterizing valve behavior. Since LIM valve motion is controlled by the instantaneous pressure differential across the valve, cylinder #3 was instrumented with high speed in-cylinder and manifold pressure transducers, as well as valve motion sensors on two of the four intake valves.

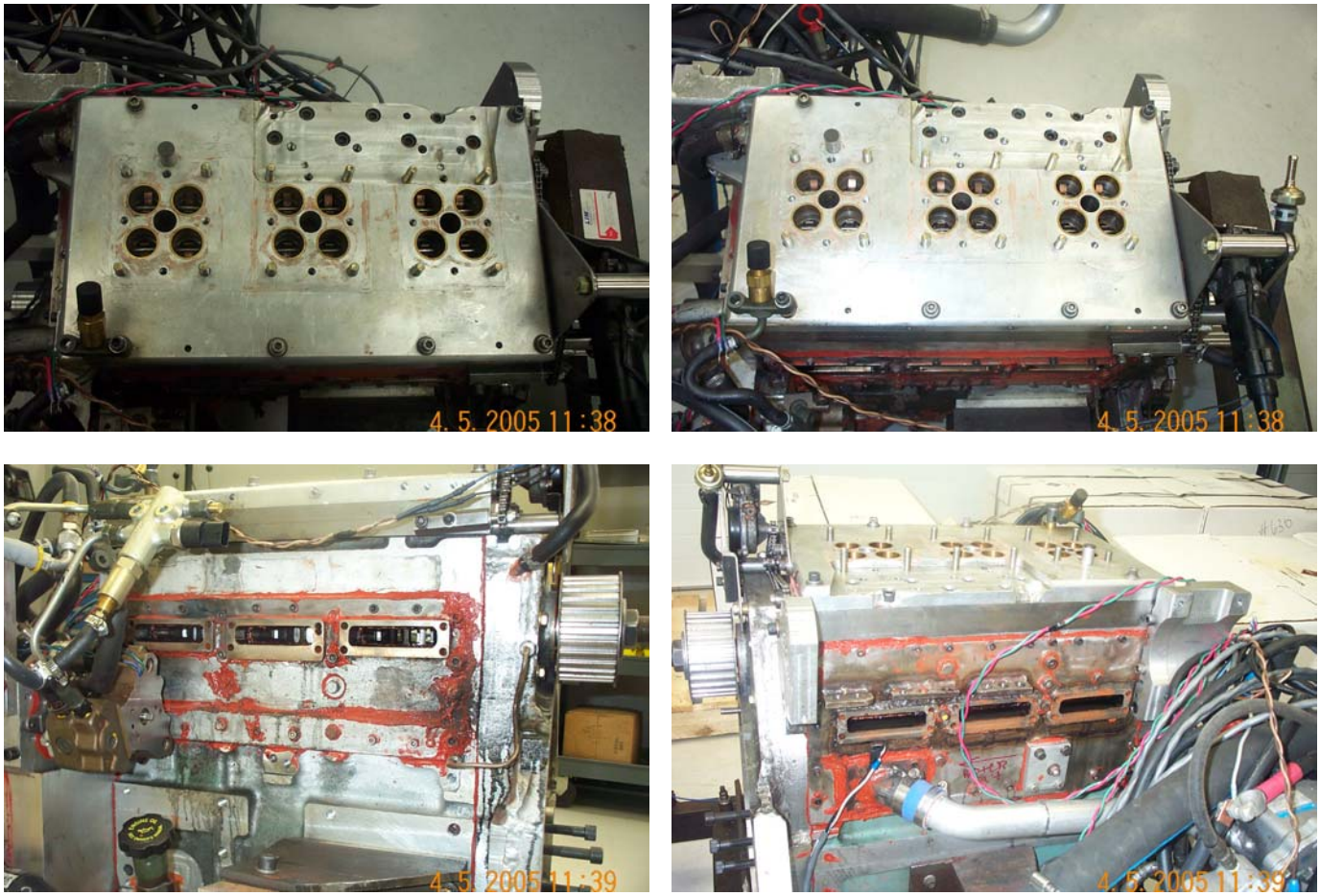

Figure 5 – Teardown of the test engine to improve leaking intake runners and exhaust manifold.

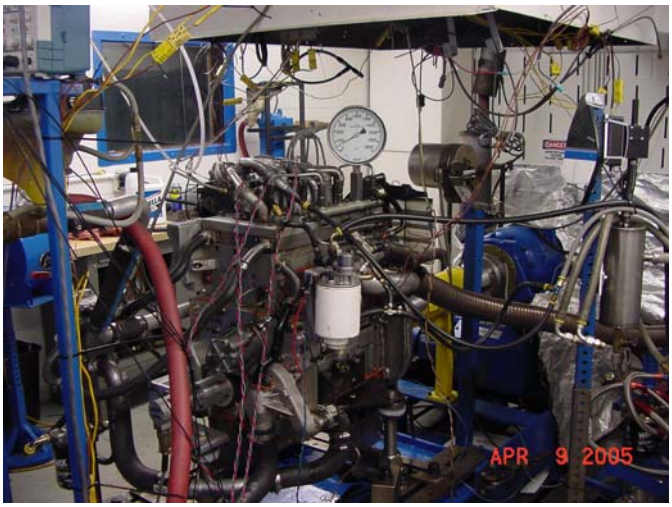

Figure 6 – Instrumentation of test engine including dynamometer.

Figure 7 – New Intake Plenum with side-mounted blower.

In-cylinder pressure measurements from cylinder #3 were obtained using a Kistler type 6053bb miniature piezo-electric measuring probe, as illustrated in Figure 8. A Kistler charge amplifier converted charge sensed at the piezo-electric crystal into an amplified voltage. This probe is particularly suitable for direct installation in small-capacity combustion engines with more than 2 valves per cylinder.

Features include:

- Good temperature stability of the sensor
- Acceleration-compensated
- Needs only 6 mm mounting bore
- Low thermal shock error and long life
- Very high sensitivity

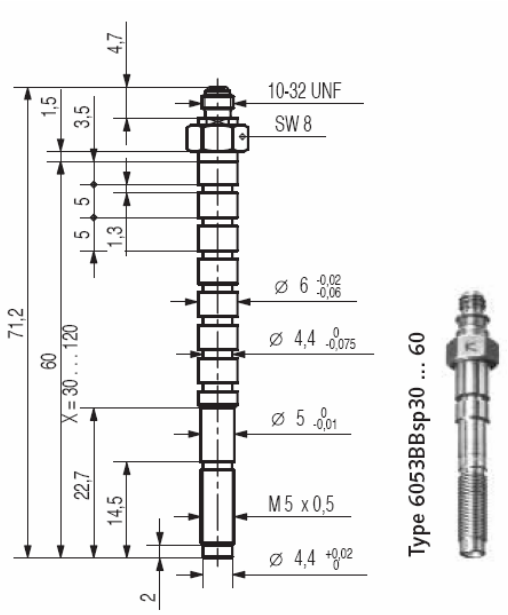

Figure 8 – High speed piezo-electric in-cylinder pressure transducer with passive cooling

Type 6053BB uses a new type of piezoelectric crystal with an achievable sensitivity of –20 pC/bar.

Instantaneous intake plenum pressures were measured using a high speed PCB piezo-resistive pressure transducer and voltage amplifier. The piezo-resistive transducer also provides a reference pressure for the in-cylinder pressure data, as piezo-electric devices only sense relative changes in pressure. The sensor was placed close to the intake valves on cylinder #3.

Capturing valve motion presented unique challenges. One option was to use a high speed laser interferometer which counts fringes produced by the laser in order to track valve position. In addition to the high cost of the laser system, installation of the laser sensor would be difficult at best. The laser system requires a good surface to reflect on and a clear view of the moving valve. Additionally, oil splash would normally present a problem for this kind of measurement.

A second researched option was the use of a Linear Variable Displacement Transducer, or LVDT, shown in Fig. 9. Of particular concern was the frequency response of the system as well as the amount of mass which would be added to the valve. The sensor is composed of two parts including an outer case which has a transducer coil and lead wires as well as an inner core which slides in and out of the outer case. The outer case is mounted in a fixed position with respect to the head, while the inner core is attached to the valve. The core position is detected by measuring the coil's differential reluctance, using a sine wave excitation and synchronous demodulator. This differential detection method provides a very sensitive measure of the core position, while canceling out temperature effects. The output of the demodulation device produces one volt per three millimeters of travel and has a 7 kHz frequency response. The core mass is negligible at only 25 milligrams. Therefore, the LVDT sensor was selected for measuring valve position.

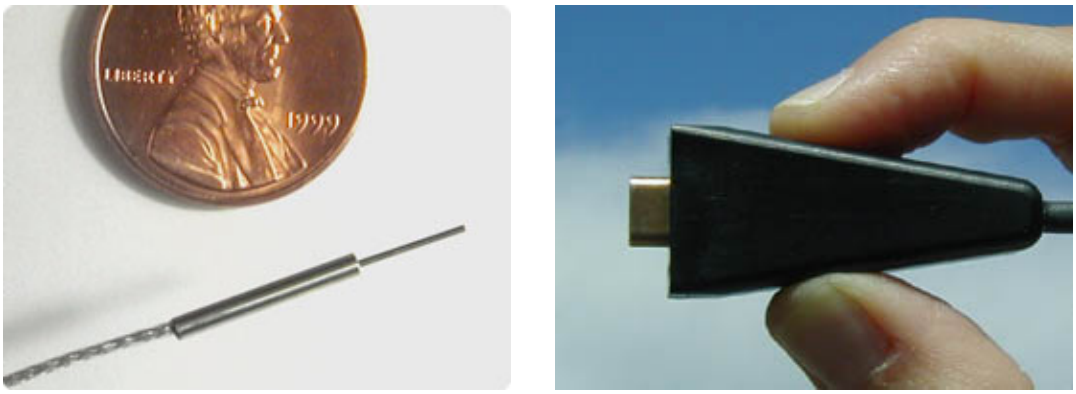

Figure 9 – Illustration of high speed LVDT used for valve motion measurement. **Left:** LVDT sensor. **Right:** Signal conditioning unit.

Figure 10 illustrates high speed raw voltages captured on the digital oscilloscope. Channel 1 (yellow trace) is the #3 in-cylinder pressure signal as a function of time over a complete engine cycle and shows the rise in pressure due to compression and combustion. Channel 2 (blue) is the intake manifold pressure signal. Note that there are three dips in manifold pressure over an engine cycle as a result of air delivery to each of the three cylinders. Channel 3 (purple) is the voltage signal delivered to the #3 injector. This trace illustrates a two pulse injection near top dead center with overdrive voltages used at the start of each injection to accelerate needle opening.

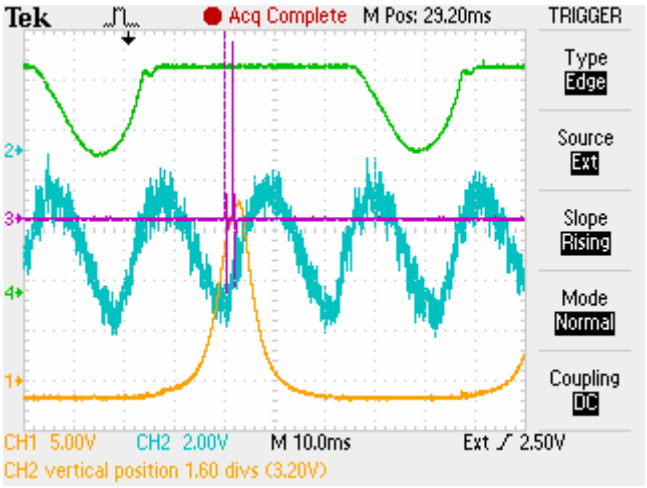

Figure 10 – High speed data capture utilizing a Tektronix TPS 2024 oscilloscope. **Yellow:** In-cylinder pressure. **Blue:** Manifold pressure. **Purple:** Injector signal. **Green:** Valve motion.

Channel 4 (green) illustrates the high speed valve motion signal from one of the #3 cylinder intake valves. The flat portions of this signal indicate that the valve is closed, while the curved portions demonstrate valve motion. A higher spring force was used in

this particular test, thus, the valve does not fully open and has much lower opening and closing velocities compared to other tests in which the spring force is reduced.

High speed voltage signals are converted to correct units using calibrated curve fits for each sensor. For in-cylinder and manifold pressure measurements, calibration charts supplied from the manufacturer were used. For LVDT measurement of valve motion, calibration charts were generated from static measurements of known position. The valves were moved in .02" increments and sensor voltages were recorded and curve fit as illustrated in Figure 11.

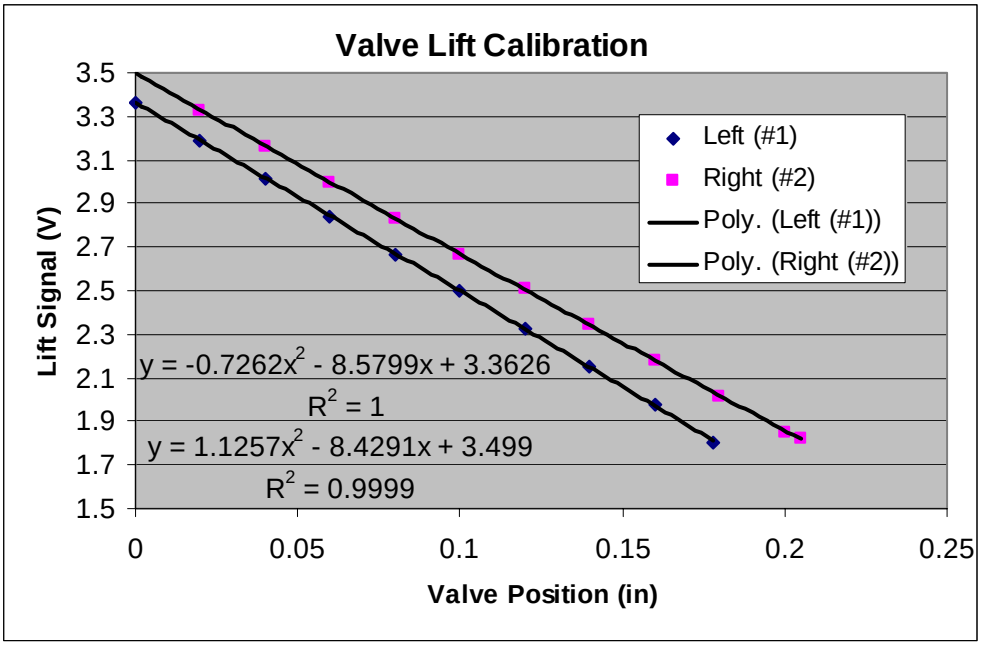

Figure 11 – Calibration curves for LVDT sensors used to measure valve positions

Low speed performance results

Six sets of low speed data runs are illustrated in Figures 12-17. Each data set includes power, torque, exhaust temps, fuel rail pressure, fueling rate, bsfc, engine speed, and boost pressure as a function of time. Boost is also plotted as a function of engine speed to indicate supercharger performance. Note in data sets D & E that boost pressure is constant with engine speed. The supercharger was deactivated during these two runs and shop air was instead supplied to the intake manifold to operate the valves and scavenge the cylinders. The data sets have points of interest indicated by vertical lines passing through a particular instance in time. A reference time stamp is indicated by each vertical line. These points of interest are identified as supplements to the following discussions.

In Figure 12, the plot of boost pressure vs. engine speed shows boost increasing with engine speed along a continuous performance curve. The blower boost has a sudden characteristic change at around 1100 rpm, however, as it increase from below 20"Hg (10psi) to over 24" Hg (12psi). This rapid rise in manifold boost occurs as the valves in

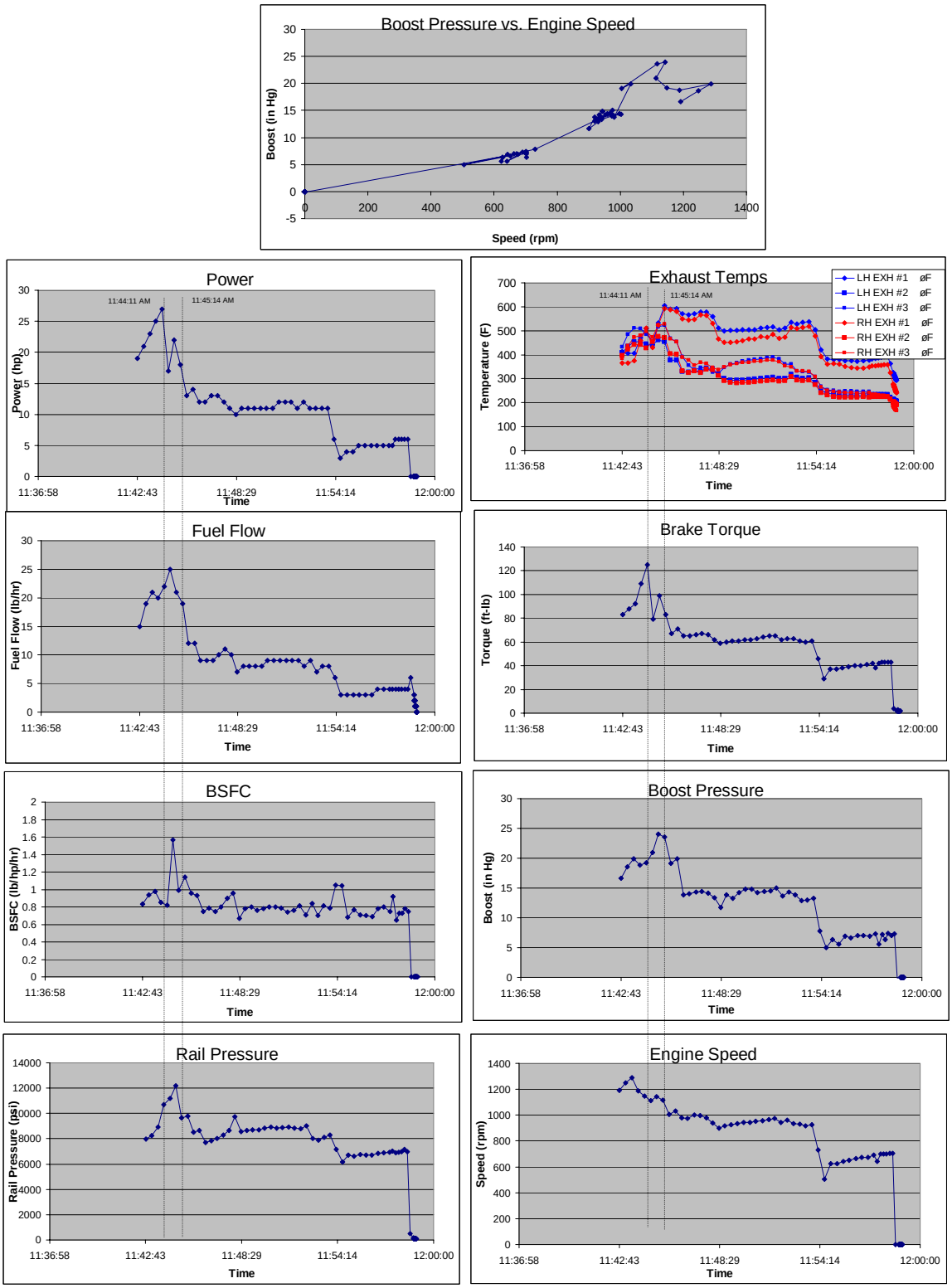

Figure 12 Set A: 08/04/05 11:58AM – Low speed data from LIM 353 test run

the #1 cylinder begin to stick closed. It was noted throughout the testing that inadequate valve operation in cylinders 1 & 3 resulted in erratic cylinder scavenging as the valves within these cylinders would intermittently stick. This was evident by observing two key indicators: 1) exhaust gas temperatures (EGT) and 2) high speed manifold pressures. Upon examination of the sticking valves, it was noted that a defect in the workmanship in

the valve seat construction caused the valve sticking and that the issue was not an inherent flaw to the valve system.

Note from the EGT plot in Fig. 12 that at around 11:45:00, cylinder #1 exhaust gas temperatures significantly diverge from the other cylinders and remain higher throughout the rest of the test session. At around 11:48:00, cylinder #3 exhibits similar behavior, however, by 11:54:00, the #3 EGT again closely tracks #2 EGT. The large discrepancy between the #1 and #2 cylinder EGT's compared to the #3 and #2 cylinder EGT's indicate that #1 cylinder valves are excessively restricting flow.

This is further demonstrated by observing swings in intake manifold pressure. Consider the two time stamps (i.e.-vertical lines) illustrated on the EGT plot of Fig. 12 at times of 11:44:11 and 11:45:14. Corresponding manifold pressures at these two instances are shown in Fig. 13. This plot shows data over two engine cycles.

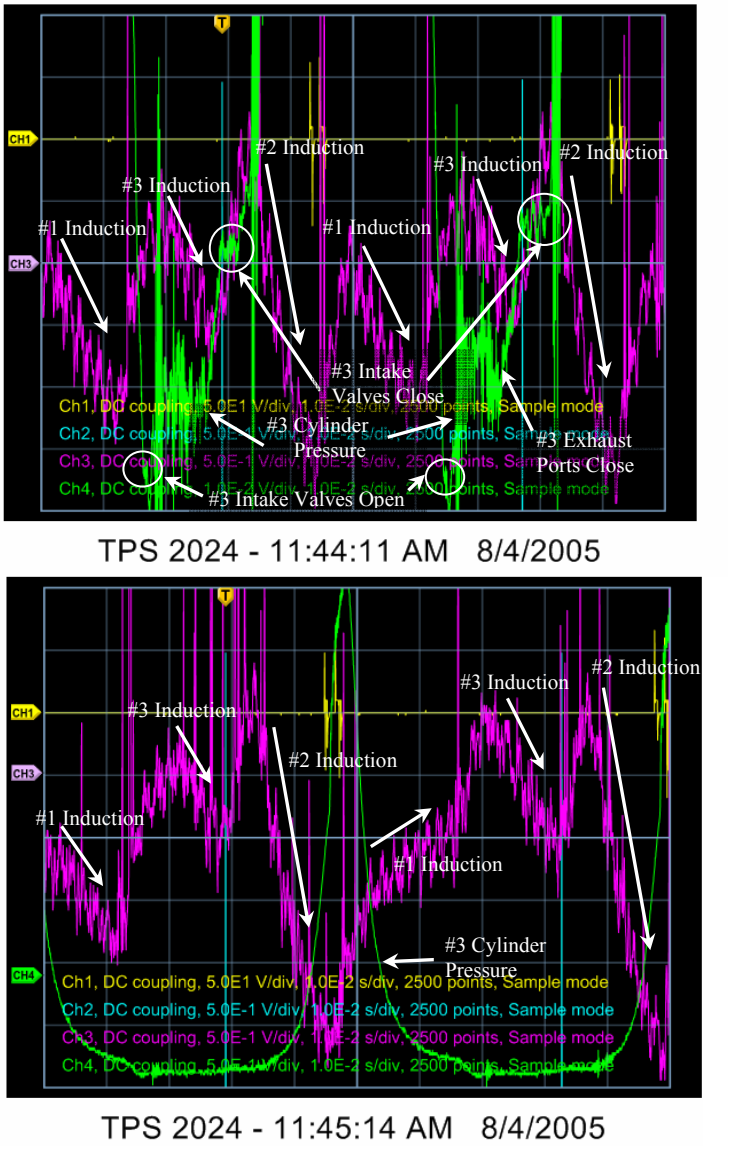

Figure 13 Instantaneous manifold pressure signal (purple), #3 cylinder pressure signal (green) and #3 injector voltage signal (yellow) at timestamps of 11:44:11 (top) and 11:45:14 (bottom).

Note the change in slope of the manifold pressure as fresh charge is delivered to each of the three cylinders. Cylinder #2 exhibits the best breathing characteristics as indicated by the largest drop in manifold pressure, followed by cylinder #3 and finally #1. Note from the zoom shot of the cylinder pressure trace (Fig.13-top) that specific port opening and closing event timings are evident. Intake valve opening occurs shortly after the cylinder blowdown pressure drops below the intake manifold pressure. The cylinder pressure recovers but remains near exhaust manifold pressures until the exhaust ports close, at which point, the cylinder pressure rapidly rises to the intake manifold pressure. Cylinder pressure subsequently tracks the intake manifold pressure until the intake valves close, and then rapidly rises due to piston compression.

One minute later at approximately the same engine speed and fueling rate, engine behavior became unstable as the #1 cylinder intake valves appeared to restrict flow (see Fig.13-bottom). Note from the figure that as manifold pressure recovers from the #2 cylinder induction, only a slight change in the manifold pressure slope is observed when the #1 valves open. The #1 cylinder flow restriction is so severe that the intake manifold inflow from the supercharger exceeds the manifold outflow to the #1 cylinder, thus, intake manifold pressure actually continues to rise during the #1 cylinder delivery event. The #3 cylinder appears to have degraded delivery as well, as indicated by the reduced downward slope of manifold pressure during its fresh charge delivery event. There is also a notable change in EGT of the #3 cylinder relative to the #2 behavior.

There are several possible reasons for the reduced lift of the #1 and #3 cylinders. Some valves may be getting stuck in the seat due to inadequate specifications for the seat angles. Alternatively, the valve body may be binding in the port due to the clearance tolerance. It was noted during one of the engine teardowns that some of the #1 and #3 intake valves appeared to stick when manually opened by hand. This indicates that a tolerancing issue was most likely the cause of poor #1 and #3 cylinder breathing performance.

Fig. 14 illustrates a second set of low speed data taken on the same day. Note from this data set that an output torque of nearly 150ft-lb was reached at an engine speed of ~1100 rpm. The injection pressure at this point was ~11,000 psi and boost was ~8 psi. Shortly after this high torque point, the #1 cylinder began to exhibit poor performance as indicated by EGT, thus rail pressure (i.e.- fueling rate) was reduced. Each subsequent attempt at increasing brake torque resulted in a significant jump in the #1 cylinder EGT and reduction in cylinder delivery as indicated by the manifold pressure trace. Note that the engine was idled as low as 600 rpm at one point in this test session.

Fig. 15 shows high speed data associated with the timestamps of Fig. 14 at 2:47:07 and 2:52:11. The first time stamp is at peak boost pressure and fueling rate. The high speed data shows a single pulse injection event with a 1.2ms duration and with an overdrive voltage applied at the beginning of injection to assist needle opening. Note that the majority of fuel is delivered before combustion actually starts. This permits a significant amount of fuel vapor to form and to pre-mix with fresh air, thus, when combustion begins, there is a rapid consumption of the pre-mixed charge resulting in a rapid increase in cylinder pressure. The detonation of pre-mixed charge creates a pressure wave that resonates within the combustion chamber as it bounces between the head face and piston. Note that the resonant frequency increases since the sound speed in the media increases proportional to the root of the combustion temperatures. This high frequency ‘noise’ creates a noticeable dieseling sound.

Later in the low speed testing session, cylinder #1 intake valve flow restrictions are again evident as an increase in #1 EGT suggests a decrease in fresh charge delivery. In addition, the manifold pressure is minimally affected by the #1 cylinder delivery event. Note, however, that the #3 cylinder intake valves appear to be operating well, as EGT’s track well with the #2 cylinder, and the manifold pressure drop during the #3 delivery event is similar to the drop during the #2 cylinder delivery event. The #3 cylinder delivery event occurs at higher manifold pressures, however, since the previous cylinder (#1) permitted minimal air delivery from the intake manifold.

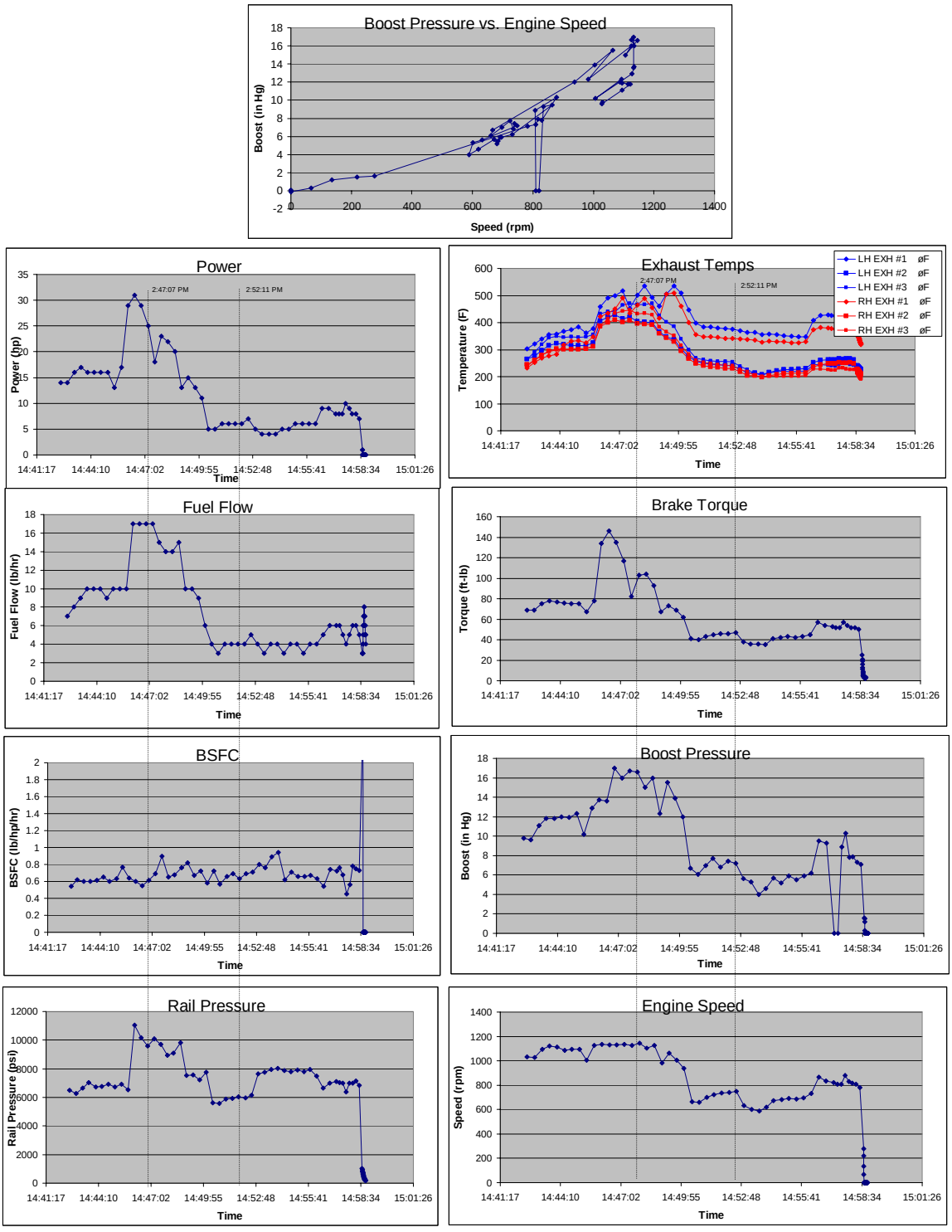

Figure 14 Set B: 08/04/05 2:58PM – Low speed data from LIM353 with max brake torque of 150ft-lb @1100rpm

Fig. 16 exhibits a low brake specific fuel consumption (BSFC) of 0.4lb/hp/hr at an engine speed of around 1000rpm, a boost pressure of ~5psi, and an injection pressure of 7000psi. As engine speed is increased to 1200rpm at a boost of 7.5psi and injection pressure of around 12,000psi, the BSFC increases to ~0.6lb/hp/hr. BSFC significantly increases as EGT's indicate a problem with valve operation. As valve performance of cylinders #1 and #3 improve near the end of the test run, BSFC again drops as torque and power increase. At the end of the test set, note the abrupt drop in intake manifold boost pressure as a result of a blower gear failure.

The next two test sessions were performed without the blower attached. Shop air was attached to the intake manifold to provide positive pressure for intake valve operation and cylinder scavenging. The boost pressure remains relatively constant with engine speed at around 2psi as seen in Figs. 17-18.

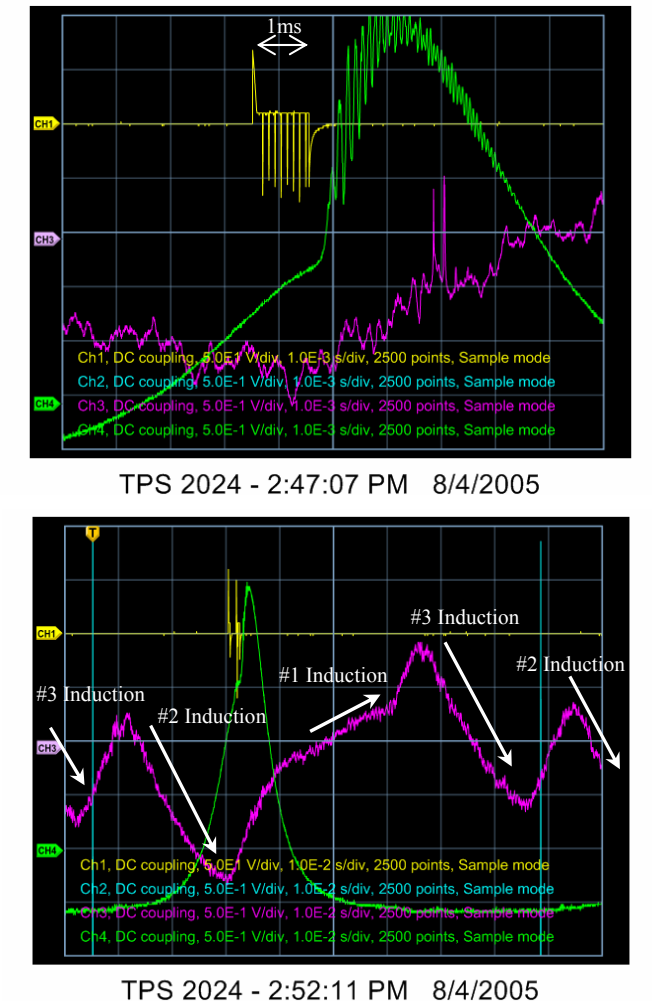

Figure 15 Instantaneous manifold pressure signal (purple), #3 cylinder pressure signal (green) and #3 injector voltage signal (yellow) at timestamps of 2:47:07 (top) and 2:52:11 (bottom).

Fig. 17 illustrates a smooth low speed operation under light load (~5hp @ 700rpm) with a BSFC of ~0.45lb/hp/hr. Valve performance is relatively consistent for all cylinders with a slight restriction noted in cylinder #1 based on irregular swings in intake manifold pressure. Only the left hand side of cylinder #1 EGT demonstrates a problem with valve operation.

Fig. 18 has an interesting operating point late in the testing period. The shop air supply was removed from the intake manifold to test the engines' ability to idle with no forced air assist. The engine ran with no forced air assist at an idle of around 180rpm. The manifold pressure was recorded at nearly 1psi of vacuum indicating that the manifold inlet was creating a flow restriction. Fuel rail pressure was ~10,000psi. Valve spring tension was reduced to maintain idle, however, the low tension resulted in significant reverse flow of burned gases back into the intake manifold. Thus, this operating condition was not maintained for an extended period of time.

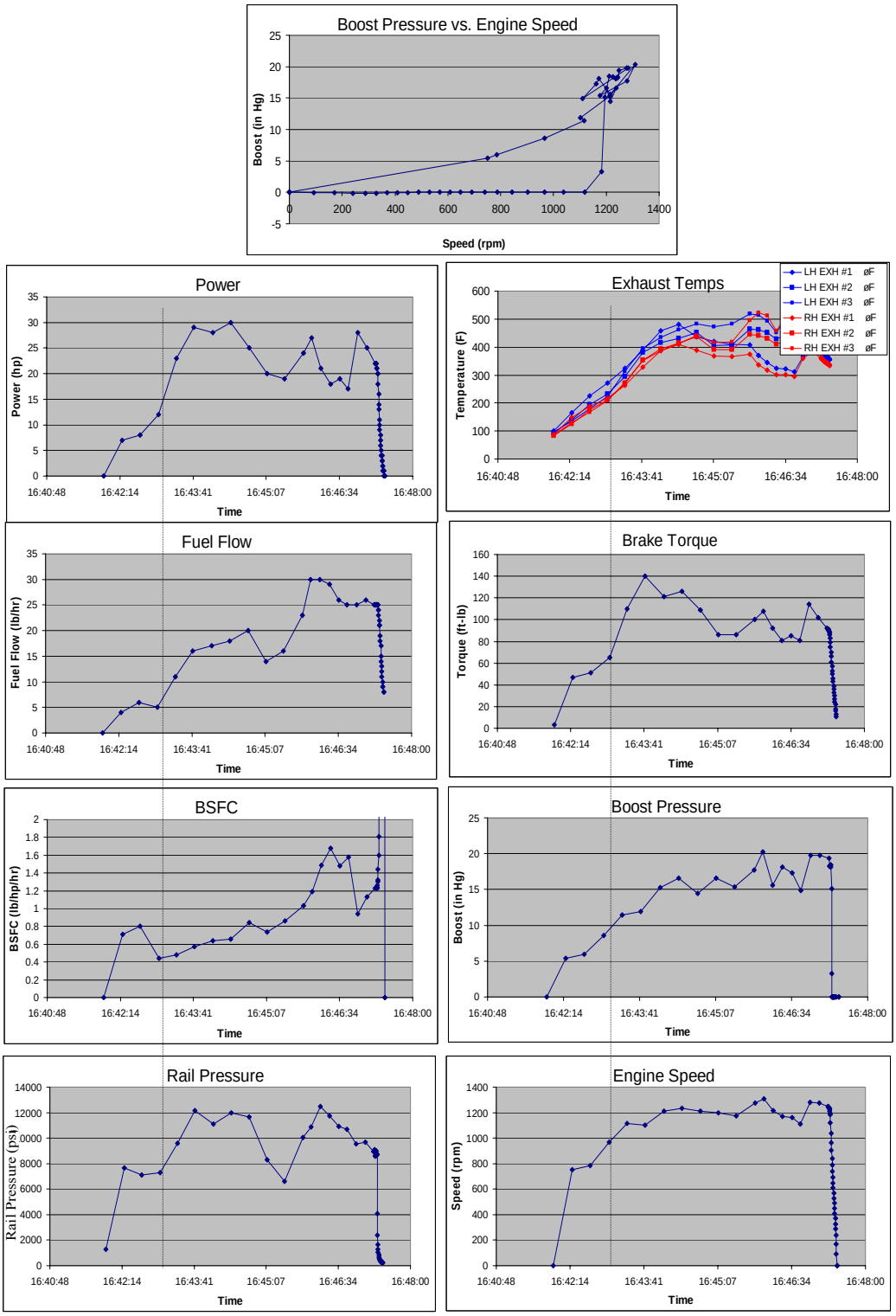

Figure 16 Set C: 08/04/05 4:47 PM – Low speed data from LIM353 illustrating minimal BSFC of 0.4lb/hp/hr @ 1000 rpm.

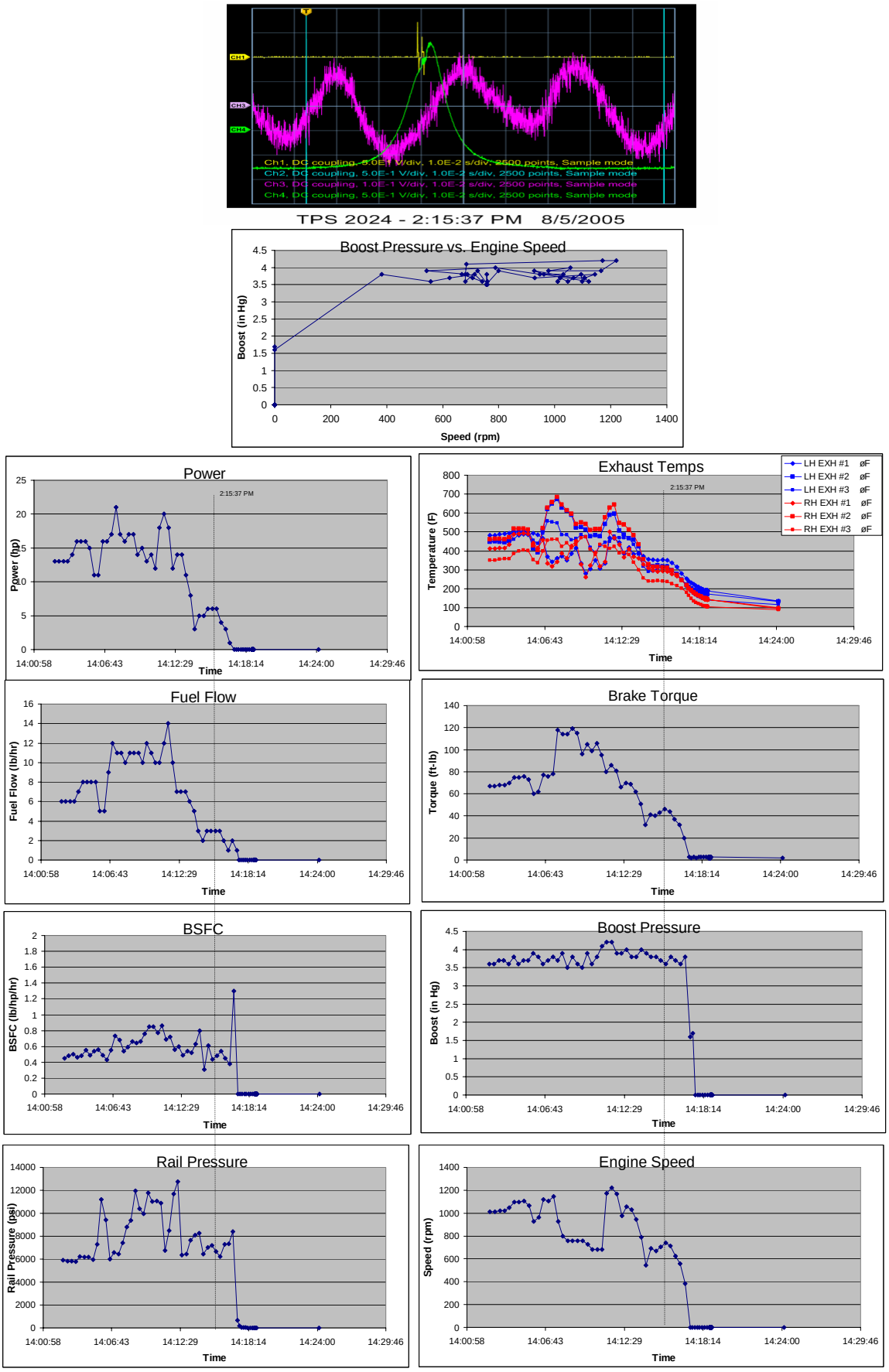

Figure 17 Set D: 08/05/05 2:24 PM – smooth low speed (~700 rpm) operation under moderate loading (100ft-lb & 40ft-lb)

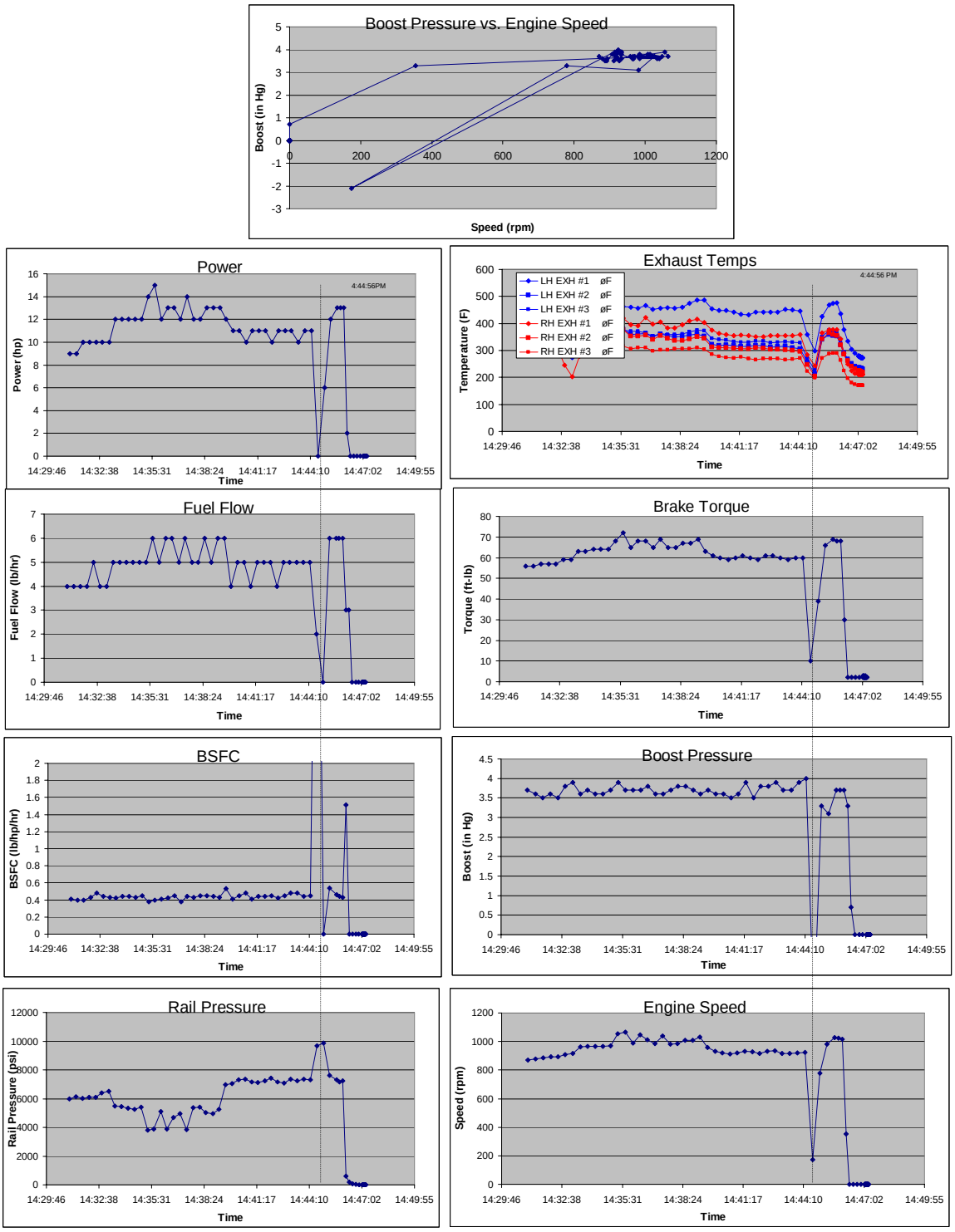

Figure 18 Set E: 08/05/05 2:47 PM – idle speed of 180 rpm achieved with a fueling rate of less than 1pph

As previously discussed, the supercharger failed at the end of the low speed test session illustrated in Fig. 16 due to a failure of a nylon coupler within the gear case. The nylon coupler was replaced with a brass coupler and the supercharger was reassembled. Fig. 19 illustrates another set of low speed data after the supercharger has been re-installed which again indicates a problem with the #1 and #3 cylinder EGT's. The timestamp indicates a point at which high speed in-cylinder data was recorded. The high speed data was taken at a brake torque of ~85ft-lb, 1100rpm, and injection pressure of ~10,000psi. High speed data is discussed in more detail in the following section.

High speed performance results

Three sets of high speed data are illustrated in Figs. 20-22. Raw data collected on the digital scope are shown at the top of each plot and include a manifold pressure signal, an in-cylinder pressure signal, and valve lift signals. High speed manifold pressure signals are converted to pressures using the transducer gain and offset. High speed in-cylinder pressure signals are reduced into pressure-volume diagrams to determine indicated work performed on the piston. Instantaneous volume is calculated from the crank-slider equation using bore, stroke, connecting rod length, and compression ratio. Piezo-electric transducers generate floating signals, thus the in-cylinder pressure is referenced to the manifold pressure at intake valve closing event. Gain for the in-cylinder pressure transducer is obtained from the transducer calibration sheet.

A plot of the isentropic ratio of specific heats (i.e.- constant pressure specific heat / constant volume specific heat), or gamma, is used to assure that all referencing, gains, and offsets are properly assigned. Unburned fresh charge during an isentropic compression should have a gamma of ~1.4 while burned gases during isentropic expansion should have a gamma of ~1.2-1.3. As gamma stabilizes towards these values, the gas process is nearly isentropic indicating that no induction, exhaust and/or heat release is occurring. Thus, the gamma plot becomes a good indication of when ports open and close, and when combustion initiates and completes. The log-log plot of pressure vs. volume is another key indicator of when ports open and close and when combustion commences. The constant slope periods during compression and expansion represent near isentropic behavior with the slope of the line defined by gamma. Curvature near TDC is an indication of heat release.

Another graph shows pressure vs. crank angle plotted against an isentropic compression / expansion curve to illustrate the start of heat release and subsequent increase in pressure due to combustion. Another plot shows the reference point at which cylinder pressure is matched to the manifold pressure. Finally, Fig. 21 and Fig. 22 also include high speed valve lift data. The curve fits of Fig. 11 were used to reduce the raw voltage signals to valve lift curves.

These three high speed data sets represent a light load, medium load, and high load condition. The area within the pressure volume diagram (on a linear scale) equals the indicated work done on the piston. Table 1 compares the indicated power (i.e.- indicated work x engine speed x number of cylinders), brake power (measured at the dyno) and friction power (= indicated power – brake power).

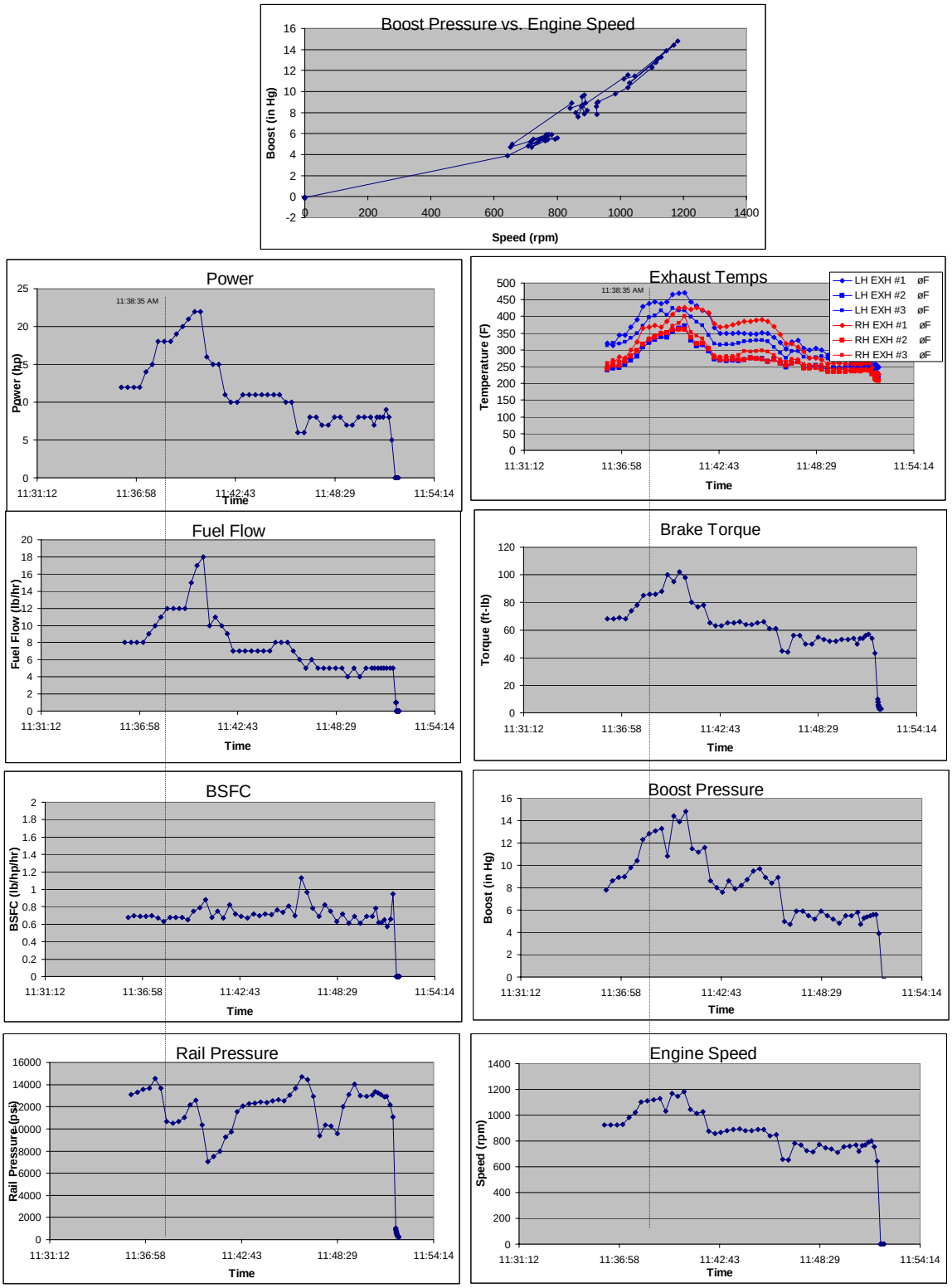

Figure 19 Set F: 08/31/05 11:52 AM – low speed data set with corresponding high speed set (Fig. 21 - HS2) taken near peak torque.

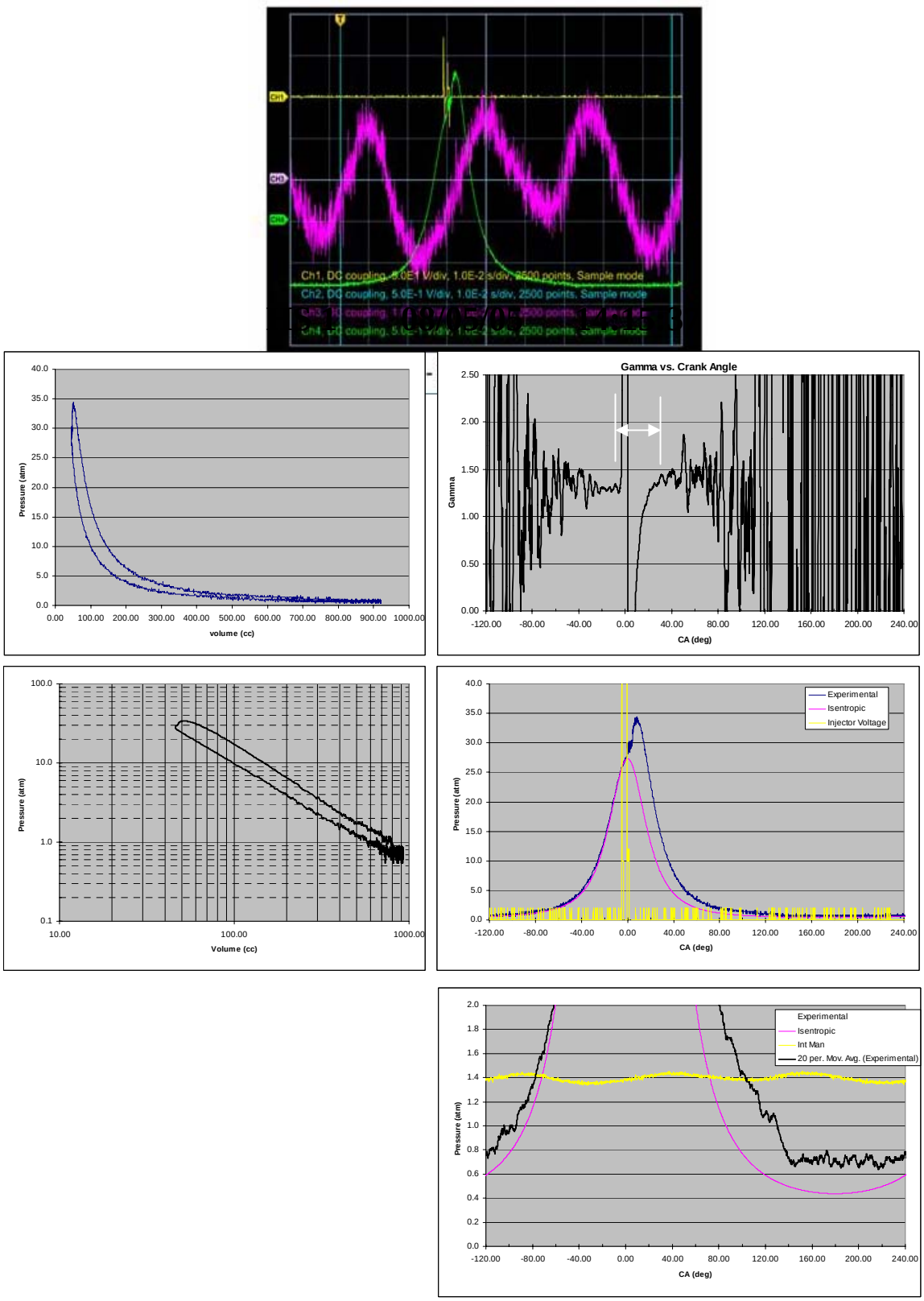

Figure 20 HS 1: 08/05/05 2:15:37 PM – Raw high speed data (top) and reduced indicated performance diagrams (bottom).

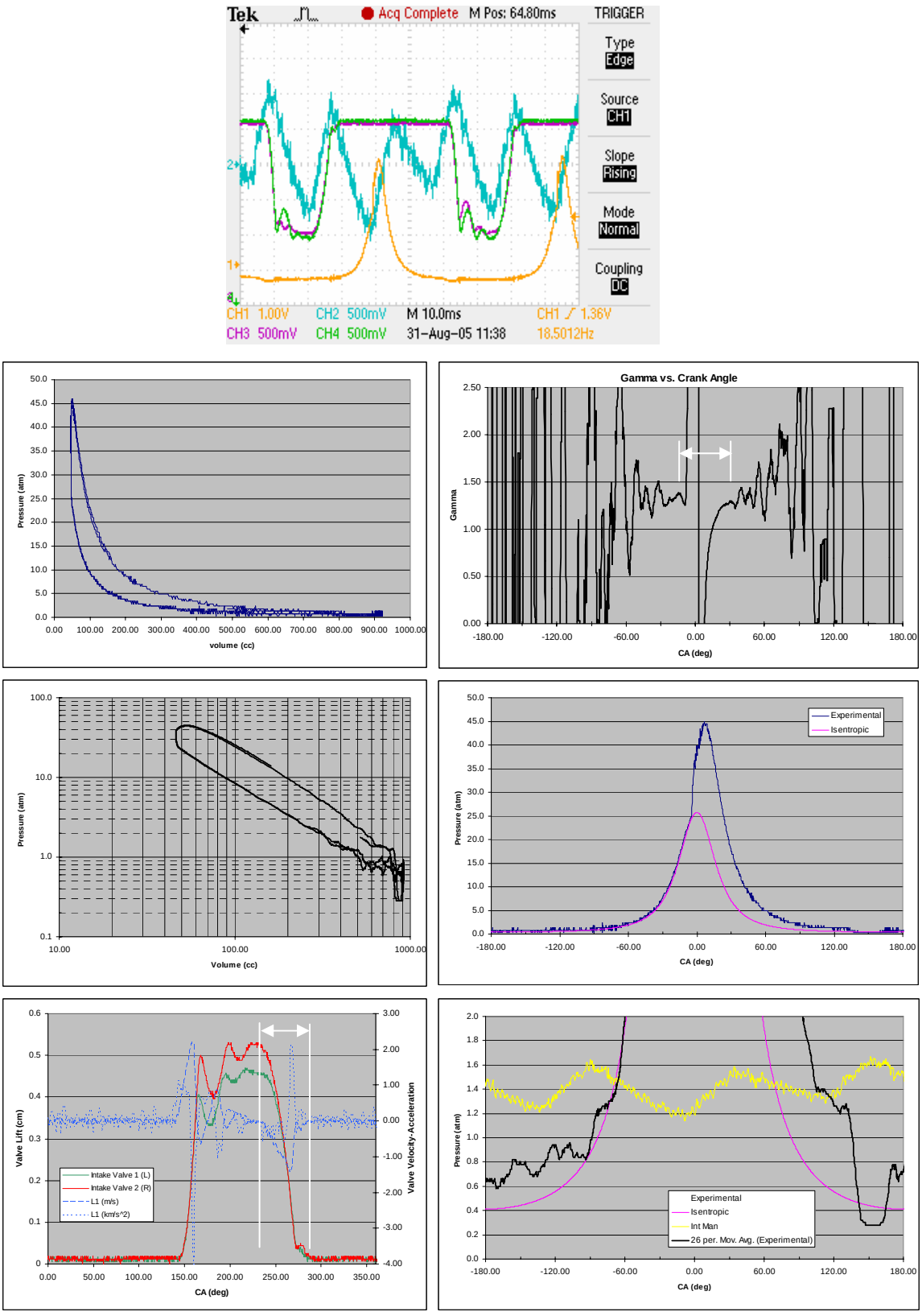

Figure 21 HS 2: 08/31/05 11:38:35 AM– Raw high speed data (top) and reduced indicated performance diagrams (bottom).

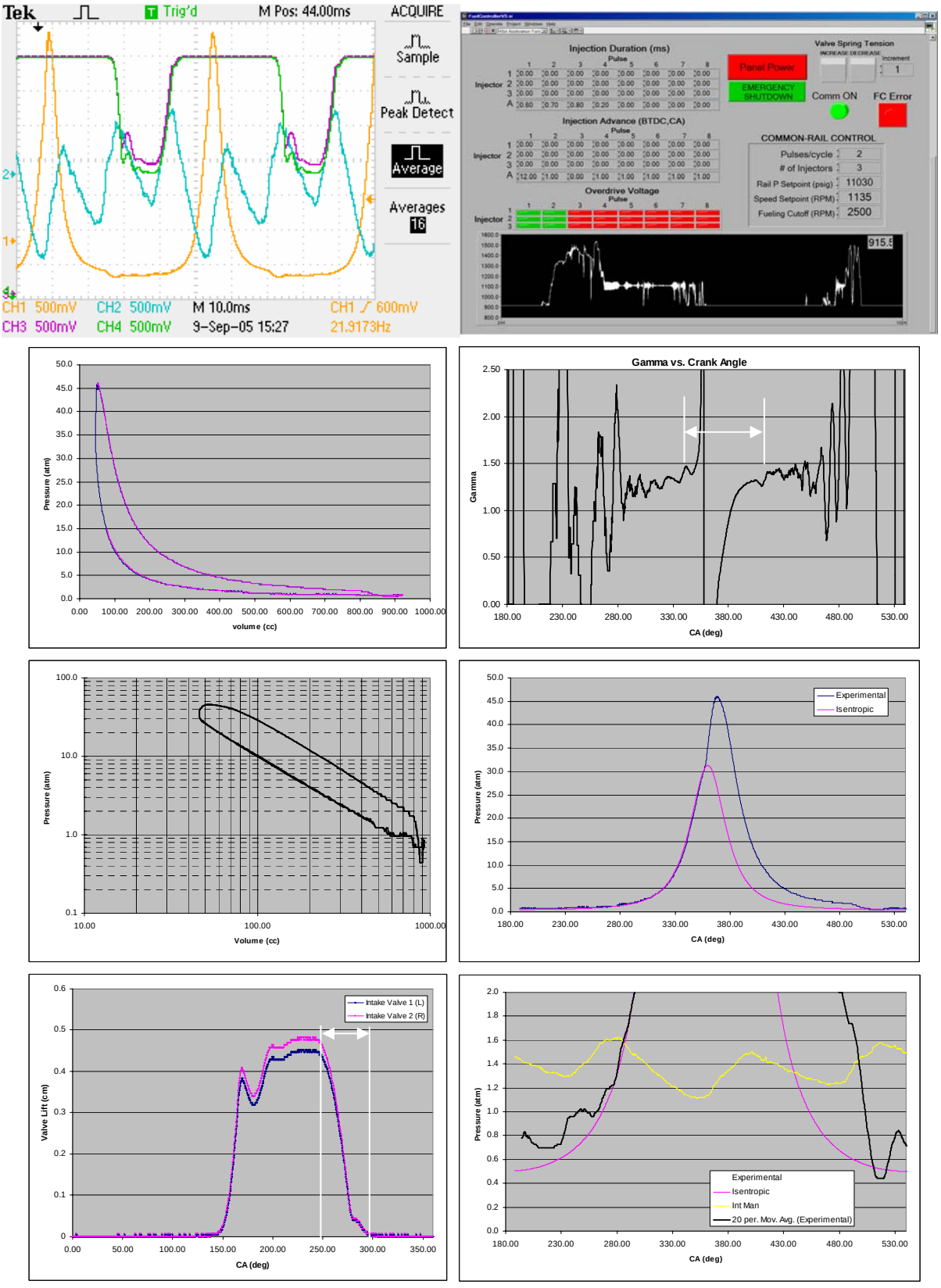

Figure 22 HS 3: 09/09/05 3:27PM– Raw high speed data (top) and reduced indicated performance diagrams (bottom).

Note that the friction horsepower is exceptionally low in all three cases, particularly in light of that fact that these three conditions are all at relatively low engine speeds. Frictional horsepower includes horsepower required to drive the supercharger, common rail high pressure fuel pump, oil pump and water pump. Indicated horsepower calculations assume that cylinders #1 and #2 behave the same as the high speed pressure data taken from the #3 cylinder.

Table 1 – Indicated, brake and friction horsepower under light, medium and high load

	Indicated Hp	Brake Hp	Friction Hp
HS1-light load @710rpm	6.6	6.0	0.6 (10%)
HS2-med load @1110rpm	20.1	18.0	2.1 (10%)
HS3-high load @1315rpm	34.3	30.0	4.3 (12.5%)

It is interesting to note the combustion duration of Figs. 20-22 as indicated by the gamma vs. crank angle plot. Durations increase with increasing load from 35°ca, to 45°ca, to 55°ca. The pressure vs. volume diagrams indicate the corresponding rapid rise in cylinder pressure near TDC. Near BDC on the logP-logV plot of each high speed data set, a rapid gas exchange process occurs as blowdown pressures rapidly recover to intake manifold pressures. However, as load and speed increase, note the extended period of time that the cylinder pressure remains at the intake manifold pressure prior to the start of compression. Inadequate spring tension slows the intake valve closing timing which reduces the effective compression ratio and thermal efficiency of the system.

Both medium and high load cases indicate a closing event duration of around 50°ca, however, the higher load, higher speed data indicate a delayed intake valve closing event by as much as 20°ca. Gas pressure forces acting on the valves are sufficient to completely open the valves to their maximum lift and cause bounce off of the lift stop as indicated by the reversed direction. The sensor frequency is limited to 7khz, thus, the high frequency bounce event is not fully captured in the data. In Fig. 21, a significant secondary bounce occurs at maximum lift. In both cases, a slight valve bounce at the valve seat is observed when the valve closes. Again, note that the high frequency bounce that occurs at valve closing is not fully captured by the sensor.

Fig. 23 illustrates good cycle-to-cycle repeatability of valve motion, cylinder pressure, and manifold pressure when spring tension is adjusted to assure that the valve reaches a controlled lift during its opening event. If the spring tension is to high, however, maximum valve lift is not reached, and due to the under damped nature of the oscillating valve spring system, pressure waves are generated in the intake manifold which affect cylinder breathing and cycle-to-cycle repeatability. Figure 24 illustrates an adequately tensioned valve response and an over tensioned valve response. Note that the adequately tensioned valve has a rapid valve opening event with a slight bounce at maximum lift, followed by a sustained period at maximum lift, and finally a slower closing event. Gas pressures on either side of the valve are more of a controlling force than the spring tension. With the over tensioned valve (Fig. 24 – right), maximum lift is never achieved and the opening duration takes longer that the closing duration, even though gas pressure forces across the valve are greatest when the valve opens. This

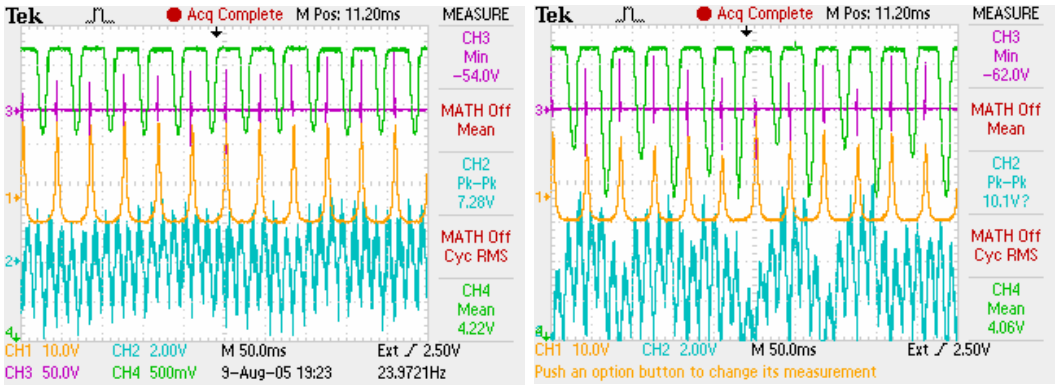

Figure 23 Cycle to cycle variation of valve lift (green), cylinder pressure (yellow) and manifold pressure with controlled valve lift operation (left) and random valve lift operation (right)

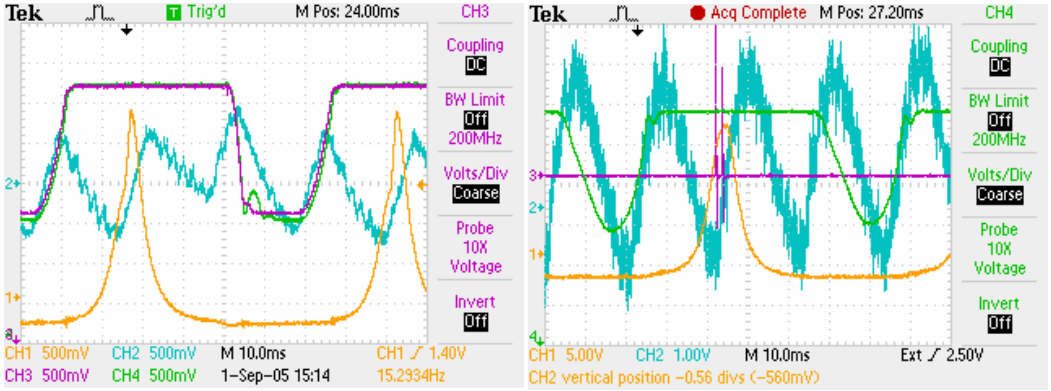

Figure 24 Valve lift behavior with light spring tension (left) and high spring tension (right).

suggests that the spring force is the dominant force controlling valve motion during this test.

The valves appear to be operating relatively well during each of these cases as indicated by the similar downward slopes in manifold pressures that result from each cylinders' scavenging process. The average manifold pressure fluctuates over time for the over tensioned valve, however, as the valve does not reach maximum lift and creates unstable control of delivered cylinder charge.

Figure 25 illustrates a transition from smooth valve behavior to erratic behavior and shows its impact on manifold pressure. The first few pressure cycles in the intake manifold suggest that all cylinders are properly scavenging, as the downward slopes in manifold pressure indicate that each cylinder is depleting a similar quantity of fresh charge from the intake manifold. One of the valves in cylinder #3 (purple) then exhibits a reduced lift which changes the downward slope of the intake manifold pressure. The next two cylinder inductions appear to continue depleting manifold mass longer than expected as a downward slope in pressure is evident for an extended period of time. This may suggest that the spring tension is too low which allows the valves to leak, or that something else is preventing proper closure. Subsequent cylinder delivery events exhibit odd behavior as the delivery cycles appear to double in frequency. This is most likely

due to excessive bounce at maximum lift resulting from low spring tension which causes an interruption in delivered charge. Observe the last valve lift trace in the figure which illustrates a significant bounce after reaching the initial peak lift. A secondary increase in manifold pressure as a result of the closing valve generates the forces necessary to accelerate the valve open again.

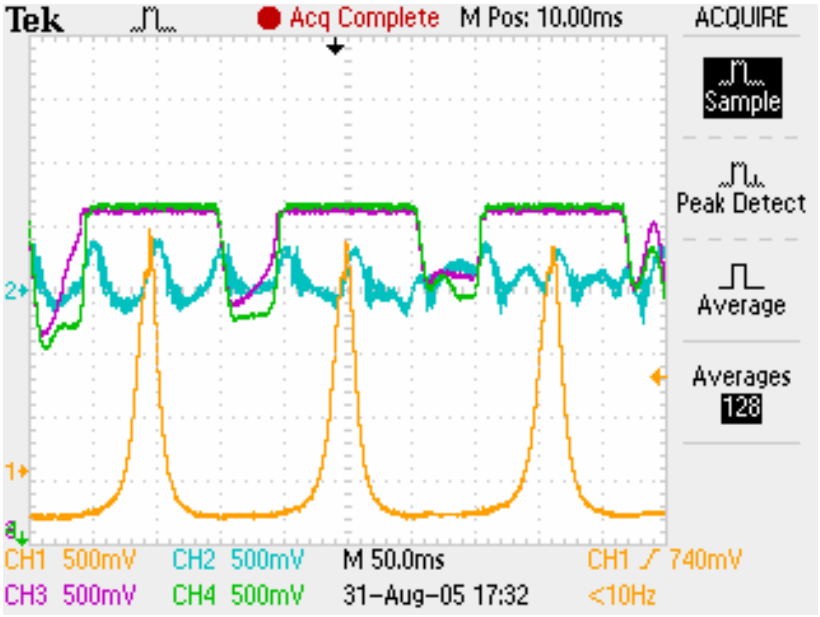

Figure 25 Effect of manifold pressure fluctuations (blue) on valve response (green & purple) and cylinder pressure (yellow)

Figure 26 illustrates the multi-pulse fuel delivery capabilities of the LIM common rail injection system, and its impact on the rate of change of cylinder pressure. The left column of plots represent a 3-pulse injection strategy with fixed durations, but altered injection timings. An overdrive voltage (~80V) is supplied to the injector for a short duration at the start of each injection pulse in order to facilitate needle opening. The high voltage decreases the time required to excite the electromagnetic transducer used to control the high pressure relief port on the back side of the needle. Thus, the needle opens sooner and with a higher opening velocity, which improves the quality of the delivered fuel spray and allows for short pulse durations.

In the first of these plots, a high frequency ripple is observed in the cylinder pressure trace and starts during the third injection pulse. As previously discussed in figure 15, a rapid heat release of pre-mixed charge creates a detonation pressure wave that resonates within the combustion chamber bouncing back and forth between the surfaces of the chamber. Detonation is a process of supersonic combustion that consists of a shock wave and a reaction zone behind it. The shock compresses the gaseous mixture, increasing the temperature to the point of ignition. The ignited material burns behind the shock and releases energy that supports the propagation of the shock across the chamber. This is undesirable from a noise and durability perspective.

In the next plot, the first and second pulse are slightly advanced creating an even larger quantity of pre-mixed charge, thus, an even stronger pre-mixed detonation occurs. In the third plot, the second and third pulses are retarded. This reduces the amount of

pre-mixed charge, thus, when auto-ignition occurs, the second and third pulse burn in a diffusion-controlled manner resulting in a smoother cylinder pressure rise. In the fourth plot, the third pulse is advanced closer to the second pulse. This reduces peak cylinder pressure as the third pulse injects into the burned gases of the second pulse, and is not delivered into a recirculation of fresh charge, as most likely occurs in the previous plot.

The second set of plots again illustrates a three pulse injection, however, overdrive voltages are not applied to each pulse. Pulse durations are maintained with adjustments made to injection timings. In the first of these plots, the pulses are equally spaced and advanced to produce peak torque. The second pulse timing is subsequently adjusted between the first and third pulse to again maximize torque. Unlike the pulses with overdrive, no sign of detonation is evident in these pressure traces. A slight retard in the

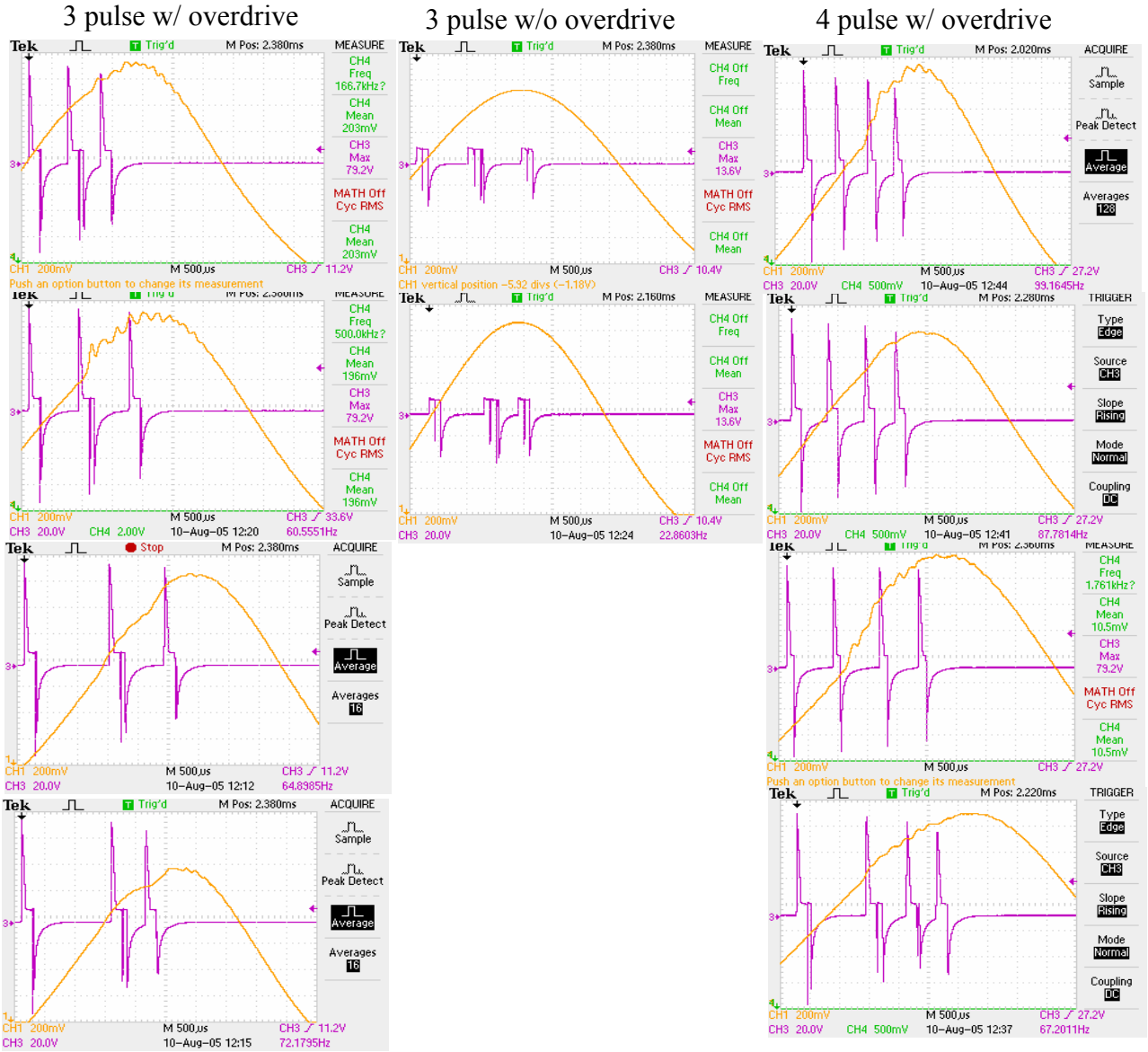

Figure 26 Effect of multi-pulse fuel delivery on rate of cylinder pressure rise.

second injection pulse increases overall heat release rate, most likely due to the overlap of needle opening between the second and third pulses which results in an increase in delivered fuel.

The third set of plots shows a four pulse injection strategy with an overdrive voltage applied to each pulse. The first three plots use equal spacing between pulses. Tight spacing used in the first plot results in a rapid pressure rise with signs of detonation evident in the pressure trace. As the pulses are slightly spread apart, the pressure rise is still rapid but does not appear to result in a detonation wave. When the pulses are again spaced further apart, a weak detonation wave appears to have occurred with a rapid pressure rise and extended burn duration. The final plot spaces to the two center pulses closer to the final pulse which weakens the detonation and reduces peak pressure while maintaining a longer burn duration. These plots illustrate the utility of the multi-pulse fuel injection system in rate shaping in-cylinder heat release.

Development of a Virtual LIM Engine SIMulation (LIMSIM)

To realize the full potential of the LIM valve technology, a comprehensive, quasi-dimensional virtual engine simulation has been developed. The first principles based system simulation models the various gas-exchange, combustion, heat transfer and frictional processes occurring throughout the LIM uniflow engine cycle. In addition, the LIM valve motion is predicted in real time based on design parameters and instantaneous operating conditions. Real turbomachinery hardware can be simulated to provide upstream boost and downstream exhaust recovery via supercharging, turbocharging and/or turbo-compounding. Experimental data taken at McLaren has been used to calibrate and validate preliminary numerical results.

The simulation was then used to assess the potential of the LIM gas cycle to reduce fuel consumption while achieving good power density. A parametric study was performed to evaluate the influence of port timing events and key engine design variables on performance and fuel economy and an improved design was achieved.

The LIM engine SIMulation, or LIMSIM, models the thermodynamic cycle of the uniflow LIM engine with passive valve control and can predict performance potential. LIMSIM predicts Mean Effective Pressure (MEP), torque vs. speed maps, volumetric and thermal efficiencies, indicated and brake engine power, cycle-resolved temperature and pressure histories of the working fluid, air and fuel mass flow rates, heat rejection rates from system components and brake specific fuel consumption.

The simulation includes the following components:

- piston and combustion chamber, induction and blowdown ports, intake and exhaust manifolds, turbo-machinery piping
- uniflow scavenging model
- port models which account for sonic flow and predict cycle-resolved Nusselt numbers for estimating wall heat loss
- variable injection timing and duration
- a combustion model for predicting pre-mixed and diffusion controlled rates of heat release
- appropriate heat transfer models to account for component to coolant heat losses

- appropriate frictional source terms to account for frictional heating which is removed by the cooling and lubricating fluids
- integrated turbomachinery model with electric assist capability
- LIM valves with passive valve control (i.e.- based on instantaneous delta-P)

Technical Description of LIMSIM

A modular format has been developed for building new engine simulations where sub-models of a cycle can be carried from an existing simulation to a new one. This commonalty of standard components allows for a more rapid build-up of new simulation programs, facilitates cross-checking of new simulation sub-models with previously tested simulations, and permits relatively easy upgrading or modification of sub-models as simulation goals change or more accurate sub-models become available. Our background expertise together with our existing base of engine component models were used to develop the system model for the LIM engine.

The parent code for LIMSIM is based on a turbocharged turbocompounded direct-injection Diesel Engine Simulation (DES) from the work of Heywood et al. at the Massachusetts Institute of Technology and Baker at the University of Illinois. In its current version, the diesel engine simulation models each component of the system as a quasi-steady, open system control volume containing a homogeneous ideal mixture of air and residual gas. A mass continuity and first law analysis of each component coupled with the equation of state form a set of non-linear differential equations which are simultaneously solved over each crank angle to give the instantaneous temperature, pressure, residual fuel fraction, and mean and turbulent kinetic energies within each system control volume. Mass flows across ports are modeled as quasi-steady, adiabatic, one-dimensional compressible flows. Experimentally measured discharge coefficients provide corrections to ideal mass flow equations. A transient heat conduction model, using the finite difference technique, predicts heat loss from manifolds, connecting pipes and combustion chamber walls. Convective boundary conditions are determined using available engine correlations based on turbulent flow in pipes and include models for nucleate boiling. Radiative boundary conditions based on the adiabatic flame temperature of the burned gas are used during combustion. Gas properties are calculated assuming ideal gas behavior. Chemical dissociation of the combustion products is considered at temperatures exceeding 1000K below which the products are considered to be an ideal mixture of non-reacting gases. A predicted ignition delay model, and an empirical correlation for two-phase heat release is incorporated into the combustion chamber.

The numerical development initially focused on reorganizing the solution algorithm to model a combustion chamber with LIM passive intake valves. The original DES treats the two-stroke diesel cycle as a sequence of continuous processes: induction, compression, combustion/expansion and exhaust. Equations assembled for each control volume were integrated during an engine cycle in sequence based on port and injection timings. In the LIM engine, however, intake port timings are variable and depend on local instantaneous boundary conditions. Thus, it is possible for these timings to occur before or after exhaust port timings and/or injection event timings. To handle this unique

characteristic of LIM valves, the solution technique no longer progresses between timelines of known event timings in order to determine the appropriate equation form, but rather determines the current cycle event by setting up root equations for all possible cycle events and then computing roots of the nonlinear equations $f_i(x)=0$, where $f_i(x)$ are continuous real functions derived from each cycle event. When any root is reached, all cycle events are tested to determine which event has occurred. Appropriate equations can subsequently be assembled once the event state is known. The root solution method uses a combination of bisection and the secant rule.

The LIM valve motion equation is constructed by first identifying the external forces acting on the valve and equating these to the body force. The external forces acting on the valve are illustrated in Fig. 27.

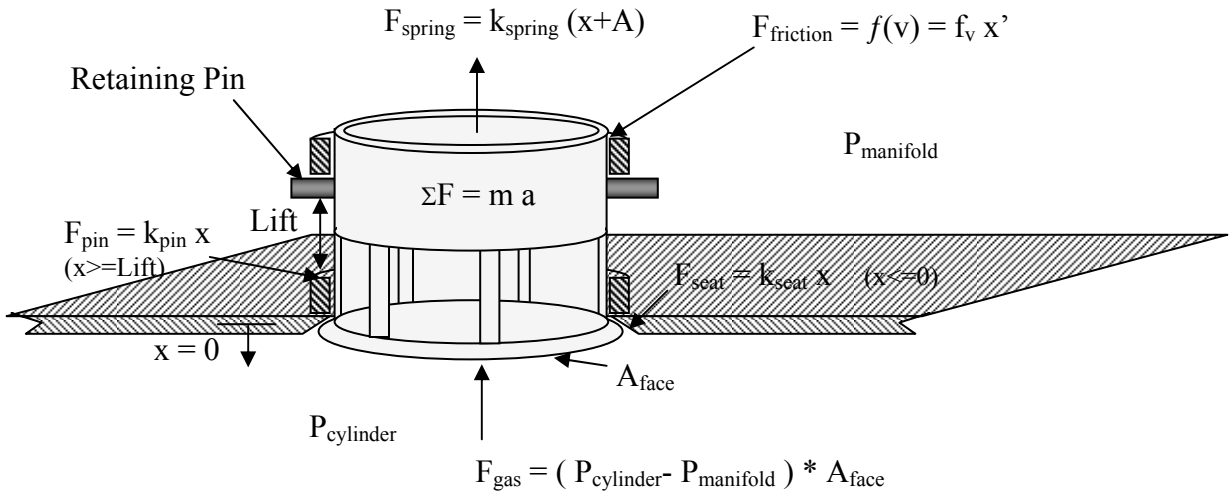

Figure 27 Forces acting on a LIM passive valve w/ spring

The equation of motion for the valve is given by

$$\sum F = m\,a \equiv m\,x''$$

Thus, from the forces identified in Fig. 27,

$$m\,x'' = (P_{man} - P_{cyl})\,A_{face} + k_{seat}x|_{x<=0} - k_{spg}\,(x+x_o) - f_v\,x' - k_{pin}\,x|_{x>=lift}$$

rearranging yields,

$$x'' + x'\,[f_v/m] + x\,[(k_{spg} + k_{pin}|_{x>=lift} - k_{seat}|_{x<=0})/m] = \{\,(P_{man} - P_{cyl})\,A_{face} - k_{spg}\,x_o\,\}\,/\,m$$

The resulting motion equation is of the form,

$$(D^2 + A\,D + B)\,x = C$$

Where $D = x'$, $D^2 = x''$, A, B and C are constant coefficients.

This equation is simultaneously solved, together with other differential equations describing the rest of the engine system, to predict instantaneous valve position, velocity and acceleration. As the valve reaches either the maximum lift or the valve seat, the equation becomes extremely stiff due to the high stiffness of the valve seat and retaining pin material. Thus, the solution time step is significantly reduced ($\Delta t <= 1.0e\text{-}9$ sec) during these events to accurately track stored energy that contributes to valve bounce.

Calibration of LIMSIM with Empirical Data

Calibration of the LIMSIM numerical model requires adjustment of coefficients for the Wiebe two-phase heat release model used for pre-mixed and diffusion controlled combustion, scaling of port discharge coefficients used to model port flow losses, adjustment of damping coefficients within the valve motion equation, and tuning of coefficients used within convective and radiative heat transfer correlations for modeling heat loss through various system surfaces.

Adjustment of coefficients for the Weibe heat release algebraic equation typically allows the model to be tailored for changes in induction turbulence, piston topologies, and injection pressures that usually vary from engine system to system. The coefficients are typically adjusted until pre-mixed and diffusion controlled heat release rates closely approximate those observed from empirical data.

Port flow discharge coefficients may need to be adjusted for irregular shaped exhaust ports to accurately assess flow separations which tend to reduce the effective flow area. Note that the actual flow area is changing with piston motion, thus, discharge coefficients are typically specified as a function of both pressure ratio across the port, and piston position relative to the top of the port. For conventional port shapes, discharge coefficient tables have previously been empirically determined and are available within the simulation. For poppet valves, discharge coefficient correlations are obtained from a General Motors publication for inflows and outflows through poppet valves of various valve, port, and seat dimensions.

LIM valve damping coefficients include terms for frictional losses between the valve body and valve port, and impact losses as the valve comes in contact with the retaining pin at full lift and the valve seat at closing. Coefficients are initially based on the material bulk modulus and adjusted to match the measured valve position for the same changes in cylinder and manifold pressures.

Heat release correlations typically only require adjustment if a unique cooling strategy is being implemented (i.e. - oil fin cooling). Current correlations model the impact of coolant passage dimensions, coolant flow rates, percent mixture of ethylene glycol and water, thermostat setpoint, and effects of local nucleate boiling.

Results from a calibrated simulation run performed at the operating conditions of high speed data set #2 (Fig. 21) are illustrated in Fig. 28. Good agreement is observed between actual and predicted in-cylinder pressures, manifold pressures, and valve motion. Similarly, actual and simulated performance and EGT's are well matched. Note in the figure that LIMSIM displays multiple graphs and numerical data while the virtual engine is running. Graphical information in Fig. 28 includes 1) the current supercharger operating line overlaid on its performance map, 2) logP vs. logV, 3) LIM valve lift, 4) velocity and 5) acceleration, 6) cylinder intake and exhaust mass flows, and 7) intake and

exhaust manifold pressures. Numerical data shown in the figure include system temperatures and pressures, cylinder and system performance, turbomachinery performance, operating conditions, and system configuration. Input design parameters and operating conditions can be changed while the virtual engine is running which provides instantaneous feedback on how these changes affect performance and fuel economy.

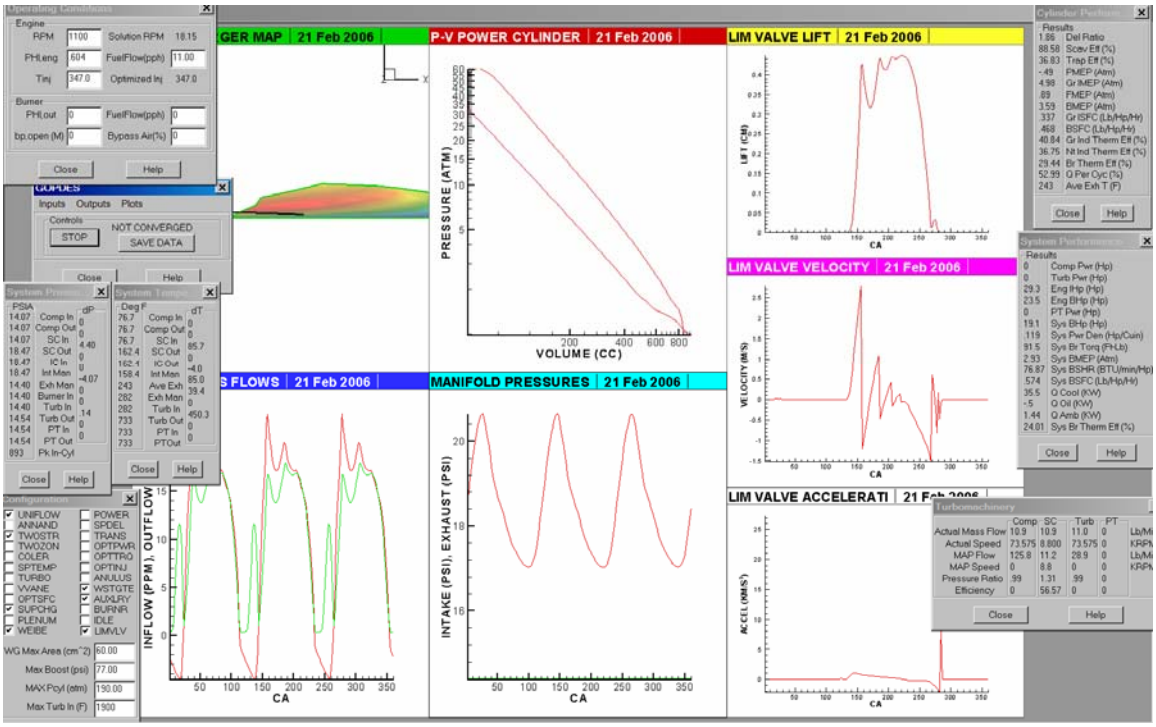

Figure 28 Results from calibration run (compare to Fig. 21)

LIM Engine Optimization: Improved LIM 353 spring and valve

Using the calibrated LIMSIM, the LIM353 prototype was simulated over a range of engine speeds and engine fueling rates (see Table 2). The simulated valve spring tension, pre-load, and maximum lift were optimized to improve performance compared to what was experimentally obtained from the baseline prototype. Predicted performance maps from LIMSIM are illustrated in Fig. 29 and Fig. 30. For fueling rates less than 20pph, only engine speeds below 1500 were simulated as insufficient power was generated to

Table 2 – Engine operating conditions simulated using LIMSIM

		Engine Speed (rpm)									
		1000	1200	1300	1400	1500	1600	1700	1800	2000	2200
Fueling Rate (pph)	10	x	x	x	x						
	20	x	x	x	x	x	x	x	x	x	x
	30			x	x	x	x	x	x	x	x
	35					x	x	x	x	x	x
	40						x	x	x	x	x
	45							x	x	x	x
	50								x	x	x
	55									x	x
	60										x

sustain greater speeds.

The equivalence ratio contour plot (Fig. 29 – top right) is used to define an operational region that is most likely to produce visible smoke in the exhaust stream. Equivalence ratio (ϕ) is defined as the actual fuel/air ratio divided by the stoichiometric fuel/air ratio. As engine fueling increases, available fresh charge within the cylinder is consumed and at some point, additional fueling significantly increases soot production.

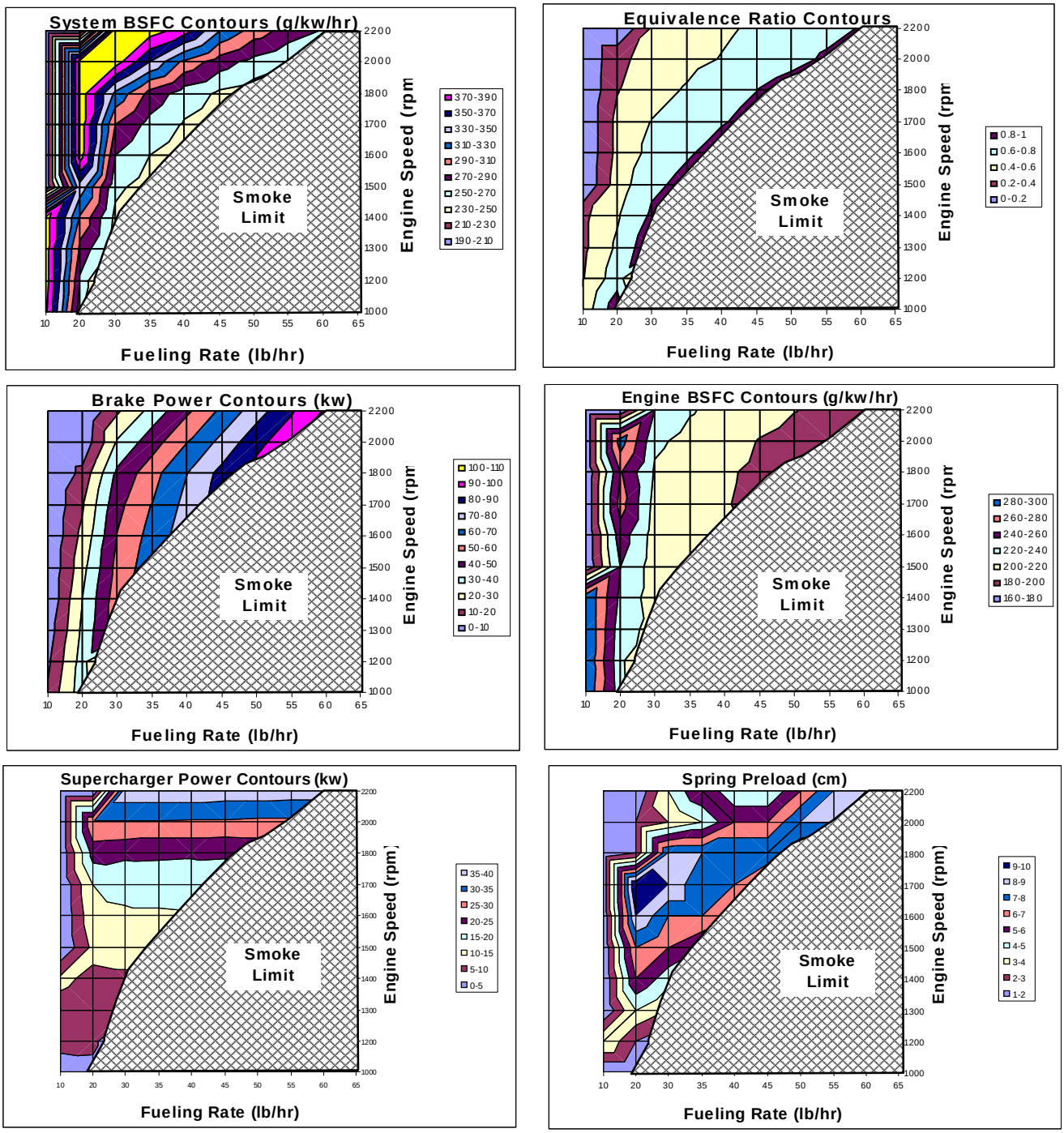

Figure 29 System performance variables mapped over various engine fueling rates and speeds.

This typically occurs for a $\phi > 0.8$. Note that in diesels, not all of the fresh cylinder charge can be consumed due to incomplete mixing associated with direct injection. Therefore, a 'Smoke Limit' region is defined on the equivalence ratio graph slightly above $\phi = 0.8$. This smoke limit region is subsequently illustrated on all other performance graphs since the engine can not typically be operated within this range of conditions.

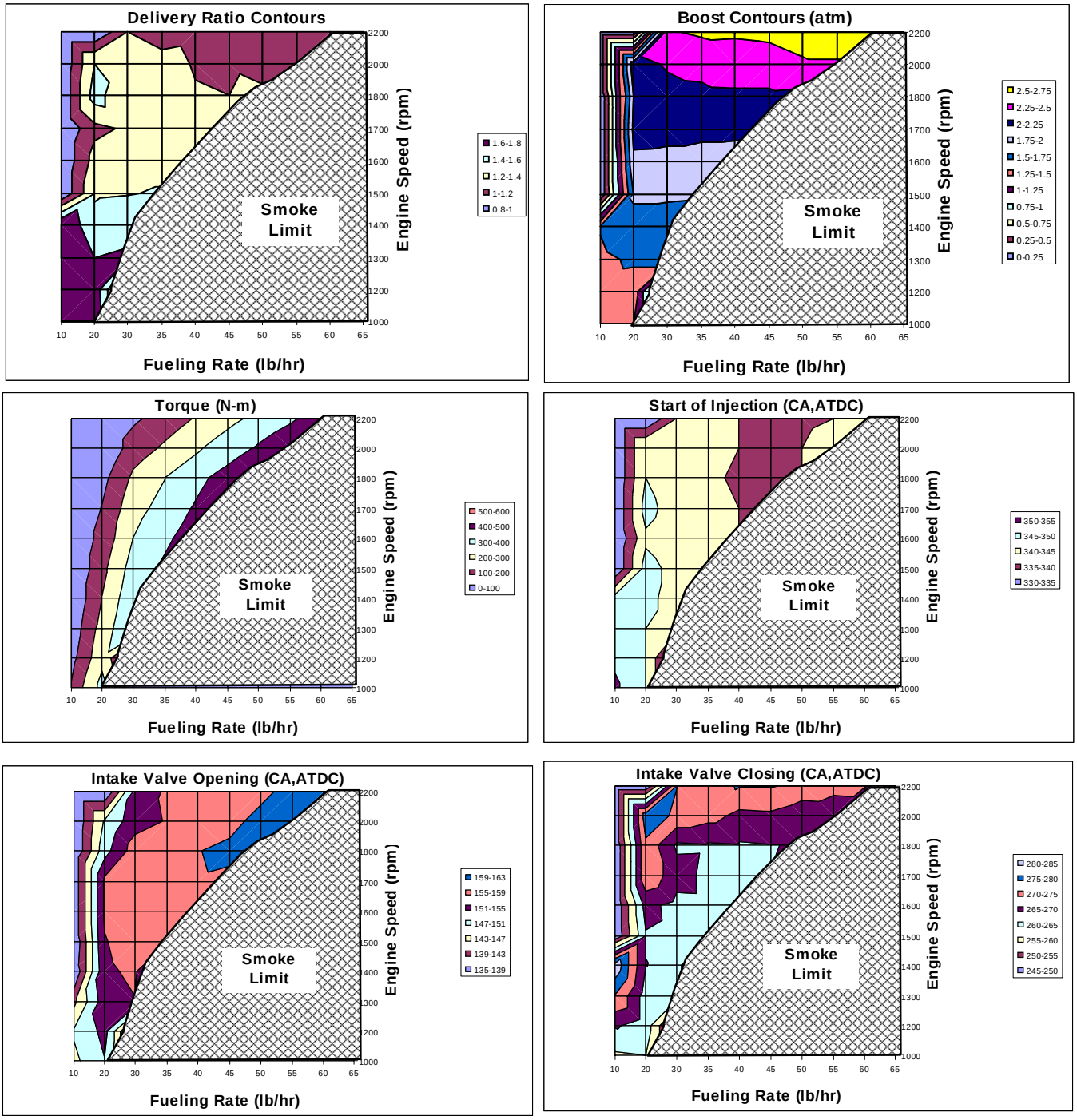

Figure 30 Additional system performance variables mapped over various engine fueling rates and speeds.

Fig. 30 illustrates boost pressures and fresh charge delivery ratios which both appear to be primarily a function of engine speed. The supercharger map is scaled from a Switzer S400 and is geared to the engine through a reduction ratio. The delivery ratio indicates a number of displacement volumes of mass at intake manifold density that have been delivered across the intake ports. Note that at higher engine speeds, the delivery ratio falls towards unity as the time for exhaust blowdown decreases. It is interesting to note that intake valve opening appears to be more closely coupled to load as blowdown pressures take longer to reach manifold pressures under higher loads, while intake valve closing is more coupled with changes in engine speed as the piston moves faster with increasing engine speed relative to the speed of the closing valve.

The current system is modeled with a valve spring constant of 390N/m with the pre-load varied over load and speed by increasing the initial spring displacement. Spring pre-load (shown as displacement – preload (N) = preload displacement (cm) x 3.9 (N/cm)) is illustrated in Fig. 29. Maximum preload is applied at light load and mid speed. Note that an increase in preload delays intake valve opening time, and advances intake valve closing time.

System specific and engine specific fuel consumption is illustrated in Fig. 29. Engine specific fuel consumption is still improving at the highest simulated engine speed, however, system specific fuel consumption peaks at around 1700 rpm and full load. As speed is increased further, the supercharger no longer operates at peak efficiency and requires significant horsepower to be driven. Optimal spring preload is actually lower at these higher speeds in order to improve delivery, however, this retards intake valve closing time and, thus, reduces effective cylinder compression ratio and system efficiency.

LIM Engine Optimization: Improved LIM 353 porting and boost

To further assess the performance potential of the LIM 353 diesel, simulated exhaust port openings were adjusted to reduce the delivery ratio and increase the effective cylinder expansion ratio in an effort to improve system fuel economy. The supercharger map was scaled accordingly to optimize supercharger efficiency throughout the range of engine operation. The modified engine design was then simulated with LIMSIM to search for peak fuel economy and peak power operating conditions.

Screen shots of the LIMSIM graphical user interface for these two conditions are illustrated in Figs. 31-32. Actual simulation output data can be found in Appendix A and B. Note that the valve lift profile has significantly changed from that observed in Fig.28, as the maximum valve lift (controlled by the height of the slot that houses the retaining pin – see Fig.27) has been increased from 0.45 cm to 0.8 cm. When the intake valves now reach the maximum lift pin, the resulting bounce energy provides an accelerated closing velocity. The larger port opening resulting from a higher lift helps to maintain good cylinder delivery, even though the exhaust port heights have been reduced. Note from the logP-logV diagram that the gas exchange process is extremely high frequency and occurs very close to bottom dead center (BDC) due to the late exhaust port opening and rapid intake valve opening/closing. With the intake valve closing event advanced, the start of compression occurs much closer to BDC (compare with Fig. 28) and, therefore, increases the effective compression ratio of the fresh charge. This is a

significant contributor to improved fuel economy as the P-V diagram approaches ideal cycle behavior.

Near top dead center, the multi-pulse fuel delivery enables rapid, controlled heat release which improves air utilization, reduces exhaust emissions, and improves noise, vibration and harshness. The operating line on the supercharger map indicates a wide swing in supercharger mass flow throughout an engine cycle. The intake manifold size directly affects the magnitude of the pressure and mass flow swings seen at the supercharger during each cylinder induction event. The intake manifold used in this example is sized at 12.7L. The operating characteristic is well centered over the peak efficiency portion of the supercharger map (red region). The intake manifold cyclic pressure swing is ~2psi. Fig. 32 shows the operating characteristic of the supercharger map near the top of the map under peak power operation. Efficiency of the blower is rapidly falling in this region, as the blower approaches its peak boost potential. The higher manifold density and reduced cylinder delivery ratio results in a smaller cyclic swing of the operating characteristic on the supercharger map.

Peak cylinder pressure is controlled to below 190atm in the simulation by automatically retarding fuel injection timing if this pressure limit is exceeded. The peak power condition results in a slight injection timing retard to reduce the peak cylinder pressure. The lower boost supplied at an engine speed associated with peak fuel economy results in lower peak cylinder pressures, however, so injection retard is not required. Optimal injection timing is used at this condition which contributes to improved system fuel economy.

Table 3 summarizes the key performance indicators for the two operating conditions illustrated in Figs.31-32. While this design promises excellent fuel economy, torque and emissions characteristics, valve bounce and seating velocities may need to be addressed to improve durability and further reduce noise. One possible solution is to implement a soft landing approach using a pneumatic air shock at the end of valve travel. Another possible solution is to implement a spring 'jiggle' that reduces spring force near the valve closing event. Feasibility of these techniques to provide a soft landing is currently under investigation.

Summary

The LIM concept has been examined in detail, both through an empirical investigation which observed valve behavior, and through a numerical investigation which explored performance and fuel economy potential. Good agreement was seen between experimental data and the LIMSIM virtual engine simulation, thus, lending credibility to performance and fuel economy predictions. While the majority of this work focused on the LIM353 engine, LIMSIM can now be used to assess any LIM engine configuration including changes to bore, stroke, number of cylinders, turbomachinery changes, intercooling, number of valves, etc.

The LIM technology appears to be capable of achieving excellent fuel economy (<.36) over a wide range of operating conditions due to the reduced duration and efficiency of the gas exchange process during scavenging, and due to the valves ability to trap manifold boost pressure in-cylinder. Intake valve timings self adjust based on cylinder and manifold conditions to provide optimal timings for improved cycle performance near BDC.

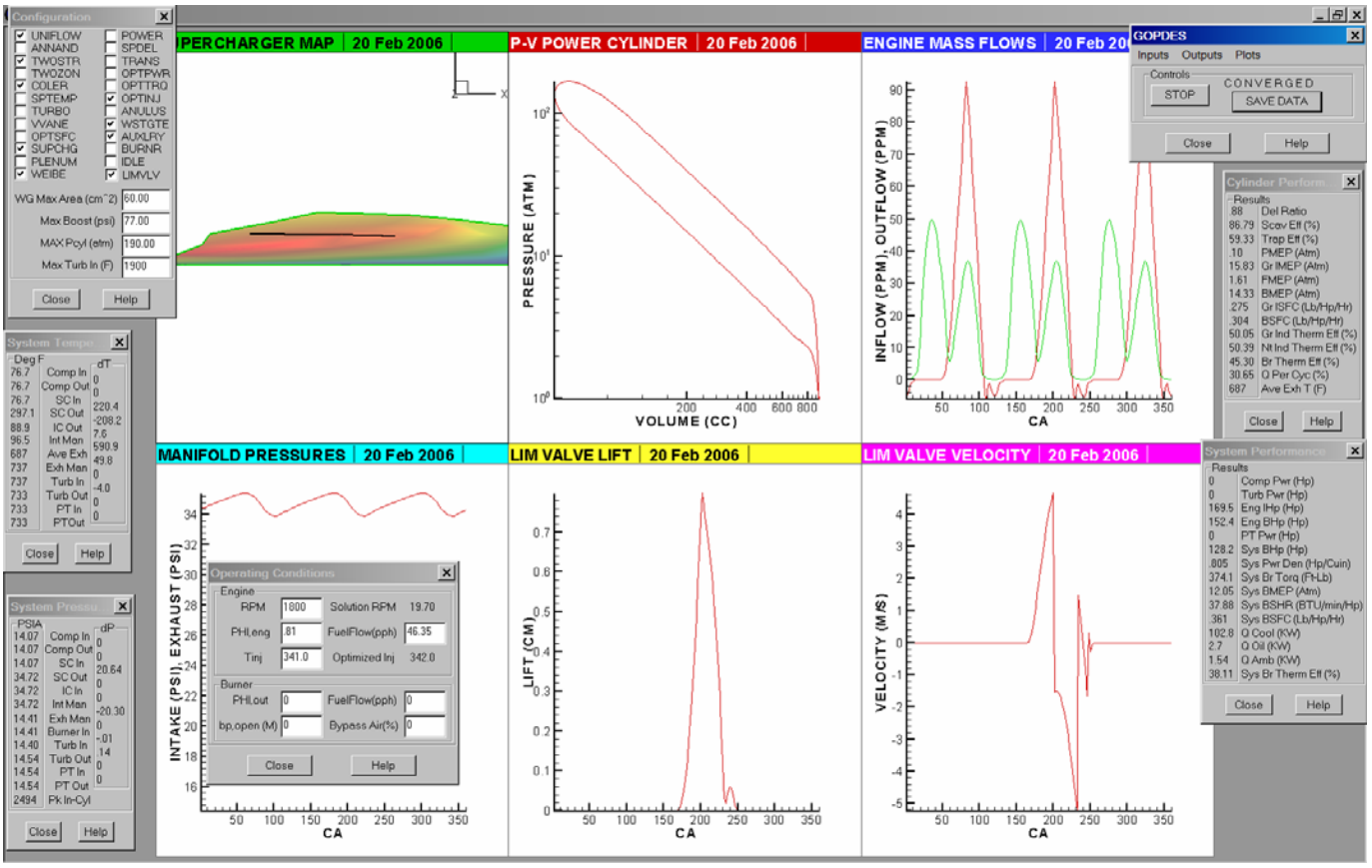

Figure 31 Peak fuel economy operating condition of a LIM 353 diesel

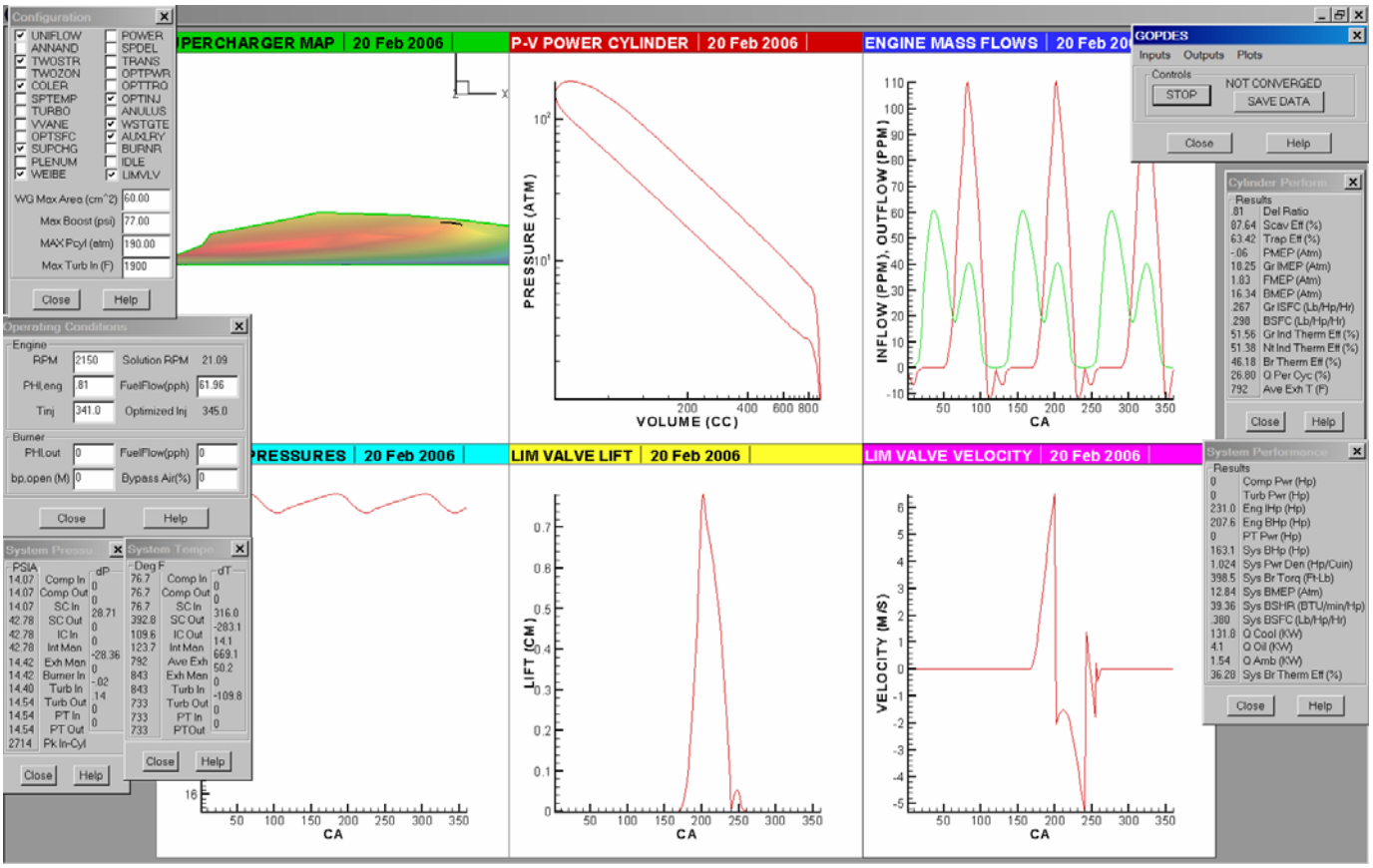

Figure 32 Peak power operating condition of a LIM 353 diesel

Table 3 – Performance indicators at peak fuel economy and peak power operation

	Peak Fuel Economy	Peak Power Output
Speed (RPM)	1800	2150
Indicated Power (IHP)	170	232
Brake Power (BHP)	128.3	163.8
BMEP (atm)	12.05	12.84
Supercharger Power (Hp)	24.2	44.5
Engine ISFC (lb/Hp/Hr)	0.274	0.255
System BSFC (lb/Hp/Hr)	0.362	0.379
Air Flow (lb/Hr)	1153	1475
Fueling Rate (lb/Hr)	46.4	62.0
Coolant Heat Rejection (kW)	82.7	109
Exhaust Gas Temp (F)	688	793
Boost Pressure (PSIA)	34.7	42.8
Peak In-Cyl Pressure (atm)	170	190

Multi-pulse, common rail fuel delivery offers excellent rate shaping ability of the heat release process, thus, improving combustion efficiency and air utilization while reducing noise and emissions. The LIM engine has the ability to idle at extremely low speeds and requires minimal starting torque. Furthermore, excellent compression at low speeds significantly enhances cold start performance as has been experimentally verified. The LIM system appears to be well suited for high power density designs utilizing a blower with an upstream intercooler and turbocharger.

Active valve management would improve higher speed performance enabling faster valve closing. Spring tensions could subsequently be optimized for valve opening, thus, good fuel economy at higher speeds could be achieved. It is anticipated that power densities for such a system would exceed 1.5Hp/cu-in with a BSFC of <0.36.

The next proposed steps include designing an optimized LIM system for a specific application, performing appropriate instrumentation of this system to rapidly analyze and correct design deficiencies, and field testing the system to evaluate durability and performance.

APPENDIX A – PEAK FUEL ECONOMY OUTPUT

```
>>>> INSTANTANEOUS CYLINDER DATA AFTER 264 ENGINE CYCLES
 ____________________________________________________________________________________________________________

                     DIESEL ENGINE CYCLE SIMULATION - LIMSIM

                                        - SUPERCHARGER INSTALLED
 ____________________________________________________________________________________________________________



 >>>>> INPUT DATA
 ____________________________________________________________________________________________________________

 >>>>> OPERATING MODE

   PREDICTED IGNITION DELAY OPTION
   PREDICTED QUASI-STEADY WALL TEMPERATURES
   FLAME RADIATION MODEL
   OPTIMIZED INJECTION TIMING SEARCH ENABLED
 ____________________________________________________________________________________________________________

 >>>>> OPERATING CONDITIONS

   FUEL USED IS DIESEL #2
   ENGINE SPEED                 =   1800.0 RPM
    NITROGEN-TO-OXYGEN RATIO    =     3.76
   PHI,ENGINE (F/A / F/A|s)     =   0.8103
   PHI,EXH MNFLD (F/A / F/A|s)  =   0.5534
   PHI,OVERALL (F/A / F/A|s)    =   0.0000
   INJECTION TIMING             =    342.0 DEG CA
   COMPRESSOR INLET PRESSURE    =   0.9577 ATM
   COMPRESSOR INLET TEMPERATURE =   298.00 K
   ATMOSPHERIC PRESSURE         =   0.9800 ATM
   ATMOSPHERIC TEMPERATURE      =   298.00 K

   LIM VALVE SPRING CONSTANT    =   390.00 N/M
   LIM VALVE SPRING PRELOAD     =    11.00 CM
 ____________________________________________________________________________________________________________


 >>>>> ENGINE DESIGN PARAMETERS

   NUMBER OF CYLINDERS     =    3
   CYLINDER BORE           =     9.842 CM
   CRANKSHAFT STROKE       =    11.430 CM
   CONNECTING ROD LENGTH   =    25.400 CM
   GEOM.COMPRESSION RATIO  =    21.000
```

```
   EFF. COMPRESSION RATIO  =    15.425
   EFF. EXPANSION RATIO    =    15.425
   DISPLACED VOLUME        =   869.655 CC
   CLEARANCE VOLUME        =    43.483 CC
   ENGINE DISPLACEMENT     =     2.609 LT
   INTAKE PORT OPENS       =     165.9 DEG CA
   INTAKE PORT CLOSES      =     252.8 DEG CA
   EXHAUST PORT OPENS      =     125.0 DEG CA
   EXHAUST PORT CLOSES     =     235.0 DEG CA
   EXHAUST CRANK ADVANCE   =       0.0 DEG CA
```

```
>>>> MANIFOLD DIMENSIONS             INTAKE     EXHAUST

   LENGTH                    (CM)        50.00       30.00
   DIAMETER                  (CM)        18.00       10.00
   CROSS-SECTIONAL AREA    (CM**2)      254.47       78.54
   INTERNAL SURFACE AREA   (CM**2)     2827.43      942.48
   VOLUME                    (LT)       12.723       2.356
```

```
>>>> CONNECTING PIPE DIMENSIONS       COMPRESSOR    TURBINE

   LENGTH                    (CM)        21.00       41.00
   DIAMETER                  (CM)        10.00       10.00
   CROSS-SECTIONAL AREA    (CM**2)       78.54       78.54
   INTERNAL SURFACE AREA   (CM**2)      659.73     1288.05
   VOLUME                    (LT)        2.356       3.220
```

```
>>>> TURBOMACHINERY DATA

         SUPERCHARGER  Schwitzer S400-105/55 compressor map (HP)
   T/C INERTIA        (KG-CM**2)        9.13
   T/C DAMPING        (G-CM**2/S)       0.29
   P.TURBINE TRANSMISSION EFF.(%)      60.00
   P.TURBINE GEAR RATIO                13.00
   SUPERCHARGER MULTIPLIERS         0.260  1.000  0.700  0.600
   COMPRESSOR MULTIPLIERS           1.000  1.000  1.000  1.000
   TURBINE MULTIPLIERS              1.000  1.000  1.000  1.000
   POWER TURBINE MULTIPLIERS        1.000  1.000  1.000  1.000
```

```
>>>> SYSTEM PRESSURE DROPS (PA)

   COMPRESSOR EXIT-SUPERCHARGER INLET          0.0
   SUPERCHARGER EXIT-INTERCOOLER INLET         0.0
   INTERCOOLER INLET - INTAKE MANIFOLD         0.0
   EXHAUST MANIFOLD - TURBINE INLET            0.0
   TURBINE EXIT - POWER TURBINE INLET          0.0
```

```
  POWER TURBINE EXIT - ATMOSPHERIC         1000.0
```

```
>>>>> HEAT TRANSFER AND TURBULENCE PARAMETERS

  NUSSELT COEFFICIENT   (CHAMBER)=     0.0350
  NUSSELT COEFFICIENT   (INT MAN)=     0.0350
  NUSSELT COEFFICIENT   (EXH MAN)=     0.0350
  NUSSELT COEFFICIENT   (C. PIPE)=     0.0350
  REYNOLDS EXPONENT              =     0.8000
  INT. MANIFOLD WALL TEMPERATURE =   304.26   K
  EXH. MANIFOLD WALL TEMPERATURE =   370.16   K
  CONN. PIPE WALL TEMPERATURE    =   596.00   K
  TURBULENT DISSIPATION CONSTANT =     1.1000
```

```
>>>>> COMPUTATIONAL PARAMETERS

  MAXIMUM # OF ITERATIONS =   8000
  OUTPUT AT ITERATION #   =    264
  TCALL                   =      1.00
  TPRINT                  =      2.00
  TSCREN                  =   8000.00
  CIINTG                  =      0.000001
  CCINTG                  =      0.000010
  CBINTG                  =      0.000010
  CEINTG                  =      0.000010
  AREROT                  =      0.000000
  REL                     =      0.000000
  MAXERR                  =      0.000010
  MAXTRY                  =    100
```

```
 >>>>> START OF BLOWDOWN PROCESS
```

CA (DEG)	P (ATM)	TEMP (K)	MEX (G)	PHI (-)	PIM (ATM)	TIM (K)	PEM (ATM)	TEM (K)	PANL (ATM)	TANL (K)	IFG (-)
126.0	6.0256	1028.02	0.00013	0.81027	2.3456	308.49	0.9800	596.07	3.5000	420.00	2
128.0	5.9147	1023.34	0.00077	0.81027	2.3486	308.61	0.9800	596.35	3.5000	420.00	2
130.0	5.8097	1018.84	0.00158	0.81027	2.3515	308.72	0.9800	596.71	3.5000	420.00	2
132.0	5.7085	1014.43	0.00289	0.81027	2.3543	308.83	0.9800	597.21	3.5000	420.00	2
134.0	5.6088	1010.03	0.00508	0.81027	2.3570	308.93	0.9800	598.13	3.5000	420.00	2
136.0	5.5114	1005.67	0.00800	0.81027	2.3597	309.03	0.9800	599.34	3.5000	420.00	2
138.0	5.4003	1000.67	0.01470	0.81027	2.3624	309.13	0.9799	601.58	3.5000	420.00	2
140.0	5.2521	993.90	0.02995	0.81027	2.3650	309.22	0.9801	607.24	3.5000	420.00	2
142.0	5.0581	984.83	0.05578	0.81027	2.3677	309.32	0.9802	617.08	3.5000	420.00	2
144.0	4.8194	973.29	0.09245	0.81027	2.3704	309.42	0.9804	630.81	3.5000	420.00	2
146.0	4.5437	959.39	0.13890	0.81027	2.3730	309.52	0.9807	647.26	3.5000	420.00	2
148.0	4.2401	943.30	0.19366	0.81027	2.3756	309.61	0.9816	665.10	3.5000	420.00	2
150.0	3.9190	925.28	0.25492	0.81027	2.3782	309.71	0.9820	682.97	3.5000	420.00	2
152.0	3.5904	905.62	0.32077	0.81027	2.3808	309.80	0.9824	699.77	3.5000	420.00	2
154.0	3.2635	884.60	0.38932	0.81027	2.3834	309.89	0.9828	714.69	3.5000	420.00	2
156.0	2.9458	862.55	0.45886	0.81027	2.3859	309.98	0.9827	727.25	3.5000	420.00	2
158.0	2.6433	839.74	0.52789	0.81027	2.3883	310.07	0.9827	737.26	3.5000	420.00	2
160.0	2.3600	816.46	0.59520	0.81027	2.3907	310.16	0.9827	744.75	3.5000	420.00	2
162.0	2.0985	792.96	0.65984	0.81027	2.3931	310.24	0.9825	749.89	3.5000	420.00	2
164.0	1.8601	769.45	0.72115	0.81027	2.3955	310.32	0.9823	752.96	3.5000	420.00	2

>>>>> OUTPUT DATA

>>>>> ENGINE CRANK-ANGLE BY CRANK-ANGLE RESULTS

>>>>> START OF INTAKE PROCESS

CA (DEG)	P (ATM)	TEMP (K)	MIN (G)	MEX (G)	PHI (-)	PIM (ATM)	TIM (K)	PEM (ATM)	TEM (K)	PANL (ATM)	TANL (K)	IFG (-)
165.9	1.6582	747.62	0.00000	0.77508	0.81027	2.3976	310.40	0.9821	754.21	8		
166.0	1.6453	746.16	0.00000	0.77858	0.81027	2.3978	310.41	0.9813	754.28	3.5000	420.00	2
168.0	1.4565	723.62	0.00002	0.83101	0.81023	2.4000	310.49	0.9817	754.67	3.5000	420.00	2
170.0	1.2969	702.49	0.00033	0.87705	0.80974	2.4022	310.56	0.9814	753.51	3.5000	420.00	2
172.0	1.1694	683.35	0.00155	0.91541	0.80767	2.4044	310.64	0.9810	751.78	3.5000	420.00	2
174.0	1.0762	666.61	0.00455	0.94513	0.80225	2.4063	310.70	0.9806	749.83	3.5000	420.00	2
176.0	1.0181	652.33	0.01042	0.96578	0.79131	2.4079	310.76	0.9804	748.07	3.5000	420.00	2
178.0	0.9923	639.78	0.02043	0.97829	0.77269	2.4090	310.80	0.9802	746.79	3.5000	420.00	2
180.0	0.9885	626.78	0.03605	0.98648	0.74473	2.4097	310.81	0.9801	745.90	3.5000	420.00	2
182.0	0.9939	610.96	0.05888	0.99540	0.70669	2.4096	310.81	0.9801	744.94	3.5000	420.00	2
184.0	1.0048	591.90	0.09047	1.00734	0.65909	2.4088	310.77	0.9802	743.47	3.5000	420.00	2
186.0	1.0216	570.48	0.13202	1.02318	0.60405	2.4070	310.70	0.9802	741.30	3.5000	420.00	2
188.0	1.0452	548.12	0.18412	1.04343	0.54500	2.4043	310.59	0.9804	738.17	3.5000	420.00	2
190.0	1.0759	526.26	0.24660	1.06838	0.48571	2.4007	310.45	0.9805	733.84	3.5000	420.00	2
192.0	1.1138	505.97	0.31883	1.09810	0.42921	2.3961	310.27	0.9807	728.13	3.5000	420.00	2
194.0	1.1576	487.12	0.40023	1.13239	0.37725	2.3908	310.06	0.9812	720.99	3.5000	420.00	2
196.0	1.2099	470.48	0.49085	1.17088	0.33034	2.3846	309.83	0.9812	712.56	3.5000	420.00	2
198.0	1.2740	456.33	0.59157	1.21334	0.28830	2.3776	309.56	0.9816	702.87	3.5000	420.00	2
200.0	1.3531	444.50	0.70400	1.25942	0.25072	2.3696	309.25	0.9820	692.15	3.5000	420.00	2
202.0	1.4505	434.85	0.82942	1.30869	0.21740	2.3604	308.90	0.9817	680.50	3.5000	420.00	2
204.0	1.5494	427.21	0.95563	1.36014	0.19061	2.3506	308.52	0.9818	668.31	3.5000	420.00	2
206.0	1.6391	421.21	1.07360	1.41179	0.17006	2.3417	308.18	0.9824	656.08	3.5000	420.00	2
208.0	1.7217	416.54	1.18243	1.46187	0.15405	2.3337	307.87	0.9819	644.41	3.5000	420.00	2
210.0	1.7986	413.01	1.28137	1.50889	0.14146	2.3267	307.60	0.9825	633.66	3.5000	420.00	2
212.0	1.8712	410.48	1.36982	1.55156	0.13151	2.3208	307.37	0.9814	624.09	3.5000	420.00	2
214.0	1.9406	408.86	1.44731	1.58883	0.12366	2.3159	307.19	0.9811	615.93	3.5000	420.00	2
216.0	2.0078	408.08	1.51349	1.61989	0.11753	2.3121	307.04	0.9809	609.27	3.5000	420.00	2
218.0	2.0735	408.10	1.56813	1.64414	0.11282	2.3095	306.94	0.9804	604.12	3.5000	420.00	2
220.0	2.1384	408.90	1.61113	1.66115	0.10932	2.3080	306.88	0.9806	600.48	3.5000	420.00	2
222.0	2.2019	410.39	1.64252	1.67126	0.10689	2.3077	306.87	0.9802	598.26	3.5000	420.00	2
224.0	2.2616	412.42	1.66255	1.67577	0.10538	2.3084	306.90	0.9801	597.18	3.5000	420.00	2
226.0	2.3102	414.65	1.67111	1.67771	0.10475	2.3102	306.97	0.9800	596.77	3.5000	420.00	2
228.0	2.3312	416.07	1.66413	1.67915	0.10475	2.3136	307.11	0.9800	596.48	3.5000	420.00	2
230.0	2.3538	417.55	1.65639	1.68000	0.10475	2.3176	307.29	0.9800	596.28	3.5000	420.00	2
232.0	2.3869	419.54	1.65183	1.68052	0.10475	2.3213	307.45	0.9800	596.17	3.5000	420.00	2
234.0	2.4320	422.10	1.65101	1.68094	0.10475	2.3243	307.57	0.9800	596.09	3.5000	420.00	2
236.0	2.4758	424.54	1.64824	1.68110	0.10475	2.3275	307.70	0.9800	596.05	3.5000	420.00	2
238.0	2.5170	426.83	1.64317	1.68110	0.10475	2.3309	307.84	0.9800	596.05	3.5000	420.00	2
240.0	2.5568	429.01	1.63647	1.68110	0.10475	2.3346	308.00	0.9800	596.05	3.5000	420.00	2
242.0	2.5980	431.22	1.62918	1.68110	0.10475	2.3384	308.17	0.9800	596.05	3.5000	420.00	2
244.0	2.6441	433.63	1.62256	1.68110	0.10475	2.3421	308.34	0.9800	596.05	3.5000	420.00	2
246.0	2.6999	436.45	1.61818	1.68110	0.10475	2.3456	308.49	0.9800	596.05	3.5000	420.00	2

>>>>> START OF COMPRESSION PROCESS

CA (DEG)	P (ATM)	TEMP (K)			PHI (-)	PIM (ATM)	TIM (K)	PEM (ATM)	TEM (K)	PANL (ATM)	TANL (K)	IFG (-)
248.0	2.7697	439.85	1.61732	1.68110	0.10475	2.3486	308.61	0.9800	596.31	3.5000	420.00	2
250.0	2.8441	443.38	1.61640	1.68110	0.10475	2.3514	308.72	0.9799	596.66	3.5000	420.00	2

>>>>> START OF COMPRESSION PROCESS

CA (DEG)	P (ATM)	TEMP (K)			PHI (-)	PIM (ATM)	TIM (K)	PEM (ATM)	TEM (K)	PANL (ATM)	TANL (K)	IFG (-)
252.0	2.9255	447.14	1.61610	1.68110	0.10475	2.3542	308.82	0.9798	597.16	3.5000	420.00	2

>>>>> START OF COMPRESSION PROCESS

CA (DEG)	P (ATM)	TEMP (K)	PHI (-)	PIM (ATM)	TIM (K)	PEM (ATM)	TEM (K)	PANL (ATM)	TANL (K)	IFG (-)

>>>>> START OF COMPRESSION PROCESS

CA (DEG)	P (ATM)	TEMP (K)	PHI (-)	PIM (ATM)	TIM (K)	PEM (ATM)	TEM (K)	PANL (ATM)	TANL (K)	IFG (-)
254.0	3.0133	451.09	0.10475	2.3569	308.92	0.9800	598.04	3.5000	420.00	2
256.0	3.1073	455.20	0.10475	2.3596	309.02	0.9800	599.25	3.5000	420.00	2
258.0	3.2079	459.47	0.10475	2.3623	309.12	0.9800	601.49	3.5000	420.00	2
260.0	3.3156	463.92	0.10475	2.3650	309.22	0.9799	607.15	3.5000	420.00	2
262.0	3.4311	468.56	0.10475	2.3677	309.32	0.9800	616.96	3.5000	420.00	2
264.0	3.5550	473.38	0.10475	2.3703	309.42	0.9805	630.67	3.5000	420.00	2
266.0	3.6882	478.41	0.10475	2.3730	309.51	0.9811	647.10	3.5000	420.00	2
268.0	3.8315	483.66	0.10475	2.3756	309.61	0.9814	664.96	3.5000	420.00	2
270.0	3.9857	489.13	0.10475	2.3782	309.70	0.9821	682.84	3.5000	420.00	2
272.0	4.1521	494.83	0.10475	2.3808	309.80	0.9820	699.65	3.5000	420.00	2
274.0	4.3315	500.77	0.10475	2.3833	309.89	0.9822	714.60	3.5000	420.00	2
276.0	4.5242	506.83	0.10475	2.3858	309.98	0.9828	727.23	3.5000	420.00	2
278.0	4.7327	513.14	0.10475	2.3883	310.07	0.9829	737.21	3.5000	420.00	2
280.0	4.9585	519.72	0.10475	2.3907	310.15	0.9826	744.65	3.5000	420.00	2
282.0	5.2034	526.57	0.10475	2.3931	310.24	0.9825	749.82	3.5000	420.00	2
284.0	5.4696	533.72	0.10475	2.3954	310.32	0.9824	752.91	3.5000	420.00	2
286.0	5.7591	541.18	0.10475	2.3977	310.40	0.9821	754.23	3.5000	420.00	2
288.0	6.0748	548.97	0.10475	2.4000	310.48	0.9818	753.89	3.5000	420.00	2
290.0	6.4195	557.09	0.10475	2.4022	310.56	0.9813	752.75	3.5000	420.00	2
292.0	6.7966	565.58	0.10475	2.4043	310.63	0.9809	750.98	3.5000	420.00	2
294.0	7.2098	574.45	0.10475	2.4062	310.70	0.9806	749.04	3.5000	420.00	2
296.0	7.6635	583.71	0.10475	2.4078	310.75	0.9803	747.30	3.5000	420.00	2
298.0	8.1627	593.39	0.10475	2.4090	310.79	0.9801	746.04	3.5000	420.00	2
300.0	8.7131	603.52	0.10475	2.4096	310.81	0.9800	745.18	3.5000	420.00	2
302.0	9.3211	614.11	0.10475	2.4095	310.80	0.9801	744.21	3.5000	420.00	2
304.0	9.9942	625.20	0.10475	2.4087	310.76	0.9801	742.75	3.5000	420.00	2
306.0	10.7412	636.80	0.10475	2.4069	310.69	0.9802	740.57	3.5000	420.00	2
308.0	11.5719	648.95	0.10475	2.4042	310.58	0.9803	737.42	3.5000	420.00	2
310.0	12.4979	661.68	0.10475	2.4005	310.44	0.9805	733.06	3.5000	420.00	2
312.0	13.5323	675.02	0.10475	2.3959	310.26	0.9806	727.33	3.5000	420.00	2
314.0	14.6906	688.99	0.10475	2.3905	310.05	0.9809	720.19	3.5000	420.00	2
316.0	15.9905	703.63	0.10475	2.3843	309.81	0.9810	711.76	3.5000	420.00	2
318.0	17.4523	718.96	0.10475	2.3773	309.55	0.9815	702.09	3.5000	420.00	2
320.0	19.0997	735.02	0.10475	2.3693	309.24	0.9815	691.39	3.5000	420.00	2
322.0	20.9596	751.83	0.10475	2.3600	308.88	0.9814	679.78	3.5000	420.00	2
324.0	23.0627	769.42	0.10475	2.3503	308.51	0.9815	667.68	3.5000	420.00	2
326.0	25.4437	787.79	0.10475	2.3414	308.17	0.9817	655.55	3.5000	420.00	2
328.0	28.1413	806.95	0.10475	2.3335	307.86	0.9818	643.97	3.5000	420.00	2
330.0	31.1976	826.88	0.10475	2.3265	307.59	0.9812	633.27	3.5000	420.00	2
332.0	34.6577	847.57	0.10475	2.3206	307.37	0.9810	623.87	3.5000	420.00	2
334.0	38.5669	868.94	0.10475	2.3157	307.18	0.9811	615.75	3.5000	420.00	2
336.0	42.9683	890.91	0.10475	2.3120	307.03	0.9805	609.09	3.5000	420.00	2
338.0	47.8967	913.33	0.10475	2.3094	306.93	0.9803	604.00	3.5000	420.00	2
340.0	53.3708	936.01	0.10475	2.3079	306.88	0.9802	600.43	3.5000	420.00	2
342.0	59.3821	958.66	0.10475	2.3076	306.87	0.9800	598.29	3.5000	420.00	8
344.0	65.8798	980.95	0.10475	2.3084	306.90	0.9800	597.27	3.5000	420.00	2
346.0	72.7538	1002.39	0.10475	2.3103	306.97	0.9800	596.86	3.5000	420.00	2
346.4	73.9954	1006.06	0.10475	2.3108	306.99	0.9800	596.80	8		

>>>>> START OF COMBUSTION AND EXPANSION PROCESSES

CA (DEG)	P (ATM)	TEMP (K)	PHI (-)	PIM (ATM)	TIM (K)	PEM (ATM)	TEM (K)	PANL (ATM)	TANL (K)	IFG (-)
348.0	79.7288	1021.31	0.10497	2.3135	307.10	0.9800	596.56	3.5000	420.00	2
350.0	87.0611	1043.53	0.10705	2.3175	307.28	0.9800	596.37	3.5000	420.00	2
352.0	95.0986	1075.31	0.11305	2.3211	307.44	0.9800	596.26	3.5000	420.00	2
354.0	104.0925	1121.45	0.12484	2.3242	307.56	0.9800	596.18	3.5000	420.00	2
356.0	114.1487	1185.45	0.14401	2.3273	307.69	0.9800	596.14	3.5000	420.00	2
358.0	125.1008	1268.77	0.17170	2.3308	307.83	0.9800	596.14	3.5000	420.00	2
360.0	136.4538	1370.53	0.20846	2.3345	308.00	0.9800	596.14	3.5000	420.00	2

362.0	147.4192	1487.50	0.25407	2.3383	308.17	0.9800	596.14	3.5000	420.00	2
364.0	157.0443	1614.46	0.30753	2.3420	308.33	0.9800	596.14	3.5000	420.00	2
366.0	164.4035	1744.82	0.36703	2.3455	308.48	0.9800	596.14	3.5000	420.00	2
368.0	168.7833	1871.39	0.43012	2.3485	308.60	0.9800	596.41	3.5000	420.00	2
370.0	169.8063	1987.21	0.49393	2.3513	308.71	0.9800	596.77	3.5000	420.00	2
372.0	167.4704	2086.33	0.55554	2.3541	308.81	0.9800	597.27	3.5000	420.00	2
374.0	162.1123	2164.56	0.61229	2.3568	308.91	0.9799	598.18	3.5000	420.00	2
376.0	154.3158	2219.84	0.66215	2.3595	309.01	0.9799	599.37	3.5000	420.00	2
378.0	144.7883	2252.33	0.70387	2.3622	309.11	0.9798	601.58	3.5000	420.00	2
380.0	134.2412	2263.88	0.73708	2.3649	309.21	0.9799	607.13	3.5000	420.00	2
382.0	123.3016	2257.46	0.76218	2.3676	309.31	0.9801	616.96	3.5000	420.00	2
384.0	112.4671	2236.57	0.78018	2.3702	309.41	0.9802	630.67	3.5000	420.00	2
386.0	102.0958	2204.75	0.79238	2.3729	309.50	0.9804	647.12	3.5000	420.00	2
388.0	92.4174	2165.36	0.80020	2.3755	309.60	0.9802	664.95	3.5000	420.00	2
390.0	83.5555	2121.31	0.80492	2.3781	309.69	0.9816	682.87	3.5000	420.00	2
392.0	75.5522	2074.95	0.80760	2.3807	309.79	0.9819	699.69	3.5000	420.00	2
394.0	68.3919	2028.03	0.80903	2.3832	309.88	0.9824	714.64	3.5000	420.00	2
396.0	62.0234	1981.72	0.80974	2.3857	309.97	0.9829	727.26	3.5000	420.00	2
398.0	56.3763	1936.74	0.81007	2.3882	310.06	0.9826	737.27	3.5000	420.00	2
400.0	51.3741	1893.46	0.81022	2.3906	310.15	0.9828	744.76	3.5000	420.00	2
402.0	46.9410	1852.02	0.81028	2.3930	310.23	0.9826	749.87	3.5000	420.00	2
404.0	43.0073	1812.45	0.81030	2.3954	310.31	0.9823	752.93	3.5000	420.00	2
406.0	39.5101	1774.70	0.81031	2.3977	310.40	0.9821	754.28	3.5000	420.00	2
408.0	36.3942	1738.69	0.81031	2.3999	310.48	0.9817	753.92	3.5000	420.00	2
410.0	33.6116	1704.32	0.81031	2.4021	310.55	0.9814	752.77	3.5000	420.00	2
412.0	31.1207	1671.51	0.81031	2.4042	310.63	0.9809	750.99	3.5000	420.00	2
414.0	28.8855	1640.15	0.81031	2.4061	310.69	0.9806	749.06	3.5000	420.00	2
416.0	26.8750	1610.15	0.81031	2.4078	310.75	0.9803	747.31	3.5000	420.00	2
418.0	25.0624	1581.45	0.81031	2.4089	310.78	0.9801	746.04	3.5000	420.00	2
420.0	23.4243	1553.95	0.81031	2.4095	310.80	0.9801	745.18	3.5000	420.00	2
422.0	21.9406	1527.59	0.81031	2.4095	310.79	0.9801	744.21	3.5000	420.00	2
424.0	20.5938	1502.29	0.81031	2.4086	310.76	0.9801	742.76	3.5000	420.00	2
426.0	19.3686	1478.00	0.81031	2.4069	310.68	0.9802	740.59	3.5000	420.00	2
428.0	18.2518	1454.66	0.81031	2.4042	310.58	0.9804	737.47	3.5000	420.00	2
430.0	17.2317	1432.20	0.81031	2.4005	310.43	0.9806	733.12	3.5000	420.00	2
432.0	16.2980	1410.58	0.81031	2.3959	310.26	0.9807	727.41	3.5000	420.00	2
434.0	15.4418	1389.75	0.81031	2.3906	310.05	0.9809	720.28	3.5000	420.00	2
436.0	14.6553	1369.65	0.81031	2.3844	309.81	0.9810	711.85	3.5000	420.00	2
438.0	13.9315	1350.26	0.81031	2.3774	309.54	0.9813	702.18	3.5000	420.00	2
440.0	13.2643	1331.53	0.81031	2.3693	309.23	0.9815	691.48	3.5000	420.00	2
442.0	12.6483	1313.44	0.81031	2.3601	308.88	0.9819	679.86	3.5000	420.00	2
444.0	12.0786	1295.93	0.81031	2.3504	308.51	0.9816	667.76	3.5000	420.00	2
446.0	11.5511	1279.00	0.81031	2.3415	308.17	0.9816	655.63	3.5000	420.00	2
448.0	11.0617	1262.60	0.81031	2.3335	307.86	0.9814	644.06	3.5000	420.00	2
450.0	10.6073	1246.72	0.81031	2.3266	307.59	0.9815	633.36	3.5000	420.00	2
452.0	10.1847	1231.32	0.81031	2.3207	307.36	0.9810	623.94	3.5000	420.00	2
454.0	9.7911	1216.38	0.81031	2.3158	307.18	0.9809	615.85	3.5000	420.00	2
456.0	9.4242	1201.89	0.81031	2.3121	307.03	0.9808	609.23	3.5000	420.00	2
458.0	9.0817	1187.81	0.81031	2.3095	306.93	0.9806	604.14	3.5000	420.00	2
460.0	8.7616	1174.14	0.81031	2.3080	306.88	0.9802	600.55	3.5000	420.00	2
462.0	8.4622	1160.85	0.81031	2.3077	306.87	0.9801	598.41	3.5000	420.00	2
464.0	8.1818	1147.93	0.81031	2.3085	306.90	0.9800	597.39	3.5000	420.00	2
466.0	7.9189	1135.36	0.81031	2.3104	306.97	0.9800	596.98	3.5000	420.00	2
468.0	7.6723	1123.12	0.81031	2.3138	307.12	0.9800	596.69	3.5000	420.00	2
470.0	7.4407	1111.20	0.81031	2.3178	307.29	0.9800	596.50	3.5000	420.00	2
472.0	7.2229	1099.59	0.81031	2.3214	307.45	0.9800	596.40	3.5000	420.00	2
474.0	7.0180	1088.27	0.81031	2.3245	307.57	0.9800	596.32	3.5000	420.00	2
476.0	6.8249	1077.20	0.81031	2.3276	307.70	0.9800	596.28	3.5000	420.00	2
478.0	6.6429	1066.39	0.81031	2.3311	307.85	0.9800	596.28	3.5000	420.00	2
480.0	6.4712	1055.82	0.81031	2.3348	308.01	0.9800	596.28	3.5000	420.00	2
482.0	6.3091	1045.49	0.81031	2.3386	308.18	0.9800	596.28	3.5000	420.00	2
484.0	6.1560	1035.39	0.81031	2.3423	308.34	0.9800	596.28	3.5000	420.00	2

>>>>> START OF BLOWDOWN PROCESS

CA (DEG)	P (ATM)	TEMP (K)	MEX (G)	PHI (-)	PIM (ATM)	TIM (K)	PEM (ATM)	TEM (K)	PANL (ATM)	TANL (K)	IFG (-)

>>>> CYCLE-AVERAGED SYSTEM DATA AFTER 264 ENGINE CYCLES

>>>> MANIFOLD HEAT TRANSFER DATA INTAKE EXHAUST

WALL TEMPERATURE (K) 304.22 370.66

AVERAGE VELOCITY (M/S)	0.34	0.21
REYNOLDS NUMBER (FILM)	8911.9	616.8
PRANDTL NUMBER	0.6470	0.6827
NUSSELT NUMBER	44.39	5.33
HEAT TRANSFER COEFF. (W/K/M**2)	6.86	2.03
HEAT TRANSFER RATE (KW)	0.004	0.210

>>>SYSTEM PRESSURES (ATM) (PSI)

SUPERCHARGER INLET	0.96	14.07
SUPERCHARGER OUTLET	2.36	34.72
DELTA P ENGINE	1.38	20.31
PEAK IN-CYLINDER	169.81	2495.25

>>>>SYSTEM TEMPERATURES (K) (F)

SUPERCHARGER INLET	298.00	76.71
SUPERCHARGER OUTLET	420.45	297.12

>>>TURBOMACHINERY DATA SUPERCHARGER

ACTUAL MASS FLOW (LB/MIN)	19.224
ACTUAL SPEED(KRPM OR U/V0)	48.600
MAP FLOW (LB/MIN)	19.810
MAP SPEED (KRPM OR U/V0)	48.600
PRESSURE RATIOS:	2.467
EFFICIENCIES:	0.728

>>> CYLINDER WALL ZONAL BREAKS FROM CENTERLINE

|----|----|----|----|---|-----|-----|-----------|-----|-----|-----------|-----------|-----------|-----------|------------|

>>>TOP RING ZONE POSITION - 14.87

>>>TOP RING REVERSAL TEMP(C) - 232.72

>>>>COMPONENT TEMPERATURE DATA

	IN-CYL (K)	IN-CYL (F)	OUTER (K)	HEAT FLUX (KW/M^2)	TCOOL (K)
PISTON	494.32	430.08			
HEAD	615.53	648.27			
CYLINDER WALL ZONE 1	438.59	329.77	414.95	163.16	375.86
CYLINDER WALL ZONE 2	427.04	308.99	406.42	145.65	374.69
CYLINDER WALL ZONE 3	427.11	309.11	406.02	148.16	373.74
CYLINDER WALL ZONE 4	432.99	319.69	409.22	167.29	372.77
CYLINDER WALL ZONE 5	450.46	351.14	418.77	216.22	371.68
CYLINDER WALL ZONE 6	433.22	320.12	398.01	254.90	370.25
CYLINDER WALL ZONE 7	426.78	308.51	394.82	233.40	369.40

CYLINDER WALL ZONE 8	430.95	316.02	405.77	170.56	368.62
CYLINDER WALL ZONE 9	425.37	305.99	392.92	233.49	367.49
CYLINDER WALL ZONE 10	428.79	312.14	393.29	244.03	366.71
CYLINDER WALL ZONE 11	431.08	316.25	387.21	326.20	365.89
CYLINDER WALL ZONE 12	441.94	335.80	394.19	332.30	365.24
CYLINDER WALL ZONE 13	458.50	365.61	400.10	410.34	364.35
CYLINDER WALL ZONE 14	480.23	404.72	407.96	513.09	363.26
CYLINDER WALL ZONE 15	526.52	488.05	423.27	704.57	361.89
INT. MANIFOLD WALL	304.22	87.90			
EXH. MANIFOLD WALL	370.66	207.50			

>>>>> CYLINDER PERFORMANCE RESULTS

DELIVERY RATIO ; (-)	0.89	
SCAVENGING EFFICIENCY	0.87	
TRAPPING EFFICIENCY	0.59	
FACTOR IN FORMULA FOR B1 & B2	3.850	
PUMPING MEAN EFF. PRESSURE (ATM, PSI) : PMEP	0.11	1.58
GROSS IND. MEAN EFF. PRESSURE (ATM, PSI) : IMEP	15.84	232.76
FRICTION MEAN EFF. PRESSURE (ATM, PSI) : FMEP	1.61	23.67
BRAKE MEAN EFF. PRESSURE (ATM, PSI) : BMEP	14.34	210.67
GROSS INDICATED S.F.C. (G/KW/HR, LB/HP/HR) : ISFC	167.590	0.276
BRAKE S.F.C. (G/KW/HR, LB/HP/HR) : CBSFC	185.157	0.304
GROSS INDICATED THERMAL EFFICIENCY; (%)	50.1	
NET INDICATED THERMAL EFFICIENCY; (%)	50.4	

CYLINDER BRAKE THERMAL

CYLINDER BRAKE THERMAL EFFICIENCY; (%)	45.3
(CYL. HEAT TRANSFER PER CYCLE)/ (MASS OF FUEL TIMES LHV) : (%)	30.7
(PISTON SKIRT-TO-ANNULUS HEAT INPUT)/ (GAS-TO-PISTON HEAT INPUT) : (%)	0.0
(WALL-TO-ANNULUS COOLING)/ (GAS-TO-WALL HEAT INPUT) : (%)	0.0

MEAN EXHAUST
TEMPERATURE; (deg C, deg F) 364.54 688.16

>>>>> SYSTEM PERFORMANCE RESULTS

SUPERCHARGER BRAKE POWER
(KW, HP) : SCBHP 18.0 24.2

ENGINE INDICATED POWER
(KW, HP) : ENIHP 126.5 169.6

ENGINE BRAKE POWER
(KW, HP) : ENBHP 113.7 152.5

OVERALL BRAKE POWER
(KW, HP) : OVBHP 95.7 128.3

OVERALL POWER DENSITY
(W/CC, HP/CU-IN) 36.67 0.81

OVERALL BRAKE TORQUE
(N-M, FT-LBf) 507.54 374.29

ENGINE BRAKE WORK
PER CYCLE; (KJ) 3.790

OVERALL BRAKE WORK
PER CYCLE (KJ) 3.189

TOTAL HEAT INPUT
PER CYCLE (KJ) 8.364

HEAT REJECTION TO COOLANT
(KW) 82.662

HEAT REJECTION TO OIL
(KW) 2.753

HEAT REJECTION TO AMBIENT
(KW) 1.546

TOTAL BRAKE SPECIFIC
HEAT REJECTION (BTU/HP/MIN, %) 37.86 89.28

OVERALL BRAKE S.F.C.
(G/KW/HR, LB/HP/HR) : BSFC 220.05 0.362

OVERALL BRAKE THERMAL
EFFICIENCY; (%) 38.1

>>>> CYLINDER MASS SUMMARY

MASS IN CYLINDER AT TIPO = 1.39877 G

MASS IN CYLINDER AT TIPC = 1.33375 G

MASS OF AIR INDUCTED = 1.61608 G

MASS OF COOLING AIR = 0.00000 G

MASS OF FUEL INJECTED = 0.06498 G

>>>> ENGINE MASS SUMMARY

TOTAL AIR FLOW RATE = 1153.32 LB/HR

TOTAL FUELING RATE = 46.37 LB/HR

TOTAL COOLANT FLOW RATE = 18.00 GPM

>>>> SYSTEM MASS SUMMARY

TOTAL AIR FLOW RATE = 1153.32 LB/HR

TOTAL FUELING RATE = 46.37 LB/HR

BURNER BYPASS AIR = 0.00 %

>>>> CYLINDER HEAT & WORK TRANSFERS

HEATI = -0.006683 KJ (TIPO - TPC)
WORKI = -0.058546 KJ

HEATC = 0.047013 KJ (TPC - TIGN)
WORKC = -0.743272 KJ

HEATCE = 0.795418 KJ (TIGN - TEPO)
WORKCE = 2.139024 KJ

HEATE = 0.019036 KJ (TEPO - TIPO)
WORKE = 0.068048 KJ

>>>> COMBUSTION SUMMARY

IGNITION DELAY PERIOD = 4.354 DEG CA

IGNITION TIMING = 346.354 DEG CA

BURN DURATION = 180.000 DEG CA

WEIGHTING FACTOR = 0.000

PREMIXED CONSTANT 1 = 2.092

PREMIXED CONSTANT 2 = 5000.000

DIFFUSION CONSTANT 1 = 315.759

DIFFUSION CONSTANT 2 = 2.944

CFACTR = 0.830

APPENDIX B – PEAK POWER OUTPUT

```
>>>> INSTANTANEOUS CYLINDER DATA AFTER  35 ENGINE CYCLES
 ____________________________________________________________________________________________________

                      DIESEL ENGINE CYCLE SIMULATION - LIMSIM

                                        - SUPERCHARGER INSTALLED
 ____________________________________________________________________________________________________


 >>>>> INPUT DATA
 ____________________________________________________________________________________________________

 >>>>> OPERATING MODE

   PREDICTED IGNITION DELAY OPTION
   PREDICTED QUASI-STEADY WALL TEMPERATURES
   FLAME RADIATION MODEL
   OPTIMIZED INJECTION TIMING SEARCH ENABLED
 ____________________________________________________________________________________________________

 >>>>> OPERATING CONDITIONS

   FUEL USED IS DIESEL #2
   ENGINE SPEED                 =   2150.0 RPM
    NITROGEN-TO-OXYGEN RATIO    =     3.76
   PHI,ENGINE (F/A / F/A|s)     =   0.8104
   PHI,EXH MNFLD (F/A / F/A|s)  =   0.5751
   PHI,OVERALL (F/A / F/A|s)    =   0.0000
   INJECTION TIMING             =    343.0 DEG CA
   COMPRESSOR INLET PRESSURE    =   0.9577 ATM
   COMPRESSOR INLET TEMPERATURE =   298.00 K
   ATMOSPHERIC PRESSURE         =   0.9800 ATM
   ATMOSPHERIC TEMPERATURE      =   298.00 K

   LIM VALVE SPRING CONSTANT    =   390.00 N/M
   LIM VALVE SPRING PRELOAD     =    11.00 CM
 ____________________________________________________________________________________________________


 >>>>> ENGINE DESIGN PARAMETERS

   NUMBER OF CYLINDERS     =    3
   CYLINDER BORE           =     9.842 CM
   CRANKSHAFT STROKE       =    11.430 CM
   CONNECTING ROD LENGTH   =    25.400 CM
   GEOM.COMPRESSION RATIO  =    21.000
   EFF. COMPRESSION RATIO  =    15.425
```

```
   EFF. EXPANSION RATIO    =    15.425
   DISPLACED VOLUME        =   869.655 CC
   CLEARANCE VOLUME        =    43.483 CC
   ENGINE DISPLACEMENT     =     2.609 LT
   INTAKE PORT OPENS       =     166.6 DEG CA
   INTAKE PORT CLOSES      =     260.5 DEG CA
   EXHAUST PORT OPENS      =     125.0 DEG CA
   EXHAUST PORT CLOSES     =     235.0 DEG CA
   EXHAUST CRANK ADVANCE   =       0.0 DEG CA
```

```
>>>> MANIFOLD DIMENSIONS             INTAKE     EXHAUST

   LENGTH                    (CM)        50.00       30.00
   DIAMETER                  (CM)        18.00       10.00
   CROSS-SECTIONAL AREA    (CM**2)      254.47       78.54
   INTERNAL SURFACE AREA   (CM**2)     2827.43      942.48
   VOLUME                    (LT)       12.723       2.356
```

```
>>>> CONNECTING PIPE DIMENSIONS       COMPRESSOR    TURBINE

   LENGTH                    (CM)        21.00       41.00
   DIAMETER                  (CM)        10.00       10.00
   CROSS-SECTIONAL AREA    (CM**2)       78.54       78.54
   INTERNAL SURFACE AREA   (CM**2)      659.73     1288.05
   VOLUME                    (LT)        2.356       3.220
```

```
>>>> TURBOMACHINERY DATA

         SUPERCHARGER  Schwitzer S400-105/55 compressor map (HP)

   T/C INERTIA        (KG-CM**2)        9.13
   T/C DAMPING        (G-CM**2/S)       0.29
   P.TURBINE TRANSMISSION EFF.(%)      60.00
   P.TURBINE GEAR RATIO                13.00
   SUPERCHARGER MULTIPLIERS         0.260  1.000  0.700  0.600
   COMPRESSOR MULTIPLIERS           1.000  1.000  1.000  1.000
   TURBINE MULTIPLIERS              1.000  1.000  1.000  1.000
   POWER TURBINE MULTIPLIERS        1.000  1.000  1.000  1.000
```

```
>>>> SYSTEM PRESSURE DROPS (PA)

   COMPRESSOR EXIT-SUPERCHARGER INLET          0.0
   SUPERCHARGER EXIT-INTERCOOLER INLET         0.0
   INTERCOOLER INLET - INTAKE MANIFOLD         0.0
   EXHAUST MANIFOLD - TURBINE INLET            0.0
   TURBINE EXIT - POWER TURBINE INLET          0.0
   POWER TURBINE EXIT - ATMOSPHERIC         1000.0
```

>>>>> HEAT TRANSFER AND TURBULENCE PARAMETERS

NUSSELT COEFFICIENT (CHAMBER)= 0.0350

NUSSELT COEFFICIENT (INT MAN)= 0.0350

NUSSELT COEFFICIENT (EXH MAN)= 0.0350

NUSSELT COEFFICIENT (C. PIPE)= 0.0350

REYNOLDS EXPONENT = 0.8000

INT. MANIFOLD WALL TEMPERATURE = 312.44 K

EXH. MANIFOLD WALL TEMPERATURE = 389.87 K

CONN. PIPE WALL TEMPERATURE = 596.00 K

TURBULENT DISSIPATION CONSTANT = 1.1000

>>>>> COMPUTATIONAL PARAMETERS

MAXIMUM # OF ITERATIONS = 8000

OUTPUT AT ITERATION # = 35

TCALL = 1.00

TPRINT = 2.00

TSCREN = 8000.00

CIINTG = 0.000001

CCINTG = 0.000010

CBINTG = 0.000010

CEINTG = 0.000010

AREROT = 0.000000

REL = 0.000000

MAXERR = 0.000010

MAXTRY = 100

>>>>> START OF BLOWDOWN PROCESS

CA (DEG)	P (ATM)	TEMP (K)	MEX (G)	PHI (-)	PIM (ATM)	TIM (K)	PEM (ATM)	TEM (K)	PANL (ATM)	TANL (K)	IFG (-)
126.0	7.2706	1115.51	0.00013	0.81040	2.8884	323.44	0.9800	647.49	3.5000	420.00	2
128.0	7.1383	1110.59	0.00075	0.81040	2.8923	323.58	0.9800	647.80	3.5000	420.00	2
130.0	7.0132	1105.87	0.00153	0.81040	2.8963	323.73	0.9800	648.20	3.5000	420.00	2
132.0	6.8929	1101.26	0.00280	0.81040	2.9003	323.88	0.9800	648.77	3.5000	420.00	2
134.0	6.7752	1096.69	0.00492	0.81040	2.9039	324.01	0.9800	649.79	3.5000	420.00	2
136.0	6.6606	1092.18	0.00774	0.81040	2.9069	324.11	0.9800	651.15	3.5000	420.00	2
138.0	6.5327	1087.10	0.01424	0.81040	2.9099	324.21	0.9800	653.68	3.5000	420.00	2
140.0	6.3665	1080.43	0.02903	0.81040	2.9129	324.30	0.9801	660.05	3.5000	420.00	2
142.0	6.1526	1071.64	0.05415	0.81040	2.9158	324.38	0.9804	671.19	3.5000	420.00	2
144.0	5.8914	1060.57	0.08996	0.81040	2.9186	324.47	0.9807	686.85	3.5000	420.00	2
146.0	5.5898	1047.27	0.13553	0.81040	2.9215	324.56	0.9814	705.77	3.5000	420.00	2
148.0	5.2567	1031.87	0.18960	0.81040	2.9244	324.64	0.9818	726.48	3.5000	420.00	2
150.0	4.9023	1014.60	0.25053	0.81040	2.9273	324.73	0.9831	747.50	3.5000	420.00	2
152.0	4.5365	995.68	0.31658	0.81040	2.9301	324.82	0.9834	767.50	3.5000	420.00	2
154.0	4.1691	975.42	0.38597	0.81040	2.9330	324.90	0.9843	785.53	3.5000	420.00	2
156.0	3.8081	954.12	0.45704	0.81040	2.9359	324.99	0.9848	800.95	3.5000	420.00	2
158.0	3.4601	932.04	0.52835	0.81040	2.9387	325.07	0.9845	813.48	3.5000	420.00	2
160.0	3.1300	909.43	0.59863	0.81040	2.9416	325.16	0.9847	823.17	3.5000	420.00	2
162.0	2.8212	886.52	0.66691	0.81040	2.9444	325.24	0.9844	830.08	3.5000	420.00	2
164.0	2.5355	863.52	0.73242	0.81040	2.9473	325.33	0.9843	834.53	3.5000	420.00	2
166.0	2.2740	840.61	0.79463	0.81040	2.9501	325.41	0.9838	836.83	3.5000	420.00	2

>>>>> OUTPUT DATA

>>>>> ENGINE CRANK-ANGLE BY CRANK-ANGLE RESULTS

>>>>> START OF INTAKE PROCESS

CA (DEG)	P (ATM)	TEMP (K)	MIN (G)	MEX (G)	PHI (-)	PIM (ATM)	TIM (K)	PEM (ATM)	TEM (K)	PANL (ATM)	TANL (K)	IFG (-)
166.5	2.2101	834.70	0.00000	0.81018	0.81040	2.9509	325.44	0.9836	837.09	8		
168.0	2.0364	817.94	0.00000	0.85318	0.81040	2.9530	325.50	0.9834	837.41	3.5000	420.00	2
170.0	1.8223	795.57	0.00014	0.90788	0.81022	2.9558	325.58	0.9831	836.54	3.5000	420.00	2
172.0	1.6315	773.41	0.00087	0.95859	0.80923	2.9586	325.66	0.9826	834.56	3.5000	420.00	2
174.0	1.4661	751.44	0.00292	1.00469	0.80619	2.9612	325.74	0.9821	831.70	3.5000	420.00	2
176.0	1.3281	729.61	0.00724	1.04558	0.79936	2.9637	325.81	0.9819	828.29	3.5000	420.00	2
178.0	1.2189	707.81	0.01496	1.08089	0.78657	2.9658	325.87	0.9814	824.64	3.5000	420.00	2
180.0	1.1394	685.75	0.02756	1.11067	0.76525	2.9674	325.92	0.9810	820.91	3.5000	420.00	2
182.0	1.0891	662.89	0.04699	1.13556	0.73283	2.9684	325.94	0.9808	817.26	3.5000	420.00	2
184.0	1.0663	638.64	0.07568	1.15711	0.68769	2.9686	325.94	0.9807	813.65	3.5000	420.00	2
186.0	1.0674	612.89	0.11599	1.17771	0.63076	2.9676	325.90	0.9806	809.84	3.5000	420.00	2
188.0	1.0883	586.46	0.16939	1.19981	0.56608	2.9652	325.82	0.9806	805.42	3.5000	420.00	2
190.0	1.1254	560.94	0.23593	1.22511	0.49950	2.9616	325.69	0.9809	799.83	3.5000	420.00	2
192.0	1.1758	537.74	0.31435	1.25442	0.43625	2.9567	325.53	0.9815	792.89	3.5000	420.00	2
194.0	1.2372	517.59	0.40293	1.28787	0.37937	2.9507	325.33	0.9812	784.32	3.5000	420.00	2
196.0	1.3090	500.55	0.50062	1.32520	0.32962	2.9438	325.10	0.9814	774.17	3.5000	420.00	2
198.0	1.3904	485.28	0.60793	1.36598	0.28632	2.9359	324.84	0.9820	762.65	3.5000	420.00	2
200.0	1.4893	472.72	0.72705	1.40971	0.24835	2.9269	324.55	0.9819	750.16	3.5000	420.00	2
202.0	1.6064	462.61	0.85770	1.45593	0.21557	2.9166	324.21	0.9822	736.83	3.5000	420.00	2
204.0	1.7193	454.74	0.98453	1.50348	0.19016	2.9064	323.88	0.9834	723.18	3.5000	420.00	2
206.0	1.8268	448.62	1.10513	1.55077	0.17031	2.8968	323.56	0.9824	709.78	3.5000	420.00	2
208.0	1.9312	443.92	1.21908	1.59648	0.15453	2.8879	323.27	0.9835	697.03	3.5000	420.00	2
210.0	2.0335	440.41	1.32584	1.63946	0.14184	2.8797	323.00	0.9829	685.31	3.5000	420.00	2
212.0	2.1348	437.94	1.42472	1.67872	0.13155	2.8724	322.75	0.9818	674.86	3.5000	420.00	2
214.0	2.2357	436.39	1.51496	1.71334	0.12322	2.8659	322.53	0.9817	665.85	3.5000	420.00	2
216.0	2.3366	435.69	1.59574	1.74246	0.11649	2.8603	322.35	0.9807	658.42	3.5000	420.00	2
218.0	2.4375	435.80	1.66619	1.76542	0.11113	2.8558	322.20	0.9811	652.65	3.5000	420.00	2
220.0	2.5384	436.66	1.72549	1.78169	0.10695	2.8524	322.08	0.9804	648.51	3.5000	420.00	2
222.0	2.6374	438.21	1.77284	1.79145	0.10381	2.8502	322.01	0.9803	645.96	3.5000	420.00	2
224.0	2.7309	440.28	1.80757	1.79584	0.10163	2.8493	321.97	0.9801	644.73	3.5000	420.00	2
226.0	2.8105	442.57	1.82911	1.79774	0.10031	2.8496	321.98	0.9800	644.24	3.5000	420.00	2
228.0	2.8605	444.60	1.83267	1.79916	0.09996	2.8515	322.04	0.9800	643.90	3.5000	420.00	2
230.0	2.8786	445.65	1.82031	1.80001	0.09996	2.8558	322.21	0.9800	643.67	3.5000	420.00	2
232.0	2.8949	446.60	1.80605	1.80053	0.09996	2.8607	322.41	0.9800	643.54	3.5000	420.00	2
234.0	2.9145	447.69	1.79208	1.80093	0.09996	2.8656	322.61	0.9800	643.44	3.5000	420.00	2
236.0	2.9419	449.11	1.77992	1.80110	0.09996	2.8703	322.80	0.9800	643.39	3.5000	420.00	2
238.0	2.9817	451.06	1.77116	1.80110	0.09996	2.8747	322.96	0.9800	643.39	3.5000	420.00	2
240.0	3.0386	453.70	1.76740	1.80110	0.09996	2.8783	323.10	0.9800	643.39	3.5000	420.00	2

>>>>> START OF COMPRESSION PROCESS

CA (DEG)	P (ATM)	TEMP (K)			PHI (-)	PIM (ATM)	TIM (K)	PEM (ATM)	TEM (K)	PANL (ATM)	TANL (K)	IFG (-)
242.0	3.1075	456.79	1.76644	1.80110	0.09996	2.8814	323.19	0.9800	643.39	3.5000	420.00	2
244.0	3.1735	459.71	1.76295	1.80110	0.09996	2.8846	323.30	0.9800	643.39	3.5000	420.00	2
246.0	3.2375	462.50	1.75727	1.80110	0.09996	2.8883	323.43	0.9800	643.40	3.5000	420.00	2
248.0	3.3016	465.25	1.75014	1.80110	0.09996	2.8922	323.58	0.9799	643.67	3.5000	420.00	2
250.0	3.3691	468.08	1.74258	1.80110	0.09996	2.8961	323.73	0.9800	644.06	3.5000	420.00	2
252.0	3.4443	471.16	1.73591	1.80110	0.09996	2.9001	323.88	0.9799	644.62	3.5000	420.00	2
254.0	3.5333	474.71	1.73173	1.80110	0.09996	2.9037	324.01	0.9800	645.61	3.5000	420.00	2

>>>>> START OF COMPRESSION PROCESS

CA (DEG)	P (ATM)	TEMP (K)			PHI (-)	PIM (ATM)	TIM (K)	PEM (ATM)	TEM (K)	PANL (ATM)	TANL (K)	IFG (-)

256.0	3.6405	478.86	1.73105	1.80110	0.09996	2.9068	324.11	0.9798	646.97	3.5000	420.00	2
258.0	3.7545	483.17	1.73014	1.80110	0.09996	2.9098	324.20	0.9795	649.37	3.5000	420.00	2

>>>>> START OF COMPRESSION PROCESS

CA (DEG)	P (ATM)	TEMP (K)			PHI (-)	PIM (ATM)	TIM (K)	PEM (ATM)	TEM (K)	PANL (ATM)	TANL (K)	IFG (-)
260.0	3.8793	487.74	1.72994	1.80110	0.09996	2.9127	324.29	0.9800	655.60	3.5000	420.00	2

>>>>> START OF COMPRESSION PROCESS

CA (DEG)	P (ATM)	TEMP (K)			PHI (-)	PIM (ATM)	TIM (K)	PEM (ATM)	TEM (K)	PANL (ATM)	TANL (K)	IFG (-)

>>>>> START OF COMPRESSION PROCESS

CA (DEG)	P (ATM)	TEMP (K)	PHI (-)	PIM (ATM)	TIM (K)	PEM (ATM)	TEM (K)	PANL (ATM)	TANL (K)	IFG (-)
262.0	4.0138	492.54	0.09996	2.9156	324.38	0.9802	666.85	3.5000	420.00	2
264.0	4.1582	497.54	0.09996	2.9185	324.47	0.9807	682.68	3.5000	420.00	2
266.0	4.3128	502.69	0.09996	2.9214	324.55	0.9816	701.82	3.5000	420.00	2
268.0	4.4785	507.99	0.09996	2.9242	324.64	0.9822	722.78	3.5000	420.00	2
270.0	4.6568	513.51	0.09996	2.9271	324.73	0.9832	744.06	3.5000	420.00	2
272.0	4.8488	519.26	0.09996	2.9300	324.81	0.9839	764.33	3.5000	420.00	2
274.0	5.0561	525.25	0.09996	2.9329	324.90	0.9845	782.61	3.5000	420.00	2
276.0	5.2799	531.49	0.09996	2.9357	324.98	0.9845	798.26	3.5000	420.00	2
278.0	5.5220	537.99	0.09996	2.9386	325.07	0.9848	811.07	3.5000	420.00	2
280.0	5.7842	544.77	0.09996	2.9414	325.16	0.9847	820.85	3.5000	420.00	2
282.0	6.0687	551.84	0.09996	2.9443	325.24	0.9846	827.93	3.5000	420.00	2
284.0	6.3777	559.22	0.09996	2.9472	325.33	0.9842	832.49	3.5000	420.00	2
286.0	6.7140	566.92	0.09996	2.9500	325.41	0.9839	834.97	3.5000	420.00	2
288.0	7.0806	574.97	0.09996	2.9528	325.50	0.9834	835.60	3.5000	420.00	2
290.0	7.4810	583.36	0.09996	2.9557	325.58	0.9830	834.83	3.5000	420.00	2
292.0	7.9189	592.14	0.09996	2.9584	325.66	0.9826	832.86	3.5000	420.00	2
294.0	8.3988	601.31	0.09996	2.9611	325.74	0.9821	830.06	3.5000	420.00	2
296.0	8.9257	610.89	0.09996	2.9635	325.81	0.9817	826.69	3.5000	420.00	2
298.0	9.5054	620.92	0.09996	2.9656	325.87	0.9813	823.06	3.5000	420.00	2
300.0	10.1445	631.40	0.09996	2.9672	325.91	0.9809	819.37	3.5000	420.00	2
302.0	10.8505	642.37	0.09996	2.9682	325.94	0.9806	815.76	3.5000	420.00	2
304.0	11.6322	653.86	0.09996	2.9683	325.93	0.9805	812.18	3.5000	420.00	2
306.0	12.4996	665.89	0.09996	2.9673	325.89	0.9805	808.40	3.5000	420.00	2
308.0	13.4642	678.49	0.09996	2.9649	325.81	0.9805	803.98	3.5000	420.00	2
310.0	14.5394	691.69	0.09996	2.9612	325.68	0.9807	798.38	3.5000	420.00	2
312.0	15.7405	705.53	0.09996	2.9562	325.52	0.9809	791.40	3.5000	420.00	2
314.0	17.0854	720.03	0.09996	2.9502	325.32	0.9813	782.79	3.5000	420.00	2
316.0	18.5946	735.23	0.09996	2.9432	325.09	0.9813	772.67	3.5000	420.00	2
318.0	20.2918	751.15	0.09996	2.9353	324.83	0.9820	761.21	3.5000	420.00	2
320.0	22.2045	767.83	0.09996	2.9263	324.53	0.9818	748.78	3.5000	420.00	2
322.0	24.3638	785.31	0.09996	2.9160	324.19	0.9823	735.50	3.5000	420.00	2
324.0	26.8056	803.58	0.09996	2.9058	323.86	0.9822	721.94	3.5000	420.00	2
326.0	29.5700	822.69	0.09996	2.8963	323.54	0.9820	708.68	3.5000	420.00	2
328.0	32.7020	842.62	0.09996	2.8874	323.25	0.9819	696.05	3.5000	420.00	2
330.0	36.2507	863.36	0.09996	2.8793	322.98	0.9816	684.54	3.5000	420.00	2
332.0	40.2683	884.90	0.09996	2.8720	322.74	0.9814	674.24	3.5000	420.00	2
334.0	44.8078	907.16	0.09996	2.8655	322.52	0.9811	665.35	3.5000	420.00	2
336.0	49.9191	930.05	0.09996	2.8600	322.34	0.9808	658.03	3.5000	420.00	2
338.0	55.6429	953.42	0.09996	2.8555	322.19	0.9804	652.23	3.5000	420.00	2
340.0	62.0012	977.08	0.09996	2.8521	322.08	0.9802	648.23	3.5000	420.00	2
342.0	68.9846	1000.73	0.09996	2.8500	322.00	0.9801	645.73	3.5000	420.00	2
344.0	76.5297	1023.95	0.09996	2.8491	321.97	0.9800	644.55	3.5000	420.00	2
346.0	84.5034	1046.19	0.09996	2.8495	321.98	0.9800	644.08	3.5000	420.00	2
346.9	88.0289	1055.36	0.09996	2.8502	322.00	0.9800	643.93	8		

>>>>> START OF COMBUSTION AND EXPANSION PROCESSES

CA (DEG)	P (ATM)	TEMP (K)	PHI (-)	PIM (ATM)	TIM (K)	PEM (ATM)	TEM (K)	PANL (ATM)	TANL (K)	IFG (-)
348.0	92.6205	1066.12	0.10003	2.8515	322.04	0.9800	643.74	3.5000	420.00	2
350.0	100.9427	1087.25	0.10144	2.8559	322.21	0.9800	643.52	3.5000	420.00	2
352.0	109.8494	1116.26	0.10629	2.8608	322.41	0.9800	643.40	3.5000	420.00	2
354.0	119.6221	1158.30	0.11652	2.8657	322.61	0.9800	643.30	3.5000	420.00	2
356.0	130.3926	1217.21	0.13380	2.8704	322.80	0.9800	643.26	3.5000	420.00	2
358.0	142.0332	1295.00	0.15942	2.8747	322.97	0.9800	643.26	3.5000	420.00	2
360.0	154.0845	1391.47	0.19408	2.8783	323.09	0.9800	643.26	3.5000	420.00	2
362.0	165.7699	1504.08	0.23778	2.8813	323.19	0.9800	643.26	3.5000	420.00	2
364.0	176.1143	1628.18	0.28971	2.8847	323.31	0.9800	643.26	3.5000	420.00	2
366.0	184.1366	1757.55	0.34825	2.8883	323.44	0.9800	643.27	3.5000	420.00	2
368.0	189.0478	1885.12	0.41106	2.8922	323.58	0.9800	643.58	3.5000	420.00	2
370.0	190.3928	2003.81	0.47535	2.8962	323.74	0.9800	643.98	3.5000	420.00	2
372.0	188.1073	2107.33	0.53815	2.9002	323.88	0.9799	644.55	3.5000	420.00	2
374.0	182.4954	2190.95	0.59670	2.9038	324.01	0.9800	645.58	3.5000	420.00	2
376.0	174.1453	2252.07	0.64877	2.9068	324.11	0.9800	646.94	3.5000	420.00	2
378.0	163.8034	2290.36	0.69288	2.9098	324.21	0.9800	649.48	3.5000	420.00	2
380.0	152.2424	2307.34	0.72845	2.9128	324.30	0.9794	655.93	3.5000	420.00	2
382.0	140.1589	2305.77	0.75570	2.9157	324.38	0.9805	667.06	3.5000	420.00	2
384.0	128.1158	2289.03	0.77550	2.9185	324.47	0.9810	682.90	3.5000	420.00	2
386.0	116.5255	2260.63	0.78912	2.9214	324.56	0.9809	702.05	3.5000	420.00	2
388.0	105.6597	2223.93	0.79798	2.9243	324.65	0.9824	722.98	3.5000	420.00	2
390.0	95.6713	2181.89	0.80341	2.9272	324.73	0.9821	744.26	3.5000	420.00	2
392.0	86.6204	2136.98	0.80655	2.9300	324.82	0.9832	764.52	3.5000	420.00	2
394.0	78.5011	2091.05	0.80824	2.9329	324.90	0.9841	782.79	3.5000	420.00	2
396.0	71.2642	2045.41	0.80911	2.9358	324.99	0.9842	798.43	3.5000	420.00	2
398.0	64.8366	2000.87	0.80952	2.9386	325.08	0.9848	811.26	3.5000	420.00	2
400.0	59.1357	1957.89	0.80970	2.9415	325.16	0.9846	821.03	3.5000	420.00	2
402.0	54.0787	1916.68	0.80978	2.9444	325.25	0.9841	828.07	3.5000	420.00	2
404.0	49.5876	1877.28	0.80980	2.9472	325.33	0.9841	832.74	3.5000	420.00	2
406.0	45.5923	1839.68	0.80981	2.9501	325.42	0.9838	835.23	3.5000	420.00	2
408.0	42.0306	1803.81	0.80982	2.9529	325.50	0.9834	835.84	3.5000	420.00	2
410.0	38.8482	1769.57	0.80982	2.9557	325.58	0.9830	834.99	3.5000	420.00	2
412.0	35.9981	1736.89	0.80982	2.9585	325.67	0.9826	833.02	3.5000	420.00	2
414.0	33.4395	1705.68	0.80982	2.9611	325.74	0.9821	830.22	3.5000	420.00	2
416.0	31.1372	1675.84	0.80982	2.9636	325.81	0.9818	826.83	3.5000	420.00	2
418.0	29.0606	1647.30	0.80982	2.9657	325.87	0.9813	823.20	3.5000	420.00	2
420.0	27.1834	1619.99	0.80982	2.9673	325.92	0.9809	819.51	3.5000	420.00	2
422.0	25.4826	1593.82	0.80982	2.9683	325.94	0.9807	815.90	3.5000	420.00	2
424.0	23.9383	1568.73	0.80982	2.9684	325.94	0.9805	812.33	3.5000	420.00	2
426.0	22.5331	1544.67	0.80982	2.9674	325.90	0.9804	808.55	3.5000	420.00	2
428.0	21.2519	1521.56	0.80982	2.9650	325.82	0.9805	804.12	3.5000	420.00	2
430.0	20.0813	1499.36	0.80982	2.9613	325.69	0.9807	798.52	3.5000	420.00	2
432.0	19.0098	1478.01	0.80982	2.9563	325.52	0.9809	791.53	3.5000	420.00	2
434.0	18.0271	1457.47	0.80982	2.9503	325.32	0.9812	782.92	3.5000	420.00	2
436.0	17.1242	1437.68	0.80982	2.9433	325.09	0.9815	772.79	3.5000	420.00	2
438.0	16.2931	1418.60	0.80982	2.9354	324.84	0.9821	761.33	3.5000	420.00	2
440.0	15.5270	1400.21	0.80982	2.9265	324.54	0.9826	748.90	3.5000	420.00	2
442.0	14.8197	1382.46	0.80982	2.9162	324.20	0.9819	735.62	3.5000	420.00	2
444.0	14.1655	1365.32	0.80982	2.9060	323.87	0.9826	722.06	3.5000	420.00	2
446.0	13.5597	1348.76	0.80982	2.8964	323.55	0.9824	708.76	3.5000	420.00	2
448.0	12.9978	1332.76	0.80982	2.8875	323.26	0.9819	696.12	3.5000	420.00	2
450.0	12.4761	1317.28	0.80982	2.8794	322.99	0.9819	684.59	3.5000	420.00	2
452.0	11.9909	1302.30	0.80982	2.8721	322.75	0.9815	674.24	3.5000	420.00	2
454.0	11.5391	1287.80	0.80982	2.8656	322.53	0.9811	665.35	3.5000	420.00	2
456.0	11.1180	1273.75	0.80982	2.8601	322.35	0.9819	658.01	3.5000	420.00	2
458.0	10.7250	1260.13	0.80982	2.8555	322.19	0.9806	652.14	3.5000	420.00	2
460.0	10.3578	1246.93	0.80982	2.8522	322.08	0.9803	648.12	3.5000	420.00	2
462.0	10.0145	1234.12	0.80982	2.8500	322.00	0.9802	645.60	3.5000	420.00	2
464.0	9.6930	1221.69	0.80982	2.8491	321.97	0.9800	644.38	3.5000	420.00	2
466.0	9.3918	1209.63	0.80982	2.8495	321.98	0.9800	643.92	3.5000	420.00	2
468.0	9.1093	1197.91	0.80982	2.8514	322.04	0.9800	643.58	3.5000	420.00	2
470.0	8.8441	1186.52	0.80982	2.8559	322.22	0.9800	643.37	3.5000	420.00	2
472.0	8.5950	1175.45	0.80982	2.8608	322.42	0.9800	643.24	3.5000	420.00	2
474.0	8.3608	1164.68	0.80982	2.8657	322.62	0.9800	643.14	3.5000	420.00	2
476.0	8.1405	1154.21	0.80982	2.8704	322.81	0.9800	643.10	3.5000	420.00	2
478.0	7.9330	1144.02	0.80982	2.8747	322.97	0.9800	643.10	3.5000	420.00	2
480.0	7.7376	1134.10	0.80982	2.8783	323.10	0.9800	643.10	3.5000	420.00	2
482.0	7.5535	1124.45	0.80982	2.8814	323.20	0.9800	643.10	3.5000	420.00	2
484.0	7.3798	1115.04	0.80982	2.8847	323.31	0.9800	643.10	3.5000	420.00	2

>>>>> START OF BLOWDOWN PROCESS

CA (DEG)	P (ATM)	TEMP (K)	MEX (G)	PHI (-)	PIM (ATM)	TIM (K)	PEM (ATM)	TEM (K)	PANL (ATM)	TANL (K)	IFG (-)

>>>> CYCLE-AVERAGED SYSTEM DATA AFTER 35 ENGINE CYCLES

 >>>> MANIFOLD HEAT TRANSFER DATA   INTAKE   EXHAUST

WALL TEMPERATURE	(K)	311.97	386.43
AVERAGE VELOCITY (M/S)		0.20	0.25
REYNOLDS NUMBER (FILM)		6242.5	659.6
PRANDTL NUMBER		0.6473	0.6914
NUSSELT NUMBER		33.39	5.64
HEAT TRANSFER COEFF. (W/K/M**2)		5.29	2.26
HEAT TRANSFER RATE	(KW)	0.013	0.258

 >>>SYSTEM PRESSURES   (ATM)   (PSI)

SUPERCHARGER INLET	0.96	14.07
SUPERCHARGER OUTLET	2.91	42.80
DELTA P ENGINE	1.93	28.38
PEAK IN-CYLINDER	190.39	2797.76

 >>>>SYSTEM TEMPERATURES (K)   (F)

SUPERCHARGER INLET	298.00	76.71
SUPERCHARGER OUTLET	473.63	392.85

>>>TURBOMACHINERY DATA   SUPERCHARGER

ACTUAL MASS FLOW (LB/MIN)	24.585
ACTUAL SPEED(KRPM OR U/V0)	58.050
MAP FLOW (LB/MIN)	25.335
MAP SPEED (KRPM OR U/V0)	58.050
PRESSURE RATIOS:	3.042
EFFICIENCIES:	0.644

 >>> CYLINDER WALL ZONAL BREAKS FROM CENTERLINE
|----!----!----!----!---!-----!-----!-----------!-----!-----!-----------!-----------!-----------!-----------!------------!

  >>>TOP RING ZONE POSITION   -   14.87

  >>>TOP RING REVERSAL TEMP(C) -   255.86

>>>>COMPONENT TEMPERATURE DATA	IN-CYL (K)	IN-CYL (F)	OUTER (K)	HEAT FLUX (KW/M^2)	TCOOL (K)
PISTON	514.30	466.06			
HEAD	654.35	718.14			
CYLINDER WALL ZONE 1	444.91	341.15	416.19	198.63	375.81
CYLINDER WALL ZONE 2	432.01	317.94	407.11	175.74	374.64
CYLINDER WALL ZONE 3	432.42	318.66	406.86	179.47	373.70
CYLINDER WALL ZONE 4	439.45	331.32	410.44	204.07	372.73
CYLINDER WALL ZONE 5	460.19	368.65	421.08	267.59	371.64
CYLINDER WALL ZONE 6	440.86	333.86	398.47	306.20	370.18
CYLINDER WALL ZONE 7	434.01	321.53	395.34	281.38	369.34
CYLINDER WALL ZONE 8	438.68	329.94	407.62	211.29	368.58
CYLINDER WALL ZONE 9	432.75	319.26	393.49	282.10	367.43
CYLINDER WALL ZONE 10	436.73	326.42	393.92	295.15	366.66
CYLINDER WALL ZONE 11	439.50	331.41	387.27	386.58	365.84
CYLINDER WALL ZONE 12	451.57	353.14	394.57	397.42	365.20
CYLINDER WALL ZONE 13	470.12	386.53	400.50	489.60	364.32
CYLINDER WALL ZONE 14	494.19	429.86	408.31	609.90	363.24
CYLINDER WALL ZONE 15	546.93	524.78	424.09	841.71	361.88
INT. MANIFOLD WALL	311.97	101.86			
EXH. MANIFOLD WALL	386.43	235.88			

>>>>> CYLINDER PERFORMANCE RESULTS

DELIVERY RATIO ; (-)	0.81	
SCAVENGING EFFICIENCY	0.88	
TRAPPING EFFICIENCY	0.63	
FACTOR IN FORMULA FOR B1 & B2	3.850	
PUMPING MEAN EFF. PRESSURE (ATM, PSI) : PMEP	-0.06	-0.94
GROSS IND. MEAN EFF. PRESSURE (ATM, PSI) : IMEP	18.31	268.99
FRICTION MEAN EFF. PRESSURE (ATM, PSI) : FMEP	1.84	27.05
BRAKE MEAN EFF. PRESSURE (ATM, PSI) : BMEP	16.40	241.00
GROSS INDICATED S.F.C. (G/KW/HR, LB/HP/HR) : ISFC	162.419	0.267
BRAKE S.F.C. (G/KW/HR, LB/HP/HR) : CBSFC	181.278	0.298
GROSS INDICATED THERMAL EFFICIENCY; (%)	51.7	
NET INDICATED THERMAL		

```
 EFFICIENCY; (%)                      51.5


CYLINDER BRAKE THERMAL
 CYLINDER BRAKE THERMAL
 EFFICIENCY; (%)                      46.3

 (CYL. HEAT TRANSFER PER CYCLE)/
 (MASS OF FUEL TIMES LHV) : (%)       27.1

 (PISTON SKIRT-TO-ANNULUS HEAT INPUT)/
 (GAS-TO-PISTON HEAT INPUT) : (%)      0.0

 (WALL-TO-ANNULUS COOLING)/
 (GAS-TO-WALL HEAT INPUT) : (%)        0.0

 MEAN EXHAUST
 TEMPERATURE; (deg C, deg F)      422.99    793.37
```

```
 >>>>>  SYSTEM PERFORMANCE RESULTS
```

```
 SUPERCHARGER BRAKE POWER
 (KW, HP) : SCBHP                  33.2      44.5


 ENGINE INDICATED POWER
 (KW, HP) : ENIHP                  172.8     231.7

 ENGINE BRAKE POWER
 (KW, HP) : ENBHP                  155.4     208.3

 OVERALL BRAKE POWER
 (KW, HP) : OVBHP                  122.2     163.8

 OVERALL POWER DENSITY
 (W/CC, HP/CU-IN)                  46.83      1.03

 OVERALL BRAKE TORQUE
 (N-M, FT-LBf)                    542.65    400.19

 ENGINE BRAKE WORK
 PER CYCLE; (KJ)                     4.336

 OVERALL BRAKE WORK
 PER CYCLE (KJ)                      3.410

 TOTAL HEAT INPUT
 PER CYCLE (KJ)                      9.368

 HEAT REJECTION TO COOLANT
 (KW)                              109.098

 HEAT REJECTION TO OIL
 (KW)                                4.185

 HEAT REJECTION TO AMBIENT
 (KW)                                1.546

 TOTAL BRAKE SPECIFIC
 HEAT REJECTION (BTU/HP/MIN, %)    39.32     92.72

 OVERALL BRAKE S.F.C.
 (G/KW/HR, LB/HP/HR) : BSFC       230.51     0.379
```

```
  OVERALL BRAKE THERMAL
  EFFICIENCY; (%)                      36.4



>>>> CYLINDER MASS SUMMARY

  MASS IN CYLINDER AT TIPO =  1.55554 G

  MASS IN CYLINDER AT TIPC =  1.48437 G

  MASS OF AIR INDUCTED     =  1.72994 G

  MASS OF COOLING AIR      =  0.00000 G

  MASS OF FUEL INJECTED    =  0.07277 G

>>>> ENGINE MASS SUMMARY

  TOTAL AIR FLOW RATE      =  1474.63 LB/HR

  TOTAL FUELING RATE       =    62.03 LB/HR

  TOTAL COOLANT FLOW RATE  =    21.50 GPM

>>>> SYSTEM MASS SUMMARY

  TOTAL AIR FLOW RATE      =  1474.63 LB/HR

  TOTAL FUELING RATE       =    62.03 LB/HR

  BURNER BYPASS AIR        =     0.00 %
```

```
>>>> CYLINDER HEAT & WORK TRANSFERS

  HEATI   =   -0.003342 KJ  (TIPO   -   TPC)
  WORKI   =   -0.089222 KJ


  HEATC   =    0.055269 KJ  (TPC    -   TIGN)
  WORKC   =   -0.854303 KJ


  HEATCE   =    0.770505 KJ  (TIGN   -   TEPO)
  WORKCE   =    2.467310 KJ


  HEATE   =    0.023377 KJ  (TEPO   -   TIPO)
  WORKE   =    0.083600 KJ
```

```
>>>> COMBUSTION SUMMARY


  IGNITION DELAY PERIOD  =   3.864 DEG CA

  IGNITION TIMING        = 346.864 DEG CA

  BURN DURATION          =  180.000 DEG CA

  WEIGHTING FACTOR       =    0.000

  PREMIXED CONSTANT 1    =    2.069

  PREMIXED CONSTANT 2    = 5000.000

  DIFFUSION CONSTANT 1   =  315.291

  DIFFUSION CONSTANT 2   =    2.943

  CFACTR                 =    0.830
```
